Study on Ring-Shaped Emitter for Subsurface Irrigation in Arid Region of Indonesia

2019.3

Agricultural and Environmental Engineering

United Graduate School of Agricultural Science

Tokyo University of Agriculture and Technology

RESKIANA SAEFUDDIN

Study on Ring-Shaped Emitter for Subsurface Irrigation in Arid Region of Indonesia

By

Reskiana Saefuddin

A dissertation submitted in partial fulfillment of the requirement for the degree of Doctor of Philosophy

March, 2019

Agricultural and Environmental Engineering
United Graduate School of Agricultural Science
Tokyo University of Agriculture and Technology

Committee Members:

Chair : Hirotaka Saito, PhD. (Professor, TUAT)
Co-chair : Tasuku Kato, PhD. (Professor, TUAT)
Co-chair : Hisao Kuroda, PhD. (Professor, Ibaraki University)
Yuji Kohgo, PhD. (Professor, TUAT)
Hiroyuki Matsui, PhD. (Professor, Utsunomiya University)

学 位 論 文 要 旨

Study on Ring-Shaped Emitter for Subsurface Irrigation in Arid Region of Indonesia

(インドネシアの乾燥地におけるリング型エミッターによる地下灌漑に関する研究)

Agricultural and Environmental Engineering
Reskiana Saefuddin
レスキアナ サフディン

Nowadays, freshwater resources are getting scarcer due to climate change, poor management and pollution. It will become a chronic problem in the future because of the rapid increase in the world population. In many water-scarce regions, farmers need to adopt one of the efficient irrigation methods for sustainable crop production. While in many developed countries high-tech micro irrigation methods such as sprinkler and drip irrigation are used increasingly, many farmers are reluctant to adopt these methods due to their high initial cost of installation, costly maintenance, and needs of highly skilled and well-trained engineers. Therefore, the use of indigenous skills and materials is crucial to promote irrigation technologies in such areas.

A ring-shaped emitter made from a common rubber hose has been developed and introduced for subsurface irrigation in some arid regions of Indonesia. It is a low-cost irrigation technology based on indigenous materials and skills. To build a ring-shaped emitter of the original design, a rubber hose is bent into a ring shape with a diameter of about 20 cm, and five 5-mm holes are drilled into it at an even interval. The entire ring-shaped hose is covered with a permeable textile so that water can infiltrate in all directions around the buried emitter. Although it has been practiced for cultivating horticulture crops, the performance of the ring-shaped emitter has not been evaluated in detail. Additionally, because the ring-shaped hose is fully covered with the textile, it may be difficult to detect any malfunctions or repair it. To promote the ring-shaped emitter for subsurface irrigation among small-scale farmers in arid or semi-arid regions, it is important to design an emitter that is easy to maintain and operate.

The main objective of this study is to investigate the performance of the ring-shaped emitter for sustainable subsurface irrigation practices in arid regions. The comprehensive study and analysis were conducted, including the improvement of the ring-shaped emitter design, the evaluation of ring-shaped emitter performance on subsurface water movement and irrigation water productivity during crop cultivation, and the assessment of long-term effect of subsurface irrigation with the ring-shaped emitter on subsurface environment. A combination of experimental and numerical analysis was applied in this study.

The laboratory experiments were first carried out in order to investigate the evaluation of the wet volume around the buried ring-shaped emitter in different soil textures (silt and sand) and inlet water pressure head application. The effect was then analyzed numerically using HYDRUS. The results indicated that hydraulic properties greatly influenced the wet volume during subsurface water application through the buried emitter. Additionally, alternative emitter designs were proposed by reducing the number of holes in the emitter and by changing the covering method to partially covered only around the holes to increase water use efficiency and to simplify the maintenance of the ring-shaped emitters. The spatial extent of the wet volume around the buried emitter in different designs was then numerically simulated with HYDRUS. As results, the non-uniformity in the wetted volume in silt for the emitter with fewer holes was not significantly different because water moved radially from the emitter, diminishing the effect of the spatial hole configuration. On the other hand, for sand, the wet volume evaluated by computed cumulative compensated root water uptake (RWU) is strongly affected by the emitter design when preceding irrigation was considered. Simulation results showed that reducing the number of holes in sand gradually increased RWU as slowly infiltrating water allowed plant roots to uptake water continuously.

The second experiments were carried out in a glass-house in order to evaluate the performance of ring-shaped emitter on soil water dynamic and irrigation water productivity during bell pepper cultivation. Two ring-shaped emitter designs were compared; original and alternative designs. HYDRUS was used to analyze soil water dynamic and root water uptake. Both experimental and numerical analysis revealed that although the alternative emitter design had lower yield and growth performance, it can increase irrigation water productivity without compromising water stress for the crops.

Finally, the long-term effect of subsurface fertilization with the ring-shaped emitter on the subsurface environment was assessed numerically using HYDRUS. The simulations were conducted for 10 years. The results indicated that potential nutrient leaching into groundwater was higher when using the original ring-shaped emitter over 10 years. On the other hand, the amount of nutrient leaching can be minimized when the alternative emitter design was used.

Overall, this study clearly demonstrated that in designing subsurface irrigation with the ring-shaped emitter involves with many factors, including the selections of an appropriate water pressure head application (i.e. emitter discharge rate), soil hydraulic characteristics, crop and climate conditions as well as plant root distribution, root and nutrient uptake, transpiration and evaporation. Understanding water and nutrient movement in the root zone around the ring-shaped emitter are important for an efficient irrigation water management and prevention of solute leaching to groundwater environment.

DEDICATION

To my parents

Acknowledgments

My diction would be inadequate to express my deepest gratitude to all those people who helped me pursuing my PhD course and dissertation. Nevertheless, I would still like to convey my appreciation and gratitude to all these people.

First and foremost, I would like to give my sincere appreciation to main supervisor Professor Hirotaka Saito, who accepted me as a PhD student. Under his supervision I learned many new things, such as HYDRUS software package and soil science. When I first started working with him, I knew nothing about it. He offered me so much advice, patiently supervising, constructive criticism and generous assistance at every stage of research work. I believed I would have never been able to finish my dissertation successfully without his valuable counsel and help. His keen observation in detecting errors and correcting the manuscript, which consuming his valuable time and beyond this his constant help has been overwhelming. I am very grateful when he gave me a chance to visit University of California Riverside (UCR) and introduced me to Professor Jirka Simunek, who developed HYDRUS. I learned HYDRUS lots during staying in UCR under guidance of Professor Jirka Simunek. I take this opportunity to express my sincere gratitude to Professor Jirka Simunek for his guidance and critical comments in order to improve our manuscript, which is enabled to publish in a strong scientific journal in this field.

I am deeply appreciating to co-chairs, and committee members, Professor Tasuku Kato, Professor Hisao Kuroda, Professor Yuji Kohgo and Professor Hiroyuki Matsui for their constructive reviews of this dissertation and make necessary improvements according to their valuable comments.

I am very thankful to the Japanese government (MEXT) scholarship for the financial support during my research. Without its support and financial help, it would not have been possible for me to complete my study and enjoy juicy life in Japan.

I would like to acknowledge my colleagues for helping me during conducting my experiments and daily campus life. I want to convey my heartfelt thanks to Soil lab members, Moeko Sasakura, Hiratsuka Masato, Iwazaki, Miyake, Rando Sekiguchi, Yamada, Kubota, Shimada, Sokhline, May, Sato, Tun-Tun, Eguchi, Kinuko Hibi, Anusron and Aline for their friendly help and kind support. Without their friendship and support it would be hard to stay in a foreign environment for long-time.

I would like as well to express my deep love and gratefulness to my dear friends, Susan Mambu, Atiqotun Fitriyah, Safirah Tasa, Aminah Balfas, Maya Agustina, Arnia Sari, Lela

Susilawati, Nurbiya, Hebatallah, Naim Mulana, Yusran, Zulham Mahasin, Nugrahaning S.Dewi, Fariha Wilis, Akmaliza Rais, Budiastuti and Sri Wahyuni, who were always by my side in hard and the dark time. Their kind support and encourage words were greatly acknowledged.

Last but not least, I am greatly indebted to my mother and father for their warm love and motivation. They trusted and encouraged me presenting their entire support while I was abroad and far away from home. Their love and confidence without any complaint or regret have enabled me to go forward on my way and complete my PhD course. I could not have come to this far by myself and would like to praise to Allah SWT. for His great loving kindness and encouragements by sending great people around me who helped me.

Contents

List of figures

List of tables

Chapter 1. Introduction

1.1. Overview

The rapid increase of the world population causes an increase in parallel with the world's food and water demand. FAO projected that the world would need to produce 60 % more food to ensure global food security in 2050 (FAO, 2015). The development of the agricultural sector has contributed to the improvement of the food security. The projected increase in the food demand will reflect a significant rise of water utilization particularly in the irrigation. Globally, the volume of fresh water withdrawn for irrigation will increase from 2.6 thousand km^3 in 2005-2007 to an estimated 2.9 thousand km^3 in 2050, especially occurring in lower income countries (FAO, 2011b).

Water is a major input in the provision of food and agricultural production. The problems of the water resources are getting more severe due to climate change, poor management and pollution. The shortages of water will result in increasing competition in many sectors, which will constrain agricultural production and will affect the income and livelihood opportunities for farmers especially in rural areas of the lower income countries. In many water-scarce regions, farmers will need to adapt in using less water for irrigation, while facing increasing demands of their products. Innovative technologies and management are required to achieve more productive use of irrigation water in agriculture.

Agriculture will continue to be the largest user of water resources in most countries, often accounting for 70 % or more of water withdrawals from rivers, lakes and aquifers. Presently, about 82 %, or about 93 km^3 of the freshwater resources in Indonesia are being used for the agricultural production while the rest is for drinking, municipal, industrial and other uses (AQUASTAT, 2011). Supply water for agriculture demand can be increased either by reducing water losses from farming practices or losses from distribution of water in irrigation network and canals. On farm practices, water losses can be further reduced by introducing more efficient irrigation systems. Micro irrigation has been developed rapidly in recent years and adopted for cultivating various high-value crops in water-scarce regions as a way to increase water use efficiency and water productivity.

Micro-irrigation is an irrigation method that applies water slowly to the roots of plants, by depositing water either on the soil surface or directly to the root zone, through a network of valves, pipes, tubing, and emitters. Micro irrigation techniques including surface and subsurface drip irrigation (trickle irrigation), pitcher irrigation, and subsurface irrigation using a clay pipe can be

used to improve irrigation efficiency on vegetable crops by reducing soil evaporation and drainage losses (Batchelor et al, 1996). Due to its ability to localize water application, a drip irrigation system can achieve higher irrigation efficiency (70 – 90%) than surface irrigation or flooding irrigation (40 – 50%) even when designed well and operated correctly (Postel, 2000).

In subsurface drip irrigation (SDI) technique, water or a mixture of water and nutrient referred to fertigation can be applied slowly to the root zone through buried plastic tubes containing embedded emitters, while maintaining a dry soil surface (Ben-Gal et al., 2004). Compared with other irrigation techniques, the subsurface irrigation has higher water saving efficiency because of its ability to decrease water loss introduced by leakage during water transport, surface evaporation and deep percolation. Another motivation of using subsurface irrigation is to reduce the extensive labor involved with seasonal installation and collection of surface drip system laterals and components (Lazarovitch et al., 2006). Many investigators advocated the use of subsurface drip irrigation to attain more crop yields and increase water irrigation efficiency. Miguel and Fransisco (2007) compared the yield and fruit quality of tomatoes in surface and subsurface drip irrigation. They found that tomatoes yield increased by 66.5% when using subsurface irrigation compared with the surface drip treatment.

Although micro irrigation methods have been conventionally used over many decades for field crops and horticultural crops, their expansion is quite limited despite of its high water use efficiency and numerous advantages. This is mainly due to the fact that the conventional "state-of-the-art" micro irrigation system is viewed as the technology for large commercial farms engaged in high value agriculture and is not appropriate nor affordable for small and marginal farmers in many developing countries (Keller et al., 2002). Furthermore, some of the modern irrigation technologies designed for large-scale farming with complex and expensive devices tend to fail when introduced in rural areas of developing countries where farming is generally practiced on a much smaller scale. In these areas, maintaining the complex irrigation systems becomes a roadblock to promoting modern technologies because there are not enough well-trained engineers and it may be difficult to find parts to repair these systems. Therefore, the use of indigenous skills and materials is crucial to spread such irrigation technologies in such areas.

The prospectus for the expansion of this technology has brightened with the development of a range of low cost/affordable micro irrigation systems, fitting to a different income level of farmers and farm sizes (Keller and Andrew, 2002; Kulkarni, 2005). Low cost and simple pressurized irrigation systems are becoming popular among the small-scale farmers in developing countries.

These systems not only help improve crop productivity, but also provide other secondary benefits such as increase employment opportunities, and food security to a large number of small holder farmers. Lowder et al (2014) reported that farm size of Indonesia is relatively small where around 78 % farm-holders have land less than 1 ha.

Subsurface irrigation with ring-shaped emitter (Saefuddin *et al*., 2014) is one of low cost-affordable irrigation techniques, which has been developed and introduced in some arid regions of Indonesia. The emitter made from a rubber hose is economically affordable, especially for small-scale farmers. After a rubber hose is bent into a ring shape with a diameter of about 20 cm, five 5-mm holes are drilled at even intervals. The entire ring-shaped hose is then covered with a permeable textile so that irrigated water can be distributed through the permeable textile in all directions around the emitter. Water is supplied through a supply tube connecting a water tank and the ring-shaped emitter. The emitter can be installed directly in the root zone at a given depth.

Although the ring-shaped emitter for subsurface irrigation has been successfully practiced for cultivating annual and perennial crops in an island of Indonesia (Saefuddin *et al*., 2014; Sumarsono *et al*., 2018), where precipitation is limited, its current design and operation are purely empirical. Understanding soil water movement and the spatial extent of the wet volume around the emitter is crucial to achieve optimum operation of subsurface irrigation with the ring-shaped emitter and to modify its design to improve usability and water use efficiency. In addition, the current design of the ring-shaped emitter does not allow one to easily detect malfunction because the emitter is fully covered with the permeable textile. As a result, it is not easy to repair it quickly. For faster promotion of the technology, it is important to have a design that is easy to maintain.

The HYDRUS (2D/3D) model (Šimůnek *et al*, 2016) solves the Richards equation numerically in 2D or 3D spatial domains based on the finite element method to simulate water flow in variably-saturated porous media. In HYDRUS, root water uptake, solute transport, and root nutrient uptake can be included in the simulations (Šimůnek *et al*., 2016). HYDRUS enables the implementation of a wide range of boundary conditions, irregular boundaries, and soil heterogeneities. It has been used to assess many subsurface irrigation applications. For example, Skaggs *et al*. (2004) compared HYDRUS-2D simulated water contents under subsurface line-source drip irrigation with observed field data in three different emitter discharge rates applied. Kandeleous and Šimůnek (2010b) used HYDRUS-2D to compare laboratory and field data of water movement in clay loam from a buried point water source at different depths and discharge rates. Kandelous *et al*. (2011) validated HYDRUS to simulate water movement from a subsurface drip irrigation system

by comparing the simulated results with the measured soil water contents from several field experiments. Hanson et al. (2008) used HYDRUS-2D to study salt leaching with subsurface drip irrigation using saline irrigation water under shallow saline ground water conditions in loamy soil. Wang et al. (2013) calibrated HYDRUS for long-term simulations with field experimental data in order to evaluate sustainable irrigation regimes of mulched drip irrigation with saline water for cotton in arid Northwest China. Overall, they concluded that HYDRUS is an effective tool for investigating and designing subsurface irrigation management practices. Moreover, HYDRUS can be used to accurately simulate short and long-term soil water dynamics and solute transport in various subsurface conditions.

1.2. Objectives of Study

In order to provide and promote sustainable subsurface irrigation with the ring-shaped emitter for cultivating the crop in arid regions, the assessment of optimal design and operation under such irrigation practice is crucial. Therefore, laboratory and cultivation experiments were conducted, while HYDRUS numerical model was used to simulate soil water dynamics and calibrate soil hydraulic parameters in various soil types and environmental conditions. The specific objectives of the research were;

1. To investigate and characterize the spatial soil water movement around the buried ring-shaped emitter for different soil types and to validate the capacity of HYDRUS to simulate such water movement.
2. To numerically evaluate the effect of modifying the ring-shaped emitter designs on soil water dynamics.
3. To investigate experimentally and numerically water dynamic distribution around the buried ring-shaped emitter during bell pepper cultivation.
4. To evaluate the performance of the ring-shaped emitter in terms of water productivity and irrigation water productivity during the cultivation of bell pepper.
5. To investigate and evaluate the long-term effect of using subsurface irrigation with the ring-shaped emitter on water movement and solute transport and its effect on the subsurface environment.

1.3. Structure of Dissertation

The main body of this dissertation is divided into four chapters (Chapter 4 to Chapter 7), addressing all specific objectives of the study. The description of each chapter is as follows:

Chapter 2 reviews the general concept of micro irrigation, including subsurface irrigation, and application of micro irrigation in Indonesia.

Chapter 3 reviews the numerical model, HYDRUS that can be used to evaluate the performance of various irrigation designs and management.

Chapter 4 describes the experimental and numerical analysis of soil water distribution around the buried ring-shaped emitter. Laboratory experiments were first carried out to monitor the changes in soil water contents during subsurface water application through the original ring-shaped emitter design buried at a given depth. The effect of soil properties and applied water pressure at the emitter inlet on soil wetting patterns was analyzed using HYDRUS.

Chapter 5 illustrates the effect of alternative ring-shaped emitter designs on soil water dynamics around the buried emitter. In this study, alternative designs of ring-shaped were proposed by reducing the number of holes in the emitter and by changing the covering method into partially covered only around the holes to increase water use efficiency and to simplify the maintenance of the ring-shaped emitters. The spatial extent of the wet volume around the buried ring-shaped emitter in different designs was numerically simulated. The numerical simulations were carried out in a full three-dimensional domain so that the asymmetry in the hole configurations could be modeled without any simplification. The results of Chapter 4 and 5 have been published in *Agricultural Water Management Journal* (Vol.211, p111-122, Saefuddin et al., 2018)

In **Chapter 6**, bell pepper cultivation experiments were carried out in glass-house during summer season of 2017 to address the third and fourth specific objectives. In this experiment, two different designs of the ring-shaped emitter, original and alternative designs were used in the cultivation experiment. The changes in the soil water content at given positions and meteorological data were monitored during the growing season as input parameters to assess the effects of the ring–shaped emitter designs on soil water distribution and plant root water uptake. HYDRUS was used to analyze soil water dynamics. The performance of the ring-shaped emitter in different designs in terms of water productivity and irrigation water productivity was then evaluated. The paper summarizing the experimental results of this chapter has been accepted for publication in *Paddy and Water Environment Journal.*

Chapter 7 describes the numerical evaluation of long-term effect of using the ring-shaped emitter for subsurface irrigation on water movement and solute distribution. HYDRUS was used to characterize the interactions between water and fertilizer application on subsurface environment and their effects on the plant root water uptake. The simulations were carried out for 10 years. In addition, two ring-shaped emitter designs were compared during fertigation applications.

Chapter 8 summarizes the conclusions of the works and the recommendations for future work.

Chapter 2. Literature Review

2.1. Management of Micro Irrigation in Arid and Semiarid Region

Meanwhile, judicious water use, long-term sustainability and increasing efficiency, as well as improving the yield to water consumption ratio become major priorities to overcome the limited availability of irrigation water in arid and semiarid regions of the world. Micro irrigation technology is considered as a higher water saving option that can be applied in these regions with alternative cropping options.

Micro irrigation is the slow application of water on, above or below the soil surface by surface drip, subsurface drip, bubbler and micro sprinkler system (Lamm et al, 2007). Water is applied as discrete or continuous drips (also called trickle), tiny stream, or miniature spray trough emitters or applicators placed along a water delivery line adjacent to the plant row (ASAE, 2011). In some parts of the world, micro irrigation is called localized irrigation to emphasize that only part of the soil volume is wetted. Micro Irrigation is usually characterized by the following features: (1) water is applied at low rates; (2) water is applied over long periods; (3) water is applied at frequent intervals; (4) water is applied near or into the root zone; (5) water is applied by a low-pressure delivery system; and (6) water is routinely used to transport fertilizers and other agricultural chemicals (Lamm et al., 2007).

Several benefits of micro irrigation are reported by many investigators such as; (1) increased water use efficiency; (2) improved crop yields and quality; (3) reduced non beneficial use by decreasing surface evaporation and elimination of irrigation run off from sloping fields or hillsides; (4) reduced deep percolation; (5) improved fertilizer and other chemical applications with minimized leaching and run off of the chemicals. Despite observed successes and possible advantages, several shortcomings have been encountered with the economics and mechanics of applying water with micro irrigation systems for some soils, water qualities and environmental conditions. The disadvantages include; (1) expensive initial and maintenance costs; (2) require expert and advanced skill to install the irrigation network, (3) potential emitter clogging due to root and solid particles intrusions; (4) salt accumulation near plants when high salinity water is used in arid regions (Lamm et al., 2007).

The continuous use of micro irrigation in arid and semi-arid environments inevitably leads to water table variations, and often to problems of water logging and salinization. Nitrate resulting

from nitrogen fertilizers used in agriculture is a widespread contaminant of groundwater and causes adverse effects on the health of humans, animals, and the ecosystem. Nitrates are not the only pollutants attributable to irrigation, so are plant nutrients in general, pesticides, and heavy metals. Pharmaceutical compounds emerge as pollutants when wastewater is used for irrigation without any previous treatment (Siemens et al., 2008).

Applying saline water continuously for irrigation through surface drip irrigation (DI) systems might result in salt accumulation close to the soil surface (DeMalach and Pasternak, 1993; Oron et al., 1995). Under conventional on-surface DI, during irrigation or precipitation, the salts that are accumulated close to the soil surface can migrate downwards and reach the main root zone. This process may inhibit water and nutrient uptake, consequently affecting the crop growth and yield (Hanson, 1995). In order to offset the osmotic shock imposed on the crop by the leached salts, a practical solution was proposed. It was suggested to further leach the accumulated salts in the main root zone to deeper layers by continuing to drip irrigate simultaneously with the periods of precipitation.

Alternatively, Oron et al. (1990) and Phene et al. (1990) have proposed that this problem can be overcome by applying saline water through a subsurface drip-irrigation (SDI) system. It is anticipated that under SDI, the salt front is partially driven down into the deeper soil bulk media and to the periphery of the root zone, thus minimizing the risk of damaging the main roots of the plants. Moreover, the improved moisture conditions in the vicinity of the emitter offsets and the inhibiting effects of the presence of the salts in the saline water (Michelakis et al., 1993). Additionally, Phene et al. (1987) reported that since the SDI is installed below the soil surface, a properly managed system can increase the advantages of conventional DI systems, especially in the areas of efficient water and nutrient utilization, salinity management and deep percolation.

2.2. Subsurface Irrigation Method

Subsurface Irrigation is one of micro irrigation methods in which water is applied below the soil surface through buried emitter including drip tapes, perforated pipe, clay pipe and tube. This method can ensure timely allocation of a suitable amount of water and nutrients to the root zone and crop water requirement, which may improve crop quality and productivity (Sun et al, 2016). The relatively dry soil on the surface during subsurface application can also prevent the growth of weeds (Sagi, 2006; Kreij et al., 2003). Other advantages of Subsurface irrigation include the increase in the working life of the system as vandalism, and solar radiation degradation are avoided; ploughing

and other cropping practices are facilitated, and the development of fungal disease are diminished (Martines and Reca, 2014). In addition, subsurface irrigation ahs a special advantage of securing system safety against pilferage and damage by animals and during intercultural operations. The value of subsurface irrigation promoted during the initial period of 1980s, rapidly promoted during the second half of 1980s and continuing its development at present mostly in areas having insufficient water and environmental problems linked to irrigation and where the wastewater is used for irrigation.

At nowadays, the most common subsurface irrigation has been used widely is subsurface drip irrigation (SDI). Camp (1998) reviewed the results of some previous works that compared the crop yield both in subsurface and other different methods of irrigation. He concluded that crop yields for subsurface drip systems were equal or better than the other systems in all cases, including different crops, soils, and cultivation condition. A few comparative studies (Fandino et al., 2012; Cancela et al., 2015) showed slightly higher grapevine water uptake and coefficient under subsurface drip irrigation than under surface drip. While Miguel and Fransisco (2007) found that tomato yields increased by 66.5 % when using subsurface drip irrigation compared with the surface drip irrigation. Despite of its numerous advantages of subsurface drip irrigation, the SDI also has a lot of issues to be solved as the associated equipment development and technical research is not mature. Many studies have regarded the hydraulic characteristics of embedded emitters and factors affecting the flow rate of embedded emitters. For example, Xu et al. (2003; 2004) explored the effects of emitter type, operating pressure on the flow rate using the orthogonal experimental design.

Lazarovicth et al (2006) stated that in contrast to surface drip irrigation, soil hydraulic properties may affect SDI dripper discharge rates. During irrigation, positive water pressure backpressure may develop in the soil near a subsurface dripper following the principles of flow from a point source (Philip 1992). The magnitude of pressure developed depends on soil texture, dripper discharge, potential cavity development near the dripper, and drip system hydraulic properties (Shani et al. 1996). Develop positive soil water pressures, resulting in a decreased discharge from subsurface drippers; this effect is most pronounced with non-pressure-compensated drippers operating at low pressures (Shani et al. 1996). In addition, variations in soil hydraulic properties within a field, and different cavity formation during installation, cause a discrepancy in pressure buildup adjacent to individual drippers—and subsequent non-uniform discharge and water

application (Warrick and Shani 1996; Ben Gal et al. 2004). Therefore, selected drippers discharge should be sufficiently low to closely match with root uptake rate of water (Lazarovitch, 2006).

Most SDI systems are designed to operate at pressure heads greater than 7 m. In general, pumps are needed to develop such pressures. There is increasing interest in SDI systems designed to operate at much lower pressures, e.g., 1.5–2.0 m e.g., (Su et al. 2000). Such systems may eliminate the need for pumps, allow an increase in an irrigated area without increasing pump capacity, or reduce the discharge rate without a decrease in orifice size. Low pressure systems generally cost less than systems designed to operate at high pressure, which may encourage their adoption. Such SDI systems are also a possible solution toward low discharge continuous irrigation, which would maintain a high root zone, soil water content and hydraulic conductivity, thus maintaining high water availability to plants (Rawlins and Raats 1975; Radin et al. 1989). Low-pressure SDI systems may be especially advantageous in developing countries, where access to electricity can be problematic. However, systems designed to operate at low pressures are particularly prone to the soil-induced changes in dripper discharge.

The performance of subsurface irrigation should be quantified for its proper design, management, operation, and provide irrigation water use efficiently. Quantification allows the users to determine and control the drippers or emitter discharge and operating pressure of system, backpressure effect on dripper discharge, formation of cavity and application of irrigation water to meet the crop water requirements. Determining the appropriate depth placement of the emitter requires consideration of soil properties and the root distribution of crop (Patel and Rajput, 2008).

Information on root distribution is useful to understand crop responses to irrigation and fertigation, especially with the limited wetted soil volume that develops under subsurface drip (Phene et al., 1991). Phene et al. (1990) showed that root length and rooted soil volume of sweet corn could be improved by frequent irrigation with shallow subsurface drip irrigation. They revealed that frequent irrigation maintained a portion of the root zone within the optimal matric potential range. In high frequent irrigated corn, root length density and water uptake patterns are determined primarily by the soil water distribution under drippers, whether the drippers are placed on, or beneath the crop row (Coelho and Or, 1999).

Most of the root system is concentrated in the top 40 cm of the soil profile in drip irrigated processing tomatoes (Machado and Oliviera, 2003). Supply of aerated water with subsurface drip irrigation can maintain aeration of the root zone in heavy clay soils significantly increase yield of vegetables soya bean and zucchini (Bhattarai et al., 2004).

In Subsurface drip irrigation, the choice of drip tape depth is influenced by crop, soil, climate characteristics and anticipated cultural practices, but generally ranges from 0.02 to 0.7 m (Camp, 1998). It is often in the range of 0.05 to 0.2 m for shallow rooted horticulture crops. From the literature, a depth of 0.15 m for lettuce would be appropriate on sandy soil. Although installation depth is generally decided for horticulture reasons, another consideration for determining depth is that deeper placement of 0.45 m may be required if the primary aim is to reduce soil evaporation and capture the potential benefit of improving water use efficiency (both in yield and quality) (Bryla et al., 2003). Camp et al., (2000) studied on SDI under different system design, installation, application and operation. They suggested that lateral SDI should be installed at a shallower depth on coarse-textured soil and slightly deeper for finer-textured soil for multi years or long-term use of SDI system.

Irrigation scheduling is one of the important components to achieve higher irrigation efficiency under any subsurface irrigation system. Irrigation scheduling is influenced by many factors such as soil, crop, climate, water supply and cultivation practices. Thus, it is essential to develop an efficient irrigation scheduling under prevailing local conditions. Various methods based on the estimated crop evapotranspiration rate, ratio of irrigation water to cumulative pan evaporation (Batra et al., 2000) and soil water depletion are widely used for scheduling irrigation in many cultivation crop practices. Irrigation application with 100% of crop evapotranspiration provided the highest yield in subsurface drip system when the drip tape was placed at a depth of 10 cm (Patel and Rajput, 2008).

2.3. Application of Micro Irrigation in Indonesia

Indonesia consists of more than 17,000 islands with over 1.9 million square miles of land, which make it the 15th largest country. Indonesia has a population estimated at 271 million in 2020, up from the 2015 estimate of 256 million (BPS, 2018). Indonesia is considered as an agricultural country where agriculture has long been serving as the contribution to the country's GDP. The predominant characteristics of Indonesian farming systems are family based, small-farm holdings, subsistence crops and traditional (non-mechanized) management. Lowder et al (2014) reported that farm size of Indonesia is relatively small where around 78 % farm-holders have land less than 1 ha.

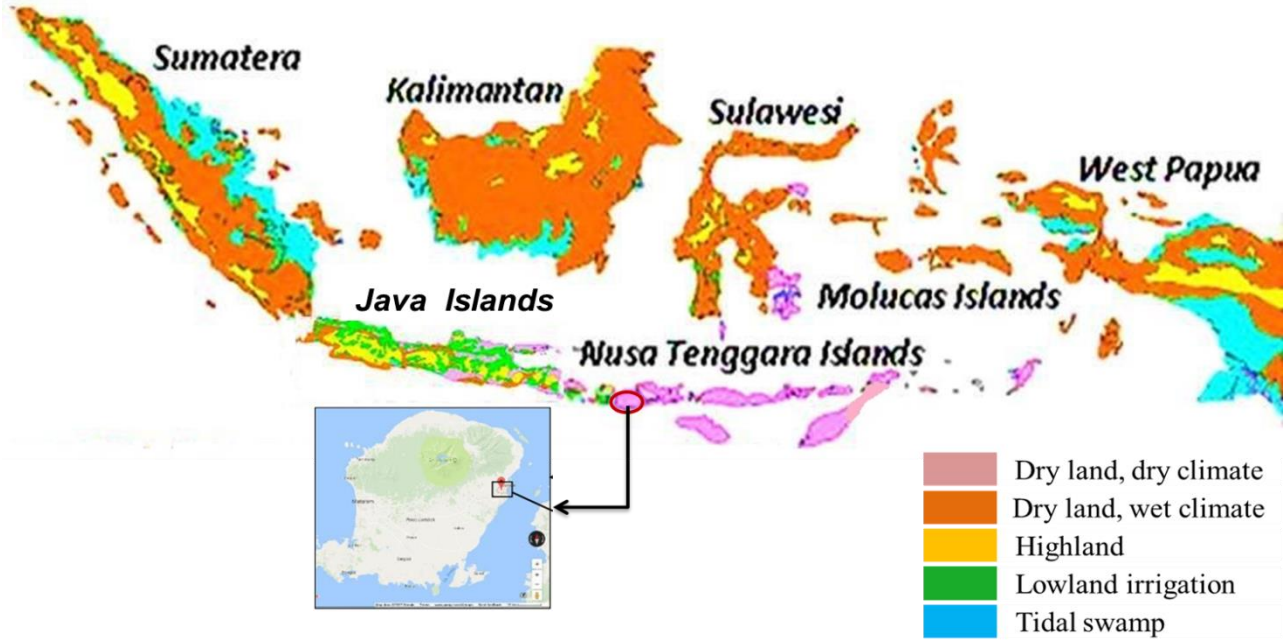

Figure 2.1 Agro-ecological zones of Indonesia (adapted from Central Agency of Soil and Agro-climate) (Syuaib, 2016). The red circle shows the region where subsurface irrigation with ring-shaped emitter was applied.

Indonesia has tropical monsoon-type climate which was characterized by slight changes of seasons and temperatures, high degree of humidity and periodically heavy rainfall. Indonesia is located in a wet tropical region with an annual average of about 2400 mm, varying from 1000 mm in East Nusa Tenggara to 4500 mm in parts of Papua (Syuaib, 2016). Generally, there are two seasons; the dry and wet. Temperatures range from 21^{o}C to 33^{o}C, but at higher altitudes the climate is cooler. The humidity is between 60 and 80% (AQUASTAT, 2011). Based on soil types, rainfall and length of growing period, five pragmatic agro-ecological zones might be recognized in the country; (1) dry land with dry climate, (2) dry land with wet climate, (3) highland, (4) lowland irrigation and (5) tidal swamp, as it is illustrated in Fig 2.1 (Syuaib, 2016). From the total of 189.2 million ha Indonesian lands, about 108.8 million ha is classified as acid upland, distributed mainly in Sumatra, Kalimantan and Papua. Semiarid uplands of 13.3 million ha are distributed in East Kalimantan, East Java, Bali, West Nusa Tenggara and East Nusa Tenggara (Mulyani and Sarwani, 2013).

In Indonesia, the expansion of micro irrigation has been accompanied by the accumulation of pilot project research which is supported by governments and NGOs. Over the past two decades drip irrigation has spread considerably in Indonesia only 9.1 million ha from the total of arid land in

Indonesia of 143 million ha (PU, 2016). The application of micro irrigation in general drip and sprinkler irrigation has been focused primarily on horticulture production and plantation (PSDA, 2008). Under micro irrigation, the agriculture water consumption in Indonesia can be reduced to 63.8% as the water use efficiency increases up to 90% on various horticulture crops (Imanudin and Prayitno, 2015).

Low-pressure micro irrigation such as drip irrigation and micro-spray irrigation has been introduced to small–scale farmers in Indonesia for almost two decades, but the adoption and application of this technology has been limited. The slow spread of micro irrigation technology due to socioeconomic characteristic of the farmers (i.e., landholding size and education) and high-cost investment (Purwartini and Suhaeti, 2017). Moreover, Palada et al. (2011) stated that the adoption and impact of affordable drip irrigation technology in Asia and Pacific countries, including Indonesia are mainly determined by climate, particularly the rainfall pattern and growing season in addition to other related technical and socioeconomic factors.

2.4. Irrigation Water Productivity and Water Use Efficiency

On-farm strategies, water productivity can be used as indicator to evaluate the performance of irrigation system. There are several definitions exist for the term of water productivity. It may convey as the physical ratio between yields and (productive or unproductive) water use (Zwart and Bastiaanssen, 2004) or between the value of the product and water use (Vasifendousta et al., 2008). Siedel et al (2015) defined five definitions of water productivity (WP) as follows;

$$WP_{I+P} = \frac{Y}{I+P} \tag{2.1}$$

$$WP_{SW} = \frac{Yield}{I+P+SW+CR} \tag{2.2}$$

$$WP_{I} = \frac{Y}{I} \tag{2.3}$$

$$WP_{RF} = \frac{Y-YRF}{I+P} \tag{2.4}$$

$$WP_{ETc} = \frac{Y}{ET_c} \tag{2.5}$$

where Y is the actual yield and YRF is the actual yield of a non-irrigated (rainfed) treatment with similar plant density and row spacing (both in Kg ha^{-1}). I is irrigation water applied, P is precipitation, SW is soil water depletion (different in soil water content between planting and

harvesting), *CR* is capillary rise and ET_c is the actual crop evapotranspiration, all during growing period (all in m^3 ha^{-1}).

According to Vazifedousta et al. (2008), WP_{I+P} is defined as the actual yield divided by the sum of irrigation water applied and precipitation. Rodrigues and Pereira (2009) determined water productivity similar to WP_{SW} as the ratio between actual yield and total water use, which is the sum of season precipitation and irrigation, capillary rise and soil depletion. While WP_I does not consider rainfall or assuming that rainfall is very low. WP can also be defined as the yield divided by actual transpiration or evapotranspiration (Perry, 2011).

Water use efficiency is defined as the ratio of the total dry matter of harvested (economic) portions of the crop produced per unit water consumed. Significant improvements in yield have been documented with micro irrigation without significant increases in the consumed water leading to improved water use efficiency (Phene et al., 1993). Intercropping or even multiple cropping of vegetables and melon crops with subsurface micro irrigation increased yields, improved water use efficiency, and reduced water applications between cropping seasons (Bucks et al., 1981). Continuous cropping is a practical way to increase water use efficiency where water prices are increasing and urbanization occurred (Lamm et al., 2007).

The irrigation water use efficiency can be defined as the yield of plant product per unit of irrigation water used during cultivation and it is a measure of the productivity of the irrigation water (Martinez and Reca, 2014). The efficiency of drip irrigation water is highly dependent on evaporation losses occurring from the constantly saturated soil beneath emitters. The Advent of subsurface drip irrigation is in part an approach to curb this inefficiency. Various methods of evaporation reduction, such as mulching that have been employed in irrigation.

Chapter 3. HYDRUS

3.1. Numerical Model of Water Flow

Irrigation design and management require some form of predictive capabilities regarding the relationships between the water application rate, soil properties and plant root water uptake pattern, and their combined effect on the resulting soil water dynamics and distribution. These relationships are formulated in models that take many forms and include those that are physically-based, analog and mathematical. The widespread availability of computer makes it possible to implement mathematical models to solve the Richards equation depicting variably saturated water flow. The most common models are numerical, analytical and empirical model (Subbaiah, 2013). For most general conditions, the Richards equation can be solved only by numerical techniques with finite differences and finite elements approach (Lamm et al., 2007).

Subbaiah (2013) stated that the highly nonlinear nature of the Richards equation due to the dependence of the hydraulic conductivity and diffusivity on the moisture content, in combination with the non-trivial forcing conditions, makes the Richards equation practically impossible to solve using analytical approaches except for a few special cases (Ju and Kung 1997; Arampatzis et al. 2001; Kavetski et al. 2002). The analytical solutions for the Richards equation exclusively dealt the absorption (moisture movement without gravity) and infiltration problems. Little attention has been paid to the redistribution and drainage problems. Philip (1991b) concluded the analyses of redistribution and drainage processes using the Richards model have almost totally relied upon numerical techniques.

The development of knowledge over time on the conceptual understanding and mathematical description of water flow, solute/nutrient transport, and root water uptake in trickle systems had been integrated in various software packages. Šimůnek (2005) presented some of the software developed for variably saturated flow. Šimůnek et al. (1999) developed a general-purpose and user-friendly two-dimensional numerical model, known as SWMS 2D (simulating the water movement and solute transport in two dimensions), or more recently as HYDRUS-1D and 2D/3D (Šimůnek et al., 2012; 2016).

HYDRUS is well known Windows-based computer software, uses the Galerkin finite element method based on the mass conservative iterative scheme proposed by Celia et al (1990).

The software enables the implementation of one, two or three-dimensional, axially symmetric water flow, solute transport, and root water and nutrient uptake based on finite element numerical solutions of flow equations. The HYDDRUS computer code uses the Richard equation for variably saturated flow and Fickian based advection-dispersion equations for both heat and solute transport. The flow equation considers water uptake by plant roots, as well as hysteresis of the unsaturated soil hydraulic properties. The software packages come with Levenberg–Marquardt type non-linear parameter optimization modules to allow estimation of a variety of soil hydraulic and solute transport parameters from experimental data. Unknown hydraulic parameters can be estimated from measured soil water contents, pressure heads, and/or boundary fluxes during transient flow by numerical inversion of the Richards' equation. Additional retention or hydraulic conductivity data, as well as a penalty function for constraining the optimized parameters to remain in some feasible regions (Bayesian estimation), can be optionally considered. The procedure similarly permits nutrient transport and/or reaction parameters to be estimated from measured concentrations and related data.

In HYDRUS, the governing equation for saturated–unsaturated flow, written as a multidimensional form of the Richards equation shown below, is solved numerically using the finite element method to simulate subsurface soil water movement.

$$\frac{\partial \theta}{\partial t} = \frac{\partial}{\partial x_i}\left[K\left(K_{ij}^{A}\frac{\partial h}{\partial x_j} + K_{iz}^{A}\right)\right] - S \qquad (3.1)$$

where θ is the soil moisture content [L^3L^{-3}], h is the pressure head [L], K is the unsaturated hydraulic conductivity [LT^{-1}], K_{ij}^{A} is the component of a dimensionless anisotropy tensor, S is the source/sink term accounting for root water uptake [T^{-1}], and x_i is the spatial coordinate [L]. For an isotropic medium, the diagonal components of K_{ij}^{A} are unity, while the off-diagonal components are all zeros. The unsaturated hydraulic conductivity function is given by

$$K(h,x,y,z) = K_s K_r(h,x,y,z) \qquad (3.2)$$

where K_r is the relative hydraulic conductivity [-] and K_s is the saturated hydraulic conductivity [LT^{-1}].

In HYDRUS numerical model, the soil hydraulic parameters can be modeled using the water retention and hydraulic conductivity function of van Genuchten-Mualem constitutive relationships (Mualem 1976; van Genuchten, 1980) as follows;

$$\theta(h) = \begin{cases} \theta_r + \dfrac{\theta_s - \theta_r}{\left(1 + |\alpha h|^n\right)^m}, & h < 0 \\ \theta_s, & h \geq 0 \end{cases} \tag{3.3}$$

$$K(h) = K_s S_e^{\,i}\left[1 - \left(1 - S_e^{\,1/m}\right)^m\right]^2 \tag{3.4}$$

$$S_e = \frac{\theta - \theta_r}{\theta_s - \theta_r}, \quad m = 1 - \frac{1}{n} \tag{3.5}$$

where θ_s is saturated water content [L^3L^{-3}]; θ_r is residual water content [L^3L^{-3}]; K_s is saturated hydraulic conductivity [LT^{-1}]; m, n and α are empirical parameters; l is shaping factor and S_e is the relative saturation (dimensionless).

3.2. The Sink Term Root Water Uptake Model

Root water and nutrient uptakes are one of the most important processes considered in numerical models simulating water content and fluxes in the subsurface, thus controlling water flow (recharge) and nutrient transport (leaching) to the groundwater (Šimůnek and Hopmans, 2009). Root water uptake is defined by the water potential gradient and hydraulic resistances in the soil-plant system (Steudle and Peterson, 1998). There are two major approaches generally used to simulate root water uptake in vadose zone hydrological models at the plot or field scale; a microscopic and macroscopic approach (Hopmans and Bristow, 2002). In the first approach, water is extracted by plant roots based on a microscopic or mesoscopic (Feddes and Raats, 2004). This approach considered a single root to be an infinitely long cylinder of uniform radius and water-absorbing properties. In the macroscopic approach, root water uptake intervenes as a sink term. The water extraction of the entire root system is included to describe the transient multidimensional water flow of the Richards equation (Clausnitzer and Hopmans, 1994), according to

$$\frac{\partial \theta}{\partial t} = \nabla \bullet \left[K \nabla (h - z)\right] - S(x, y, z, t) \tag{3.6}$$

where θ is the volumetric water content [L^3L^{-3}], K is the unsaturated hydraulic conductivity tensor [LT^{-1}], h is the soil water matric head [L], z is the depth which is included for vertical flow [L], and S in the volumetric sink term [$L^3L^{-3}T^{-1}$], representing root water uptake as a function of both time and space. This macroscopic approach allows direct integration of root water uptake with the transient soil water flow and provides natural interaction between transpiration and root water extraction. The macroscopic approach has been utilized in many vadose zone models, in which the

potential transpiration is distributed over the root zone proportionally to root density, and is locally reduced depending on soil saturation and salinity status (Feddes et al, 1978; Maas, 1990).

The distribution of root water uptake (RWU) depends, besides the root distribution, also on the water availability in the root zone. When the soil dries out and the soil water potential decreases to the wilting point, the difference in water potential between the soil and the plant causes reducing in root water uptake. The relation between RWU, soil water potential, and transpiration demand is described by a so-called stress function (Feddes et al., 1978).

Hillel (1980) stated that the rate of water uptake from a given volume of soil depends on rooting density (the effective length of roots per unit volume of soil), soil conductivity, and the difference between average soil-water suction and root suction. If the initial soil-water suction is uniform throughout all depths of the root zone, and the active roots are not uniformly distributed. The rate of water uptake will be highest where the density of roots is greatest. Therefore, more rapid uptake will result in more rapid depletion of soil water content.

The numerical model HYDRUS software package (Šimůnek et al., 2006; 2008; 2016) is capable of incorporating plant root water uptake using the macroscopic approach introduced by Feddes et al. (1978). In HYDRUS, root water uptake is modeled as a sink/source term, representing the volume of water removed per unit time from a unit volume of soil due to plant water uptake. Root water extraction, $S(h)$, from the soil can be computed either as compensated or uncompensated root water uptake.

3.2.1. Root Water Uptake without Compensation

The sink term, $S(h)$ in eq. (3.1) represents the volume of water removed per unit time from a unit volume of soil due to plant water uptake. The water stress is accounted for using the model suggested by Feddes et al. (1978), which is implemented in HYDRUS;

$$S(h) = \alpha(h)Sp \tag{3.7}$$

where S_p (LT^{-1}) is the potential water uptake and $\alpha(h)$ is a dimensionless water response function for water uptake. Feddes et al. (1978) proposed a linear model for the water stress response function $\alpha(h)$ which involves five threshold variables: P_0, the pressure head [L] below which roots start to extract water from the soil; P_{Opt}, the pressure head [L] below which roots extract water at the maximum possible rate; P_2H, the limiting pressure head [L] below which roots cannot longer extract water at the maximum rate (assuming a potential transpiration rate of r_2H); P_2L, the limiting pressure head [L] below which roots cannot longer extract water at the maximum rate (assuming a

potential rate of r_2L); P_3, the pressure head [L] below which root water uptake ceases (the wilting point); and r_2H and r_2L, potential transpiration rate [LT^{-1}]. Figure 3.1 gives a schematic plot of the stress response function used by Feddes et al. (1978). Under non-optimal conditions, i.e., either too wet or too dry, S_p is reduced by means of the factor $\alpha(h)$. The reduction of root water uptake due to water stress, $\alpha(h)$, is described as:

$$\propto (h) = \begin{cases} 0 & , h \geq h_1 \\ \frac{(h_1 - h)}{(h_1 - h_2)} & , h_1 > h \geq h_2 \\ 1 & , h_2 > h \geq h_3 \\ \frac{(h - h_4)}{(h_3 - h_4)} & , h_3 > h \geq h_4 \\ 0 & , h_4 > h \end{cases} \qquad (3.8)$$

where h_1, h_2, h_3 and h_4 are the threshold model parameters. Water uptake is at its potential rate when the pressure head between h_2 and h_3, decreases linearly when $h>h_2$ or $h<h_3$ and becomes zero when $h<h_4$ or $h>h_1$. The parameters of the stress response function for a majority of agricultural crops can be found in various databases (e.g. Taylor and Aschorft, 1972; Wesseling et al., 1991) and are directly implemented in HYDRUS. The actual root water uptake is equal to the potential uptake rate (potential transpiration rate) during the periods of no water stress ($\alpha(h)$ =1).

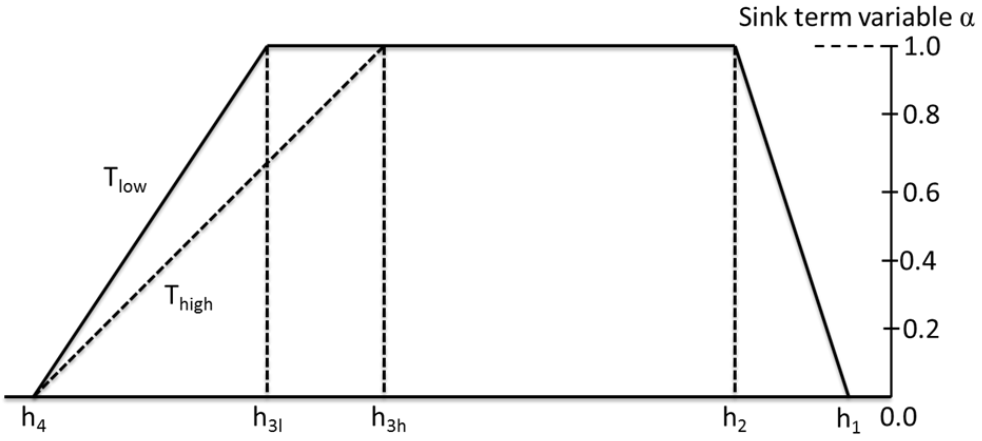

Figure 3.1 Schematic of the plant water stress response function, α (h) as proposed by Feddes et al. (1978).

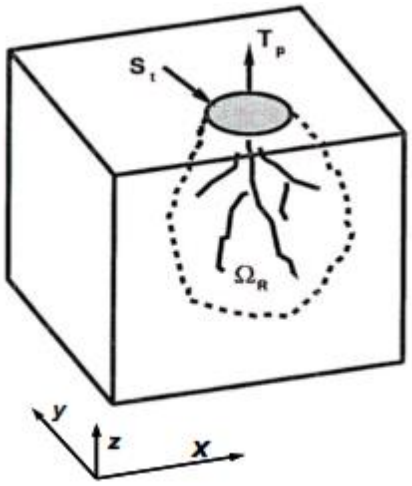

Figure 3.2 Šimůnek et al. (2008) described the schematic of the potential water uptake distribution function in three-dimensional root zone domain.

The potential water uptake, *Sp*, is affected by potential transpiration and the spatial root distribution. When the potential water uptake rate is distributed over the three-dimensional root domain (Figure 3.2), *Sp* becomes:

$$Sp = b(x, y, z) S_t T_p \tag{3.9}$$

where T_p is the potential transpiration rate [LT^{-1}], S_t is soil surface associated with the transpiration process, $b(x, y, z)$ is a spatial root distribution function. The three-dimensional model for root distribution used in HYDRUS is expressed by Vrugt et al. (2001). The function of root distribution is described by the following equation;

$$b(x,y,z) = \left[1 - \frac{x}{X_m}\right]\left[1 - \frac{y}{Y_m}\right]\left[1 - \frac{z}{Z_m}\right] e^{-\left(\frac{p_x}{X_m}\left|x^* - x\right| + \frac{p_y}{Y_m}\left|y^* - y\right| + \frac{p_z}{Z_m}\left|z^* - z\right|\right)} \tag{3.10}$$

where X_m, Y_m and Z_m are the maximum rooting lengths in the x-, y-, and z- directions [L], respectively; x, y, and z are distances from the origin of the three in the x-, y- and z- directions [L], respectively; p_x [-], p_y [-], p_z [-], x^* [L], y^* [L], and z^* [L] are empirical parameters, and b (x, y, z) is denote three-dimensional spatial root distribution of the potential root water uptake. Following Vrugt et al. (2001), p_x, p_y and p_z are set to unity for $z>z^*$, $x>x^*$ and $y>y^*$.

The actual uncompensated root water uptake, *S (h)* (Šimůnek and Hopmans, 2008) as follows;

$$S(h,x,y,z,t) = \alpha(h,x,y,z,t) * b(x,y,z,t) * S_t * T_p(t) \tag{3.11}$$

So that the actual transpiration rate, T_a [LT^{-1}] is obtained by integrating equation (3.11) over the root domain, Ω_R (Šimůnek and Hopmans, 2008);

$$T_a(t) = \frac{1}{S_t} \int_{\Omega_R} S(h,x,y,z,t)d\Omega = T_p(t) \int_{\Omega_R} \alpha(h,x,y,z,t)b(x,y,z,t)d\Omega \quad (3.12)$$

3.2.2. Root Water Uptake with Compensation

A compensated root water uptake model is also implemented in HYDRUS by introducing a threshold value, referred to as the root adaptability factor, of a dimensionless water stress index, which is defined as the ratio of actual and potential transpiration rates (Šimůnek and Hopmans, 2008). If the water stress index is above the root adaptability factor, reduced root water uptake in one part of the root zone is fully compensated for by root water uptake from other parts of the root zone where the water stress is smaller, so that the actual transpiration rate is equal to the potential transpiration rate. If the water stress index is below the root adaptability factor, reduced water uptake is only partially compensated. The ratio of actual to potential transpiration is then equal to the ratio of the water stress index to the root adaptability factor, which is less than unity. The ratio of actual and potential transpiration of uncompensated root water uptake is defined as;

$$\frac{Ta(t)}{Tp(t)} = \frac{1}{Tp(t)S_t} \int_{\Omega_R} S(h,x,y,z,t)d\Omega = \int_{\Omega_R} \alpha(h,x,y,z,t)b(x,y,z,t)d\Omega = \omega(t) \quad (3.13)$$

where ω is a dimensionless water stress index (Jarvis, 1989). Following this approach, HYDRUS implemented a critical value of the water stress index, ω_c, which is referred to also as a root adaptability factor.

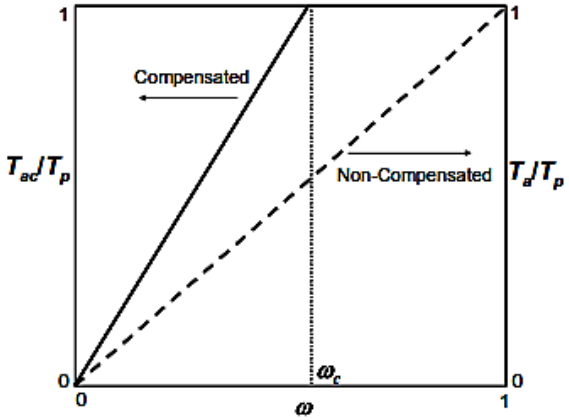

Figure 3.3 The ratio of actual to potential transpiration as a function of the stress index, ω (arrows point towards the corresponding axis; the left axis is for compensated uptake, while the right axis for uncompensated uptake) (Šimůnek and Hopmans, 2008).

The compensated actual transpiration rate, T_{ac}, is defined as the ratio of T_a/ω. When the water stress range above the critical water stress index (i.e., $\omega>\omega_c$), the ratio of the actual transpiration becomes:

$$\frac{T_{ac}(t)}{T_p(t)} = \frac{T_a(t)}{T_p(t)\omega(t)} = \frac{\int_{\Omega_R} \alpha(h,x,y,z,t)b(x,y,z,t)d\Omega}{\omega(t)} = \frac{\omega(t)}{\omega(t)} = 1$$

$$S_c(h,x,y,z,t) = \alpha(h,x,y,z,t)b(x,y,z,t,)S_t \frac{T_p(t)}{\omega(t)} \tag{3.14}$$

For the water stress range below the critical water stress index (i.e., $\omega<\omega_c$), the compensated actual transpiration rate is defined as $T_{ac}=T_a/\omega_c$, so that;

$$\frac{T_{ac}(t)}{T_p(t)} = \frac{T_a(t)}{T_p(t)\omega_c(t)} = \frac{\int_{\Omega_R} \alpha(h,x,y,z,t)b(x,y,z,t)d\Omega}{\omega_c(t)} = \frac{\omega(t)}{\omega_c(t)} < 1$$

$$S_c(h,x,y,z,t) = \alpha(h,x,y,z,t)b(x,y,z,t,)S_t \frac{T_p(t)}{\omega_c(t)} \tag{3.15}$$

where S_c is the compensated root water uptake [LT^{-1}]. For ω_c= 1 and 0, the root water uptake is either uncompensated or fully compensated. The value of the critical water stress index, ω_c for agricultural plants is relatively high. Thus their ability to compensate natural stresses is limited, as compared to natural plants, especially desert species. The plant deserts have low ω_c and correspondingly high ability to compensate for natural stresses (i.e. only take up water and nutrients from those parts of the root system where they are most available) (Šimůnek and Hopmans, 2008).

3.3. Modeling Approach of Solute Transport

Soil water and nutrient distribution around the buried ring-shaped emitter were simulated using HYDRUS 2D/3D (Šimůnek et al., 2008; 2018). The HYDRUS can simulate three-dimensional variably-saturated water flow and solute transport based on the Richards equation for water flow and the equilibrium advection-dispersion equation for solute transport. A sink term is included in these equations to account for water and nutrient uptake and the effects of water and osmotic stress (Feddes and Raats, 2004). In addition, the model allows the specification of root water and nutrient uptake, which affects the spatial distribution of water and soil water salinity between irrigation cycles. The solute transport was described using the general advection-dispersion equation given by:

$$\frac{\partial \theta c}{\partial t} = \nabla.\left(\theta D.\nabla c - qc\right) - r_a(c,h) \qquad (3.16)$$

where c is the concentration of the solute in liquid phase [ML^{-3}], q is the Darcy-Buckingham water flux vector [LT^{-1}], and D is the dispersion tensor [L^2T^{-1}], which was described using standard expressions (e.g., Bear, 1972) in terms of the longitudinal (ε_L) and transverse (ε_T) dispersivities [L]. The presented application assumes a single value for the longitudinal dispersivity (with the transverse dispersivity being one-tenth of the longitudinal dispresivity. r_a represents the root nutrient uptake [$ML^{-3}T^{-1}$], which is the sum of actual (a) passive (p_a) and active (a_a) root nutrient uptakes. The sink terms r_a, p_a and a_a represent the mass of nutrient removed per unit time from a unit volume soil due to the total passive and active plant nutrient uptake, respectively. (Šimůnek and Hopmans, 2009).

3.4. Root Nutrient Uptake

The component r_a in the presented model (Eq. 3.15) allows for both passive and active root nutrient uptake. The passive uptake describes the mass flow and root uptake of nutrients dissolved in water taken up by plant roots. The passive nutrient uptake represents flow nutrients into roots associated with flow of water supplying the plant transpiration demand. Since transpiration flow is an active process, the mass nutrient flow is also a process that is actively regulated by plants Šimůnek and Hopmans, 2009).

In HYDRUS, passive nutrient uptake is simulated by multiplying root water uptake either compensated or uncompensated with the dissolved nutrient concentration, for concentration values below a priori defined maximum concentration (c_{max});

$$p_a(x,y,z,t) = s^*(x,y,z,t)\ min\ [c(x,y,z,t),\ c_{max}] \qquad (3.17)$$

where c is the dissolved nutrient concentration [ML^{-3}] and c_{max} is the maximum allowed solution concentration [ML^{-3}] that can be taken up by plant roots during passive root water uptake. All nutrient dissolved in water is taken up by plant roots when c_{max} is large (larger than the dissolved concentration c), while no nutrient is taken up when c_{max} is equal to zero.

The reduction of water uptake also can be caused due to salinity stress. Fig 3.4 illustates the reduction of water uptake due to salinity stress, which is proposed by Maas and Hoffman (1977). The response function can be written in terms of concentration, or electrical conductivity of either the soil water or the soil saturation extract, or osmotic pressure head (Maas, 1986; Maas and Grattan, 1999; Maas and Hoffman, 1977; van Genuchten and Hoffman, 1984).

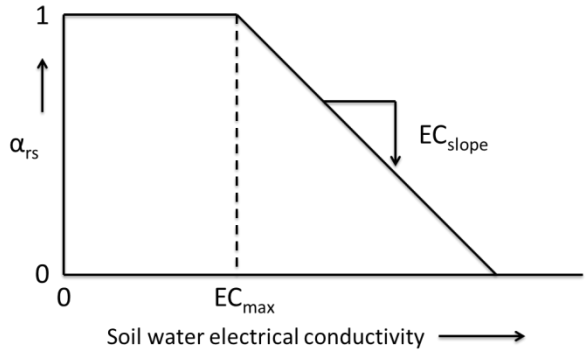

Figure 3.4 Reduction coefficient for root water uptake, α_{rs}, as a function of the electrical conductivity EC of the soil saturation extract (Maas and Hoffman, 1977)

In HYDRUS implements root water uptake for threshold model of Maas and Hoffman (1977), which describes reduction root water upake due to salinity stress as given by:

$$\alpha(h_o) = \begin{cases} 1 & 0 \geq h_o \geq h_{ot} \\ 1 - \frac{(h_{ot} - h_o)}{(h_{ot} - h_{o0})} & h_{ot} > h_o \geq h_{o0} \\ 0 & h_{o0} > h_o \end{cases} \qquad (3.18)$$

where h_o is the osmotic pressure head, h_{ot} is the threshold value of h_o above which the yield at the osmotic pressure head equal to potential yield, and h_{o0} is the threshold value of h_o below which the yield at the osmotic pressure equal to zero.

3.5. The Application of HYDRUS in Various Irrigation Designs

The HYDRUS numerical model has been tested by many researchers to assess its ability to simulate water movement from water source (e.g emitter) in various irrigation designs and management scenarios. Subbaiah (2013) reviewed the HYDRUS as a useful tool to evaluate irrigation design and management from several investigators such as Fares et al. (2001) used HYDRUS-2D to demonstrate the performance of drip irrigation in three different types of soil. The results highlighted that the water movement can be described as vertical and multidimensional in sandy soils and loam and clay soils. Skaggs et al. (2004) carried out an extensive analysis of multiple subsurface drip irrigation field experiments, and successfully compared observed wetting patterns with HYDRUS-2D model predictions. Ajdary (2005) used HYDRUS-2D model to simulate water and nitrogen distribution in drip fertigation system. Provenzano (2007) assessed the accuracy of HYDRUS-2D by comparing simulation results and experimental observations of matric potential for subsurface drip irrigation system in a sandy loam soil with a 10-cm installation depth, and also

found satisfactory agreement. Zhou et al. (2007) compared APRI and HYDRUS-2D models to simulate soil water dynamics in a vineyard under alternate partial root zone drip irrigation. Ajdary (2008) used HYDRUS-2D model to simulation of water distribution pattern under different types of soils.

Chapter 4. Experimental and Numerical Investigation Subsurface Water Flow under Ring-Shaped Emitter

4.1. Introduction

Subsurface irrigation systems are becoming increasingly popular to supply irrigation water, nutrients, and pesticides directly to the root zone efficiently. Increasing the efficiency of irrigation water use is a major concern for coping water scarcity in arid and semiarid regions. Subsurface irrigation with a ring-shaped emitter is one of subsurface irrigation methods that has been recently developed and introduced in some arid regions of Indonesia to cultivate annual and perennial crops (Saefuddin *et al*., 2014; Sumarsono *et al*., 2018). A ring-shaped emitter made from a standard water hose is economically affordable for small-scale farmers in such rural areas. To make the original design ring-shaped emitter, a water hose is first bent into a ring-shaped with a diameter of about 20 cm. Five-5 mm holes are drilled into it at an even interval. The entire ring-shaped hose is then covered with a permeable textile so that water can infiltrate through permeable textile in all directions. Water is supplied from a water tank through a tube to the inlet of the emitter. Although, subsurface irrigation with the ring-shaped emitter was successfully practiced cultivating crops in Indonesia, the design and the operation of the entire system have been purely empirical.

The dimensions spatial extent (or the volume) of wetted areas around emitter is crucial to obtain an optimum design of the emitter. The precise distribution of soil water content around a ring-shaped emitter must be known in order to properly manage subsurface irrigation with ring-shaped emitter to wet the plant root zone uniformly, which will increase water use efficiency of water or fertilizer use, and to prevent water losses due to either evaporation in soil surface or deep percolation to groundwater. Moreover, hydraulic properties of soil are critical factors to determine the infiltration phase. Therefore, by applying high pressure head of water applications in subsurface irrigation with ring-shaped emitter requires knowledge of regulating the irrigation discharge rates that involve the quantity of water passing through the root zone based on soil hydraulic properties.

Kandelous and Šimůnek (2010) compared three theoretical modeling approaches (numerical, analytical, and empirical) for calculating wetting patterns under the surface and subsurface irrigation drip irrigation that are important for optimal design. They concluded that numerical model using HYDRUS-2D (Šimůnek et al., 1999; 2008) provided good predictions of

soil water content distribution compared to other models. Recently HYDRUS numerical model (Šimůnek et al., 1999; 2006; 2008; 2016) has been widely used to simulate water movement under different irrigation designs and management scenarios. For example, Fares et al (2001) examined HYDRUS-2D to evaluate the performance of drip irrigation in three different soil types. The results highlighted the water movement more vertically in sandy soils, while the horizontal distance wetted volume was higher in clay soil. Performance of a drip system is better in clay soils than sandy soils. Whereas, Cote et al. (2003) investigated the wetting patterns under subsurface drip irrigation (SDI) without considering water uptake by plant roots. They used three different soil types including sand, silt and silt clay loam with four different irrigation fluxes. They found that subsurface drip irrigation can improve plant water availability in medium and low permeability fine-textured soil, providing that design and management were adapted to account for their soil hydraulic properties. In addition, in highly permeable soil coarse-textured soils, water and nutrients are moved quickly downwards from the emitter.

Gärdenäs et al. (2005) studied the effect of soil hydraulic properties under subsurface irrigation considering root water uptake. They concluded that percolation was highest for coarse-textured soils (sandy loam soil) and lowest for finer-textured soil (silt clay soil). Provenzano (2007) assessed the accuracy of HYDRUS-2D by comparing simulation results and experimental observations of matric potential for subsurface drip irrigation system in a sandy loam soil with a 10-cm installation depth, and also found satisfactory agreement. Siyal et al. (2009) used HYDRUS-2D to investigate the performance of pitcher irrigation system and found the close agreement between observed and simulated soil water content during subsurface water application through pitcher. While Nagazawa *et al*. (2008) examined HYDRUS-1D to investigate the performance of the buried porous bottle for subsurface irrigation by applying different water pressure head applications in quartz sand soil. They found the predicted of soil water contents generally fitted well with the observed data. In addition, the rate of deep percolation and evaporation from the soil surface can be reduced by applying the pressure head smaller than the air entry value of the soil. Overall, they concluded that HYDRUS 1D, and 2D/3D is an effective tool for investigating and designing irrigation management practices.

In order to provide of design and management for subsurface irrigation with ring-shaped emitter, the first step that should be taken into account is to investigate the wetting patterns and soil water content distributions around buried ring-shaped emitter by considering the soil hydraulic properties and the amount of water irrigation applications. Therefore, the aims of this work are to

(1) study the influence of soil hydraulic properties on soil water movement around buried ring-shaped emitter, (2) calibrate and validate the capacity of the HYDRUS 2D/3D numerical model in assessing the water flow in soil under subsurface irrigation with original design ring-shaped emitter. To address these objectives, the laboratory experiments were first carried out to monitor changes in the soil moisture content at given positions during water applied with the buried original ring-shaped emitter. While the emitter was developed to aid plant cultivation, the laboratory experiments were carried out without any plants in this work to avoid any difficulties associated with plant root water uptake. Two different water pressure head applications; 1 and 5 cmH_2O are applied for two soil types, sand and silt. Therefore, there are 4 simulations were considered to express the infiltration processes. HYDRUS was then calibrated with the experimental soil water content data collected during the subsurface water application experiments with the original ring-shaped emitter. The calibrated model was next used to predict other experimental data for validation.

4.2. Theory

4.2.1. HYDRUS Numerical Model of Water Flow

Unsaturated water flow through a porous medium is generally described using the Richards equation. The solution of this equation requires knowledge of soil hydraulic function, which is the retention curve, $\theta(h)$, and the hydraulic conductivity function, $K(h)$. Because of the highly non-linear water retention and hydraulic conductivity functions only can be solved using numerical approach. A numerical approach using HYDRUS 2D/3D (Šimůnek et al., 2008; 2016) enables simulate water, solute and heat movement in two-three dimensional variably saturated media under a wide range of complex and irregular boundary conditions and soil heterogeneities. The software uses a modified form of Richard equation, including a sink term for water uptake by plant roots to describe the water flow in isotropic variably saturated porous media, based on the mass conservative iterative schemes introduced by Celia et al. (1990). The governing flow equation (Eq 3.1) within HYDRUS was solved numerically using Galerkin finite elements (Šimůnek et al., 1999; 2006; 2008; 2016) in both two and three dimensions. This numerical scheme also allows a two-dimensional version of the Richard equation to be solved for three-dimensional exhibiting radial symmetry about the vertical axis (such as for flow from a point source). Because such problems involve only two coordinates (i.e., a vertical axis z and a radial axis r), refer to these problems as axi-symmetrical two-dimensional problems.

The two-dimensional module of the HYDRUS 2D/3D software package (Šimůnek et al., 2016) was used to simulate water movement for the specific subsurface irrigation with original design ring-shaped emitter. In order to describe water flow in an entire laboratory infiltration experiment, it is sufficient to analyze the flow in the single volume element. Because of the original ring-shaped emitter used in the experiment was fully covered by the permeable textile, we assumed that water infiltrated thorough the textile in all directions. Therefore, the infiltration processes can be viewed as an axi-symmetrical three-dimensional flow with the radius r [L] and the depth z [L] as key variables. Three-dimensional axi-symmetrical flow in variably saturated, rigid, isotropic media can be described by the following modified form of Richard's equation;

$$\frac{\partial \theta}{\partial t} = \frac{\partial}{\partial r}\left(K(h)\frac{\partial h}{\partial r}\right) + \frac{K(h)}{r}\frac{\partial h}{\partial r} + \frac{\partial}{\partial z}\left(K(h)\left(\frac{\partial h}{\partial z}+1\right)\right) \tag{4.1}$$

where θ [L^3L^{-3}] is the volumetric soil water content, h[L] is the pressure head, t [T] is time, r [L] is the radial coordinate, z [L] is the vertical coordinate taken positive upwards, and K [LT^{-1}] is the unsaturated hydraulic conductivity. The unsaturated hydraulic properties are described using van Genuchten-Mualem functional relationships (van Genuchten, 1980). The constitutive equations of van Genuchten-Mualem model is described in Chapter 2 (eq. 3.3 through eq. 3.5).

4.2.2. Soil Hydraulic Properties

In order to run the simulation of water flow using HYDRUS requires accuracy of soil hydraulic properties to describe the more realistic water flow condition in the field/laboratory experiments. HYDRUS-2D/3D numerical code (Šimůnek et al., 2006) enables to inversely estimate unsaturated soil hydraulic properties from the transient flow data. HYDRUS was used to inversely estimate soil hydraulic parameters from variably-saturated water flow data collected during the subsurface water application experiment with the original design ring-shaped emitter. The inverse method implemented in HYDRUS is based on the minimization of a given objective function, which expresses the discrepancy between observed and predicted values. The Levenberg-Marquardt optimization algorithm (Marquardt, 1963), in combination with the HYDRUS-2D/3D code was used to minimize the objective function. An inverse problem requires the same type of information as a forward problem. It also requires initial estimates of optimized parameters, potions of observation points and measured data with corresponding measurement times and weighing factors.

In this study, the optimized soil hydraulic parameters were determined by systematically minimizing the difference between observed and simulated state variables (e.g. soil water content

and cumulative infiltration). The objective function O used in this study was defined as the sum of two components:

$$O(\boldsymbol{\beta},\boldsymbol{\theta},\mathbf{q}) = \sum_{j=1}^{m_\theta} v_j \sum_{i=1}^{n_{\theta j}} w_{i,j} \left[\theta_j^*(\mathbf{x},t_i) - \theta_j(\mathbf{x},t_i,\boldsymbol{\beta})\right]^2 + \sum_{k=1}^{n_q} w_k \left[q_c^*(t_k) - q_c(t_k,\boldsymbol{\beta})\right]^2 \quad (4.2)$$

where θ_j is the soil water content (SWC) at the sensor position $\mathbf{x}$, and q_c is the cumulative emitter discharge at the inlet of the buried ring-shaped emitter [L T^{-1}]. The superscript * represents specific measurements at time t_i for SMC and t_k for the cumulative discharge. While m_θ is the number of sensor locations, $n_{\theta j}$ is the number of measurements at each sensor position. In this objective function, $\theta_j(\mathbf{x},t_j,\boldsymbol{\beta})$ and $q_c(t_k,\boldsymbol{\beta})$ are the corresponding model predictions for the vector of optimized soil hydraulic parameters, $\boldsymbol{\beta}$, and v_j, $w_{i,j}$, and w_k are weights associated with a particular measurement. During parameter estimation, the parameters of van Genuchten-Mualem model were optimized.

4.3. Materials and Method

4.3.1. Experimental Set-up

The laboratory experiments were carried out using a container (50 cm in diameter at the top, 40 cm in diameter at the bottom, and 55 cm in height) filled with air-dried soil (Fig. 4.1 and 4.2b). Two types of the soil, silt and sand, were used in the experiments. Soils were packed with a 5-cm increment at the predetermined bulk density of 1.41 g cm^{-3} and 1.52 g cm^{-3} for silt and sand, respectively. A 10-cm thick gravel layer was installed at the bottom of the container. For each experiment, the original ring-shaped emitter was installed at a depth of 15 cm. The emitter was connected to a Mariotte tank (10 cm in diameter and 44 cm in height) to control the water pressure head applied at the inlet (referred to as the inlet pressure). In this study, a constant pressure head of either 1 cm or 5 cm was maintained at the inlet of the buried emitter for 10 hours to apply water through the emitter. During experiments, the volume of water in the Mariotte tank was recorded every 30 minutes to obtain the water discharge rate (i.e., water application rate).

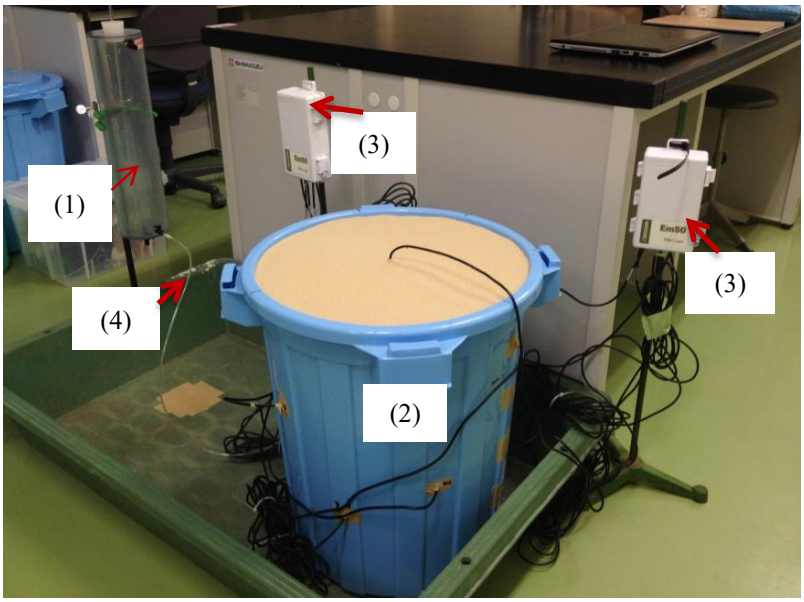

1. Marriotte tank
2. Soil container
3. EM50 data logger and soil sensors connections
4. Small tube water connecting from mariotte tank to an inlet of ring-shaped emitter

Figure 4.1 A schematic laboratory experimental set-up of subsurface water flow where ring shaped-emitter was installed at a depth of 15 cm from the soil surface.

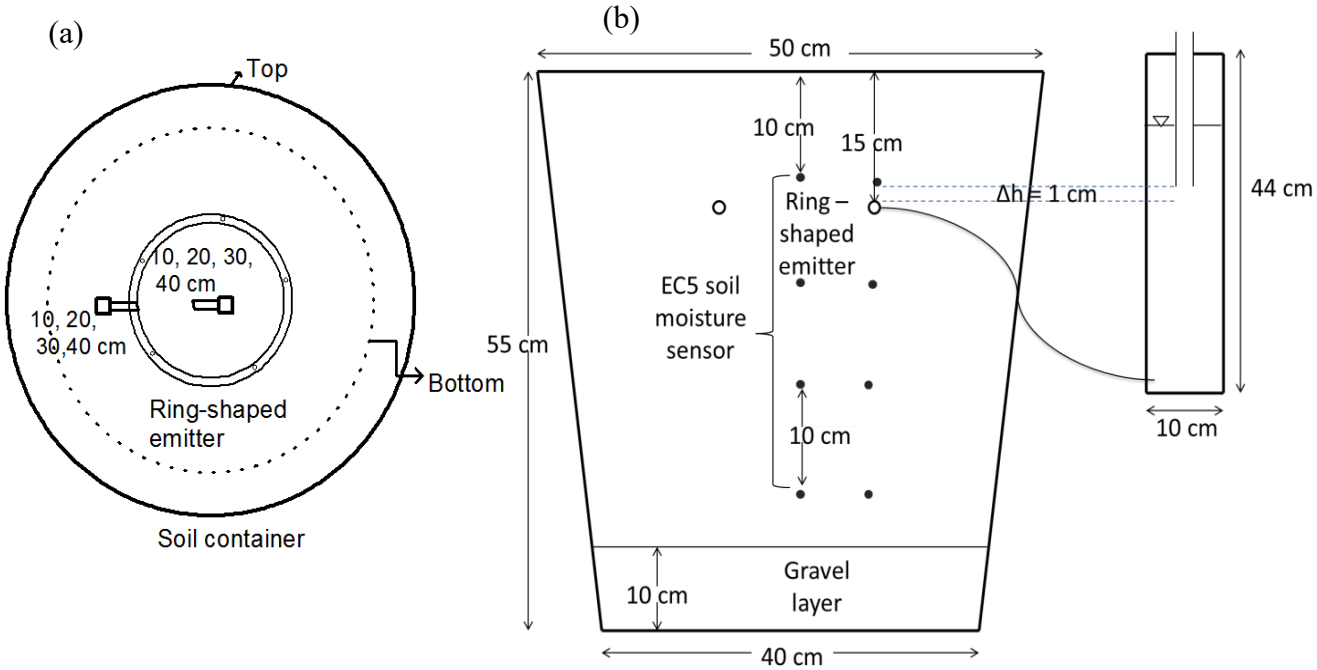

Figure 4.2 Top view (a) and cross-section (b) of the soil container used in the laboratory experiments with a ring-shaped emitter. The black dots represent soil moisture sensors.

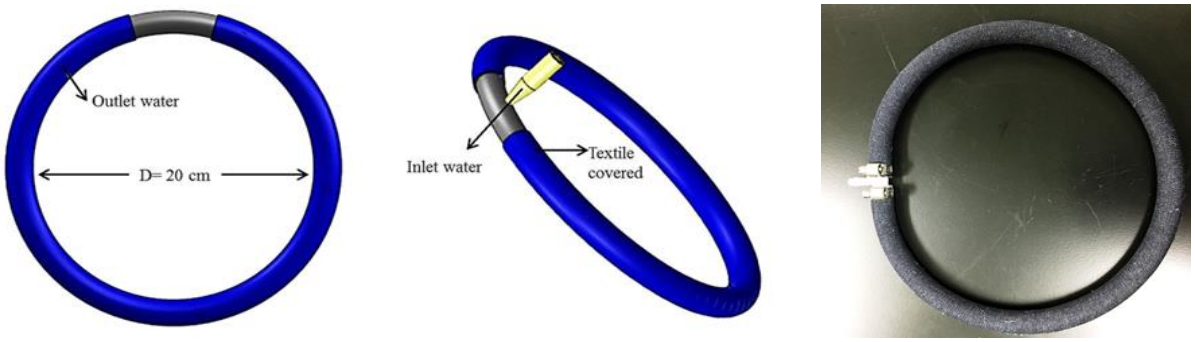

Figure 4.3 Schematic of the original ring-shaped emitter, which is fully covered with a permeable textile used in the laboratory experiment.

The ring-shaped emitter used in this study was made from a rubber water hose. The hose, which had a 1 cm inner diameter, was bent into a ring shape with a diameter of about 20 cm. There were 5 small holes with 0.5 cm in diameter drilled at even intervals on one side of the ring. The entire ring was covered with a permeable textile so that applied water could infiltrate in all directions into the soil. The original ring-shaped emitter is referred to as the 5F emitter in the remainder of this dissertation. The schematic of the ring-shaped emitter is depicted in Figure 4.3. When the ring-shaped emitter was installed in the soil, its 5 holes were all facing down to block any soil particles from entering the holes.

There were 8 capacitance soil moisture sensors, EC5, a product of METER Environment, installed around the buried emitter to monitor changes in the soil water content. Figure 4.2a shows the position of the sensors in the container. Four sensors were installed at depths of 10, 20, 30, and 40 cm directly above and below the emitter and four additional sensors were installed at the same depths in the center of the emitter. Since the ring-shaped emitter was installed at a depth of 15 cm, the four sensor installation depths were 5 cm above, and 5, 15, and 25 cm below the emitter, respectively. The soil moisture sensors were individually calibrated for the soils used in the experiments.

Toyoura sand and DL-Clay were used in this study to represent as different soil hydraulic properties. In each soil type, three disturbed soil samples were used to determine soil hydraulic parameters including bulk density, saturated water content, and soil water retention curve. The soil textures were classified as sand and silt, respectively. The average measured soil bulk density for both soil textures sand and silt was 1.52 g cm^{-3} and 1.41 g cm^{-3}, respectively. As for saturated water content measurement, the soil cores were first saturated from the bottom and then submerged in water for 24 h. After weighing, the saturated soil samples were dried at 105 °C to constant mass, and their mass-based saturated soil water content was determined. θs values were determined by

multiplying saturated mass-based soil water content with Bulk density. The average saturated water content was 0.430 $cm^3\ cm^{-3}$ and 0.468 $cm^3\ cm^3$ for sand and silt, respectively. In addition, the soil water retention curve, $\theta\ (h)$, was determined in the laboratory using a pressure plate apparatus for suctions of 0 to 1033 cm. The saturated hydraulic conductivity value, *Ks* of 29.7 cm h^{-1} and 0.35 cm h^{-1} for sand and silt, which is provided in the Soil Catalog by ROSETTA were used as initial parameters, completing the hydraulic conductivity function, $K\ (h)$, the parameters of the van Genuchten-Mualem equations (eq. 3.3, 3.4 and eq. 3.5) were fitted using simultaneously retention and conductivity data determined by the RETC program (van Genuchten et al., 1991). The van Genuchten-Mualem parameters were used as initial input parameters for optimizing soil hydraulic properties using the inverse solution.

4.3.2. Numerical Simulation of Soil Water Distribution using HYDRUS Three-Dimensional Axi-Symmetrical Flow Domain

Modeling of water flow was carried out for all laboratory experimental scenarios, including subsurface water application with 1 cm and 5 cm pressure head for each soil type, sand and silt, resulted a total of 4 simulations was considered. The HYDRUS-2D/3D software package was used to simulate the transient axi-symmetrical (or radially symmetrical) three-dimensional movement of water in the soil. In this approach, we assumed water infiltrate in all directions of ring-shaped emitter through permeable textile since ring-shaped emitter was fully covered with permeable textile. Therefore, the system could be modeled as an axi-symmetrical three-dimensional domain. The domain geometry used in the axi-symmetrical three-dimensional model is shown in Fig. 4. 4. Similar axi-symmetric modeling approaches have been used in many other studies with a subsurface point water source (Cote *et al.*, 2003; Gärdenäs *et al.*, 2005; Provenzano, 2007; Kandelous and Šimůnek, 2010a; Kandelous *et al.*, 2011; Naglic *et al.*, 2014). The simulated for water movement only consider in right side of the vertical cross section in half soil profile domain, 55 cm height, 20 cm in wide (bottom) and 25 cm wide (top). A circle with a 1-cm diameter located at a 15-cm depth in the domain represents the cross-section of the buried ring-shaped emitter (Fig. 4.4). The entire flow domain was discretized into 661 nodes and 1,246 triangular finite elements, with their sizes gradually increasing up to 2.5 cm away from the emitter. Mesh refinement of 1 cm size was done at along the perimeter of the emitter. The finite element mesh was generated using an automatic triangulation algorithm that is implemented in HYDRUS.

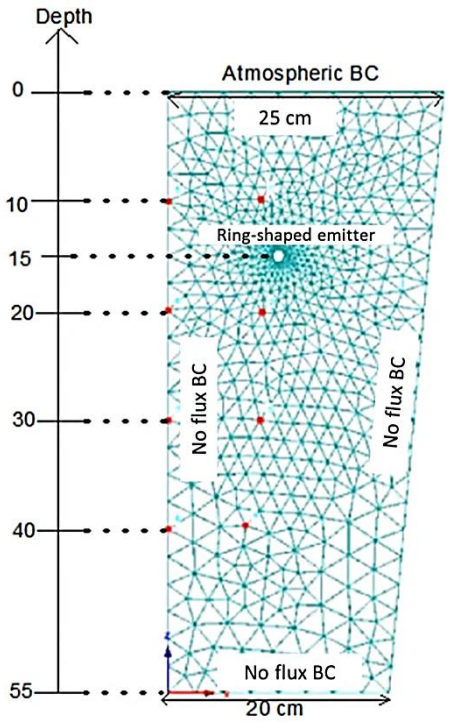

Figure 4.4 An axisymmetric three-dimensional simulation domain used in the numerical analysis of water flow from a buried ring-shaped emitter. Eight red dots in the domain depict the positions of moisture sensors.

Changes in the soil water content through time were simulated at 8 observation nodes that corresponded with the positions of the soil moisture sensors installed as shown by red dots in Figure 3.4. The initial water content value (θ_{in}) was set uniform across the flow domain. The observed average initial water content (θ_{in}) was assigned to the entire flow domain as the initial water content. The average initial water contents were 0.044 $cm^3\ cm^{-3}$ and 0.046 $cm^3\ cm^{-3}$ for silt and sand, respectively. No flow boundary conditions were considered along the two vertical sides and bottom of the transport domain, while an atmospheric boundary condition was set at the top edge of the flow domain. A constant pressure head equal to pressure head that imposed during the laboratory experiment (e.g 1 and 5 cmH_2O) as a variable head boundary condition along the circumference of emitter was assumed during the irrigation time (10 hours) and no flux in fallow time when irrigation was stopped (after 10 hours), allowing redistribution flow. This boundary condition applies a specified pressure head to the lowest nodal point of the emitter and adjusts pressure heads in the other nodal points based on the vertical coordinates. The simulation was run for 24 hours for each simulation scenario. The initial soil hydraulic properties for the van Genuchten-Mualem function are listed in the following table:

Table 4.1 Soil hydraulic parameters for van Genuchten-Mualem function (van Genuchten, 1980) and bulk density for different soil types as initial input parameters for calibration model.

Soil texture	θ_r (cm^3cm^{-3})	θ_s (cm^3cm^{-3})	α (cm^{-1})	n (-)	Ks ($cm\ h^{-1}$)	l (-)	Bulk density ($g\ cm^{-3}$)
Silt	0.034	0.400	0.249	2.992	0.35	0.5	1.52
Sand	0.045	0.430	0.012	2.421	29.7	0.5	1.41

4.3.3. Statistical Analysis

The performance of the model was evaluated by comparing observed (*O*) and HYDRUS-2D/3D simulated (*S*) of soil water content distribution at given locations using various quantitative measures of the uncertainty. In this study, three different statistical indexes were used such as, the root mean square error (RMSE), the mean absolute error (MAE) and the mean error (ME). They indicate the differences between observations and predictions. The mathematical equations of the mentioned statistics are as follows;

$$RMSE = \left[\frac{\sum_{i=1}^{n} (S_i - O_i)^2}{n} \right]^{1/2} \tag{4.3}$$

$$MAE = \frac{1}{n} \sum_{i=1}^{n} \left| O_i - S_i \right| \tag{4.4}$$

$$ME = \frac{1}{n} \sum_{i=1}^{n} \left(S_i - O_i \right) \tag{4.5}$$

where O_i and S_i are the observed and simulated values; and n is the number of measurements. The RMSE measures estimation of absolute errors, whereas the ME shows the overestimation or underestimation of the model. The obtained RMSE and ME close to zero indicate better performance of the model. In general, RMSE ≥MAE, the degree in which the RMSE value exceeds MAE is usually a good indicator of the presence and extent of outliers or the variance of the difference between the observed and the modeled values.

4.4. Results and Discussions

4.4.1. The Effect of Soil Properties on Distribution of Soil Water Dynamics

The simulations of water movement were carried out for two soils with contrasting physical properties; a highly permeable coarse-textured sand and a medium permeability fine-textured silt. The figure 4.6 shows the water retention and the hydraulic conductivity function for silt and sand. These hydraulic properties illustrate the effect of different soil properties can have on water infiltration movement in subsurface irrigation with ring-shaped emitter.

Numerical simulations of soil water content distributions in silt and sand under different applied pressure head irrigations are given in Figure 4.5 and Figure 4.7. Figure 4.5 displays simulated the wetted areas around the buried emitter in the axisymmetrical three-dimensional flow domain after 1, 5, 10, 15, 20, and 24 hours using the optimized soil hydraulic parameters listed in Table 4.2. Whereas Figure 3.7 depicts the comparison of observed and simulated soil water contents at 8 locations. Open triangles in Fig. 4.7 represent the observed (SWCs) at the center of the buried ring-shaped emitter in four depths (i.e., 10 cm, 20 cm, 30 cm, and 40 cm), whereas open circles show SWCs directly below and above the buried ring-shaped emitter in the same four depths.

For silt soil, the wetted areas expanded radially with time during the water application (i.e., during the first 10 hours). After allowing redistribution process, the wetted area has reached nearly the soil surface when applied higher irrigation water pressured at the inlet emitter. These results also can be described in Figure 4.7ab. SWCs 5 cm directly below and above the buried ring-shaped emitter (i.e., 10 and 20 cm depths) increased a few hours after the beginning of the water application for both inlet pressure heads. This indicates that water infiltrated radially in all directions around the buried emitter regardless of the inlet pressure head applied. An initially steep increase in SWCs became more gradual after a few hours, before finally reaching their maximum values after about 10 hours at the time when the application of water stopped. An increase in SWCs 5 cm directly below the emitter increased faster than SWCs observed at 5 cm directly above the emitter regardless of the inlet pressure applied because the gravitation enhanced the flow in the downward direction. During the redistribution process, SWCs gradually decreased at both locations.

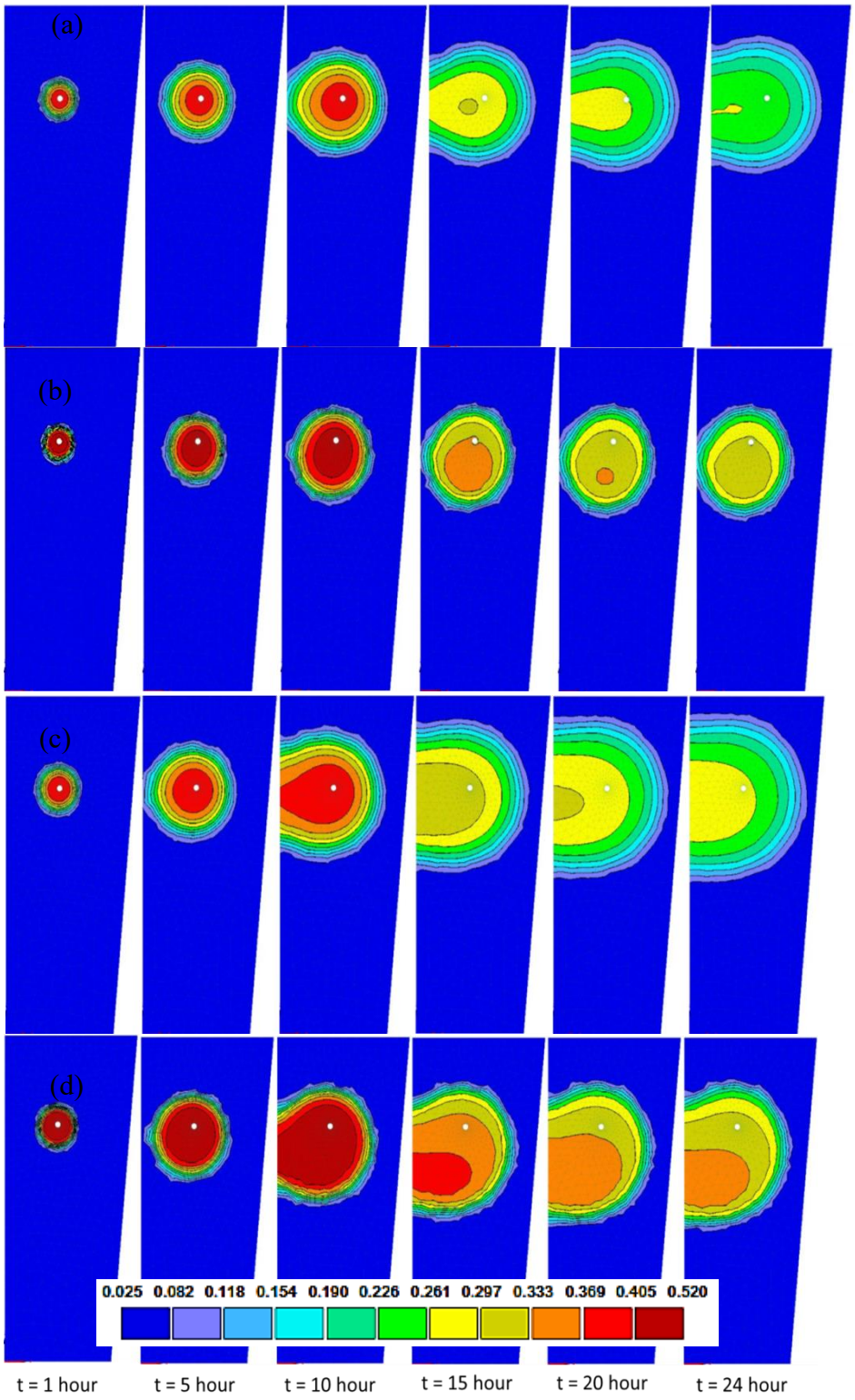

Figure 4.5 The spatial extent of simulated soil water content distribution around buried ring-shaped emitter, (a) silt with the 1-cm inlet pressure head, (b) sand with the 1-cm inlet pressure head, (c) silt with the 5-cm inlet pressure head, and (d) sand with the 5-cm inlet pressure head.

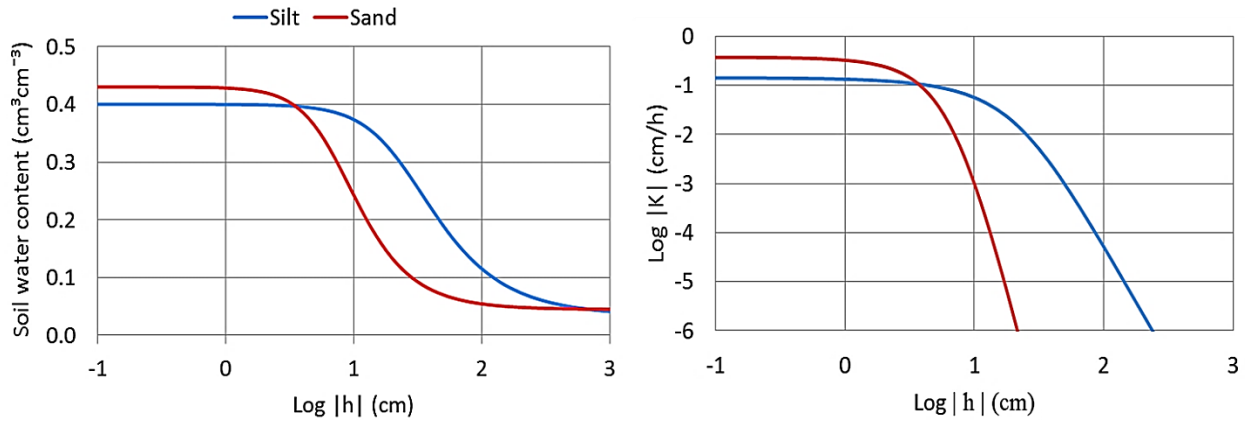

Figure 4.6 Soil water retention curves (left) and unsaturated hydraulic conductivity functions (right) for silt and sand described using the van Genuchten-Mualem model with optimized parameters.

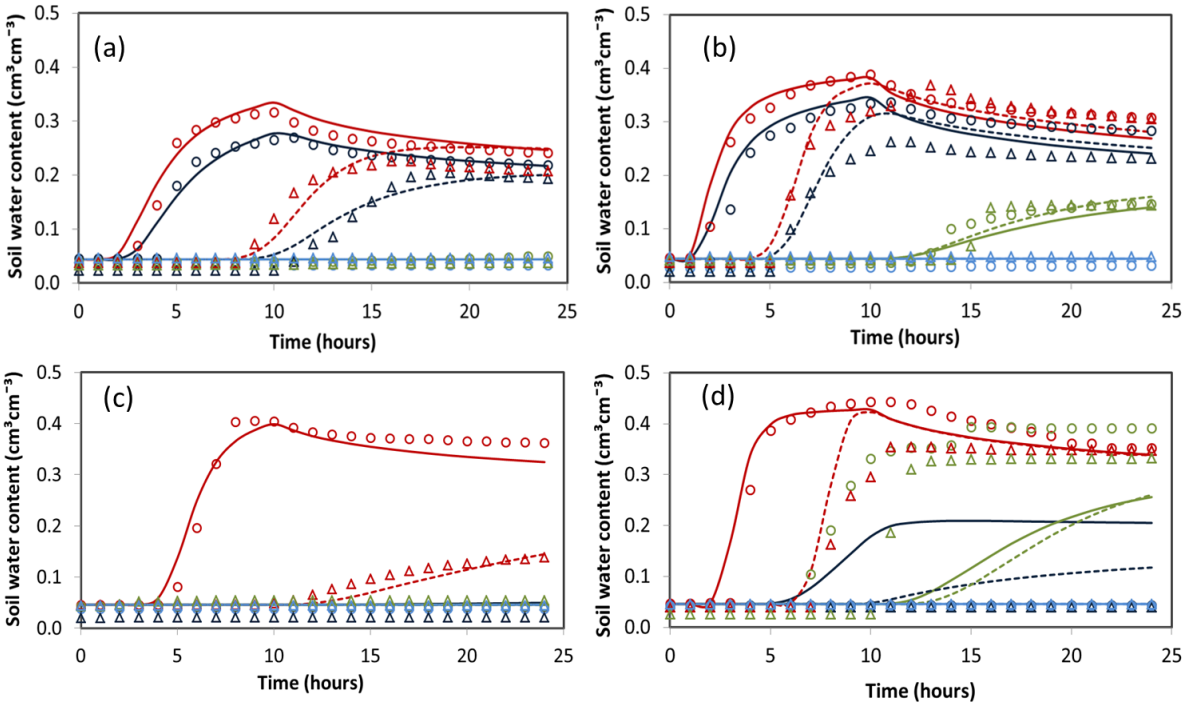

Figure 4.7 Soil water contents (SWCs) measured by 8 moisture sensors positioned in 4 depths (10, 20, 30, and 40 cm from the soil surface) during the subsurface water application experiments in silt (a and b) and sand (c and d). Open circles depict SWCs observed at positions directly above (i.e., 5 cm above) and below (i.e., 5,15, 25 cm below) the emitter (installed at a 15-cm depth), whreas open triangles show SWCs observed at the corresponding depths in the center of the container. Two different inlet pressure heads (i.e., 1 cm (a nd c) and 5 cm (b and d)) were applied during experiments. Lines depict corresponding SWCs simulated using HYDRUS. While HYDRUS was calibrated using data collected with 1-cm inlet pressure head (a and c), it was validated using the data observed with the inlet 5-cm inlet pressure head (b and c).

Table 4.2 The van-Genuchten-Mualem model parameters optimized for silt and sand. Both saturated and residual water contents are marked with * as they were not optimized during the inverse modeling.

Soil texture	θ_r *(cm^3cm^{-3})	θ_s *(cm^3cm^{-3})	α (cm^{-1})	n (-)	Ks (cm h^{-1})	l (-)
Silt	0.034	0.400	0.041	1.734	0.215	0.50
Sand	0.045	0.430	0.137	2.421	0.38	4.09

On the other hand, SWCs in the same depths (5 cm above and below the buried emitter) at the center of the buried emitter started increasing much later due to the lateral distance from the emitter (i.e., the water source). As expected, SWCs 5 cm below the emitter increased much faster than those 5 cm above the emitter. When the inlet pressure head was 1 cm, SWCs at the center kept increasing but never reached the same peaks as above and below the emitter at both depths. SWCs at other depths (i.e., 30 and 40 cm below the surface) never increased during the experiment.

The main difference between silt and sand was that observed SWCs did not increase 5 cm above the buried emitter (dark blue symbols in Figs. 4.7cd for the depth of 10 cm) in the sand. Additionally, when the applied inlet pressure head was 5 cm, increases in SWCs 5 cm and 15 cm below the buried emitter (i.e., in depths of 20 and 30 cm) were especially large. These results indicate that downward water movement was dominant in the sand profile while water moved more radially, including lateral and upward directions, from the emitter in the silt profile. This difference can be attributed to different macroscopic capillary lengths, λ_c, given below, of these two soils (Radcliffe and Šimůnek, 2010).

$$\lambda_c = \frac{\int_{h_i}^{h_0} K(h)dh}{K(h_0) - K(h_i)} \tag{4.6}$$

The macroscopic capillary length λ_c can be interpreted as the measure of the effects of capillarity as opposed to gravity. The macroscopic capillary length was 7.56 cm and 5.27 cm for silt and sand, respectively, when integrating from h_i = 0 cm to h_0 = -200 cm. Since sand typically has a much lower macroscopic capillary length than other soils, water flowing from a source will move much less laterally or upward than downward. The results corroborate the study of Cote et al. (2003) which found that the macroscopic capillary length in sand was about 3.6 cm smaller than in silt soil, which was 8.3 cm.

Philip (1968) stated the macroscopic capillary length can be used to quantify the influence of soil on water infiltration process in the soil. The macroscopic capillary length scale, λ_c is a measure of the relative importance of gravity and capillarity for water movement in soil. Slowly permeable fine-textured soils, where capillarity force tends to dominate, have large λ_c values. While highly permeable coarse-textured soils, where gravity effects manifest more readily, have small λ_c (Philip, 1968).

The numerical analyses show that in highly permeable coarse-textured soil such as sand used in this study, water drains easily and quickly from the root zone because gravity dominates in infiltration process. This can exacerbate off-site impacts, such as increased recharge or pollution of groundwater systems. On the other hand, in slowly permeable fine-textured materials such as silt soil, water is held within the root zones and as such would normally be readily available for plant roots to uptake water. In addition, This study clarified that HYDRUS is indeed a useful tool for analyzing soil water dynamics during the water application with the buried ring-shaped emitter (i.e., subsurface irrigation), as also indicated by a number of other subsurface drip irrigation studies (Bufon *et al*., 2012; Lazarovitch *et al*., 2007; Kandelous *et al*., 2012; El-Nesr *et al*., 2014; Ghazouani *et al*., 2015).

4.4.2. Cumulative Infiltration

The cumulative discharge increased almost linearly for both soils when the applied inlet pressure head was 1 cm (Fig. 4.8ac). There was no obvious difference in the cumulative discharge between silt and sand. When the inlet pressure increased to 5 cm, while the cumulative discharges for both soils increased almost linearly with time, the cumulative discharge after 10 hours of water application in sand was much larger than in silt.

For each soil, when the water pressure head was applied higher at the inlet emitter (i.e. 5 cm) resulted the wetted area (i.e., the wet volume) much larger in the soil profile compared to when applied lower inlet pressure head. For silt, SWCs at 5 cm directly below and above the buried ring-shaped emitter (i.e., 10 and 20 cm depths) (Fig. 4.7c) increased earlier and faster when the inlet pressure head of 5 cm was applied compared to those with the 1 cm inlet pressure head.

4.4.3. Model Calibration and Validation

The inverse approach was used to optimize the parameters (α, *n, Ks* and *l*) and to calibrate the HYDRUS 2D/3D model (Hopmans et al., 2002; Lazarovitch et al., 2007). The soil water content

measured at 8 locations of 1-cm inlet pressure head water application was used to calibrate the van Genuchten-Mualem parameters (Tabel 4.1) using the Levenberg-Marquardt nonlinear minimization functions (Eq.4.2). The data collected during the experiments performed with the 5-cm inlet pressure head was then used to validate HYDRUS with calibrated parameters. The calibrated parameters are summarized in Table 4.2, while Table 4.3 summarizes statistics of discrepancies between observations and simulations.

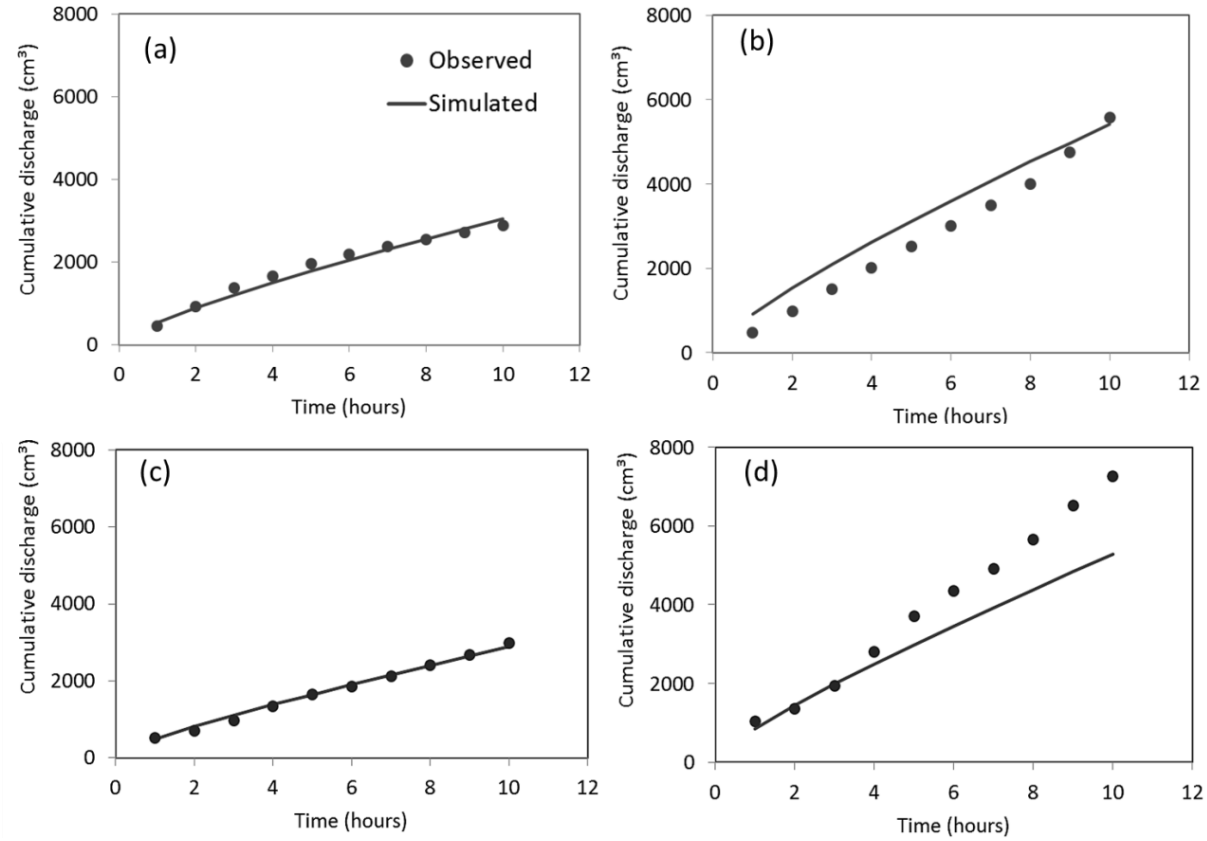

Figure 4.8 Observed (dots) and simulated (line) cumulative irrigations for silt (a and b) and sand (c and d) for the applied inlet pressure heads of 1 cm (a and c) and 5 cm (b and d). The data collected using the 1-cm inlet pressure head were used for model calibration, the data collected using 5-cm inlet pressure head were used for model validation.

Table 4.3 Summary statistics between simulated and observed soil water contents (SWC) at 8 locations where the soil moisture sensors were installed. RMSE, ME, MAE, respectively, are root mean square error, mean error, and mean absolute error computed between simulated and observed SWC.

Soil	Inlet pressure head (cm H_2O)	RMSE (cm^3 cm^{-3})	ME (cm^3 cm^{-3})	MAE (cm^3 cm^{-3})
Silt	1 (Calibration)	0.019	-0.057	0.011
	5 (Validation)	0.026	0.038	0.015
Sand	1 (Calibration)	0.015	-0.002	0.009
	5 (Validation)	0.061	-0.016	0.032

Figure 4.7ac shows a comparison between simulated and observed soil water content in calibration phase, while 4.7bd shows the comparison between simulated and observed soil water content in validation phase. Figure 4.8 shows both observed and predicted cumulative irrigation discharges during water application for different soil types in both calibration (4.8ac) and validation (4.8bd) phases. The RMSE values of the model in the simulation process of soil water content varied in the range 0.019 to 0.061 cm^3 cm^{-3} for different soil types and inlet pressure head applications during calibration and validation phases (Table 4.3). Ajdary et al. (2007); Kandelous and Simunek (2010) and Ramos et al. (2012) reported that the RMSE value in their soil water content simulation varied in the range of 0.015-0.017, 0.011-0.045, 0.028-0.033 cm^3 cm^{-3} respectively. The low values of ME and MAE describe the good performance of the model (Table 4.3). It can be concluded that the error of simulation is low enough and therefore the performance of the model is acceptable. For both soils, fitted values of SWCs and cumulative discharges agreed reasonably well with observed values.

For silt, both SWCs and cumulative discharges were predicted well using the optimized parameters. For sand, however, predicted SWCs did not agree well with observed ones, especially 15 cm directly below (i.e., in the depth of 30 cm) where SWCs were overestimated and 5 cm directly above (i.e., in the depth of 10 cm) where SWCs were underestimated. This indicates that more downward water flow occurred during the experiment than predicted by the HYDRUS simulation. When the applied inlet pressure head was 5 cm, the preferential-type flow may have occurred underneath the drilled holes of the emitter that enhanced downward water movement. This type of flow clearly creates a non-uniform asymmetrical wetted volume around the buried emitter, which may not be an ideal situation for plant roots to uptake water. Sand is known to be susceptible

to preferential flow or finger-type flow when it is initially dry. In places where preferential flow paths are formed, the soil becomes strongly wettable, increasing its ability to conduct water downward through these pathways (Dekker *et al*., 1994). It may, therefore, not be a good idea to apply a high inlet pressure when a ring-shaped emitter is installed in an initially dry sandy soil profile.

4.5. Summary

In this study, laboratory experiments were first performed to investigate the soil water content distributions around a buried ring-shaped emitter during the subsurface water application. The ring-shaped emitter used in this study was made from a rubber hose, which was bent into a ring shape with a diameter of about 20 cm. There were five holes drilled at even intervals as dripping points. The entire ring was then covered by a permeable textile so that applied water could infiltrate in all directions through the textile. Such a low-cost subsurface irrigation system can generate benefits for small-scale farmers who have scarce water resources. The experiments were carried out using a container that was filled with either silt or sand. The ring-shaped emitter was installed at a depth of 15 cm. Water was distributed through the inlet of the emitter by applying a constant pressure head of either 1 cm or 5 cm. Changes in the soil water content were monitored using 8 soil moisture sensors installed at 4 different depths: 10, 20, 30, and 40 cm below the surface (i.e., 5 cm above, and 5, 15, and 25 cm below the emitter). Four sensors were installed in the center of the emitter, and four sensors were installed directly above and below the emitter. Results showed that water moved radially around the emitter in silt, while downward water movement was dominant in sand. The difference in the flow pattern can be attributed to the difference in the macroscopic capillary length of the soil, which can be interpreted as a measure of the contribution of capillarity as opposed to gravity's effect on unsaturated water movement.

HYDRUS, a model simulating variably-saturated water flow in porous media, was then used to analyze soil water dynamics around the buried emitter during the subsurface water application. HYDRUS was first calibrated using the data observed during the subsurface water application experiment with the 1-cm inlet pressure head. The calibrated soil hydraulic parameters were then used to simulate soil water dynamics around the buried emitter during the experiments with the 5-cm inlet pressure head. Changes in the soil water contents observed by 8 sensors at different locations were predicted well using HYDRUS with parameters optimized for silt. For sand, SWCs above the buried emitter were overestimated, and those directly below the emitter were

underestimated. This indicates that downward water movement was predominant, suggesting the occurrence of preferential flow. It should be emphasized here that numerical model HYDRUS 2D/3D can capture reasonably how ring-shaped emitter with the original design for subsurface irrigation works. By analyzing the outputs of this model, design of ring-shaped emitter and management strategies can be improved to increase the efficiency of irrigation water use.

Chapter 5. Numerical Evaluation of Ring-Shaped Emitter Designs for Subsurface Irrigation

5.1. Introduction

The current design of the ring-shaped emitter does not allow one to easily detect malfunctions because the emitter is fully covered with a permeable textile. As a result, it is not easy to detect any malfunctions and to repair such malfunctions quickly. In addition, for faster promotion of the technology, it is important to have a design that is easy to maintain. It has not yet been evaluated whether the number of holes can be reduced and/or whether it is possible to cover emitters only partially with a permeable textile. Because the number of experiments that can be carried out is usually limited, numerical simulations can be used instead to evaluate the performance of ring-shaped emitters of various designs and under different soils. Using numerical simulations, a design that is more robust may be propsed.

Kandelous et al. (2011) used HYDRUS software packages to analyze the soil water content distribution between two neighboring buried emitters. Three geometry approaches were used in their analysis, in which the emitters were represented as 1) point sources in an axisymmterical two-dimensional domain, 2) a line source in a planar two-dimensional and 3) a point source in a full three-dimensional domain. They found that only a full three-dimensional model was able to describe the complex soil water dynamics at all stages of the infiltration processes and to provide accurate simulations of the water content distribution around the buried emitter with multiple drippers.

In this chapter, an alternative design of the ring-shaped emitter was proposed by reducing the number of holes and changing the covering method. The effect of changing the emitter design was evaluated numerically using HYDRUS in a fully three-dimensional spatial domain. Uncompensated and compensated root water uptake models were computed as an indirect quantitative proxy for evaluating the three-dimensional wetted volume around the buried emitter. When water around the emitter is not uniformly distributed, the uniformly distributed roots around the buried emitter may not be able to uptake water at an optimum rate because some parts of the root system are under stress. The root water uptake rate, therefore, can be used as an indirect indicator of how buried ring-shaped emitters of different designs performed compared to the original ring-shaped emitter.

5.2. Materials and Methods

The main objective of this chapter was to numerically investigate the effect of changing ring-shaped emitter designs, especially the number and locations of holes and the permeable textile covering method, on the spatial extent of the wet volume around the buried emitter. In addition to the original ring-shaped emitter with five drilled holes fully covered by the permeable textile, ring-shaped emitters with a reduced number of holes and only partially covered by the textile were considered. Modified emitters with 2, 3, 4, and 5 holes, referred to as 2P, 3P, 4P, and 5P emitters, respectively, were considered in this study. The original ring-shaped emitter is referred to as 5F. Figure 5.1 shows a top view of the five different ring-shaped emitters considered in this study. The grey sections of the ring represent the locations covered with the textile (i.e., permeable sections), while the white sections represent the ring without the textile (i.e., impermeable sections). The partially covered emitters were designed to increase the ease of inspection and maintenance.

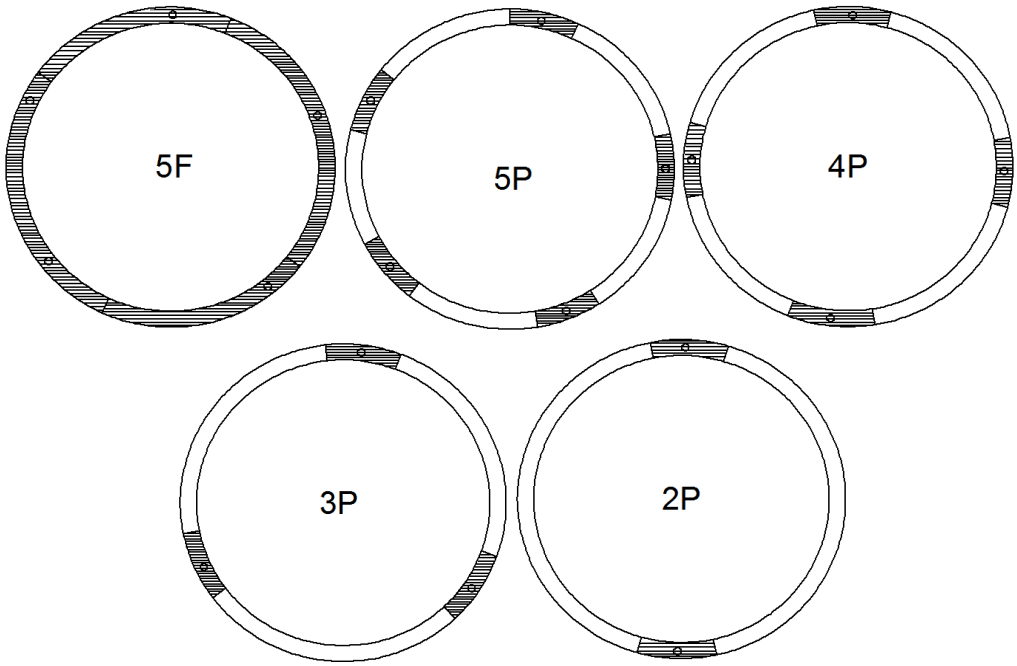

Figure 5.1 Schematics (top views) of different ring-shaped emitter designs. Black sections depict locations of holes covered with permeable textile and white sections depict rubber hoses without cover (i.e., impermeable parts).

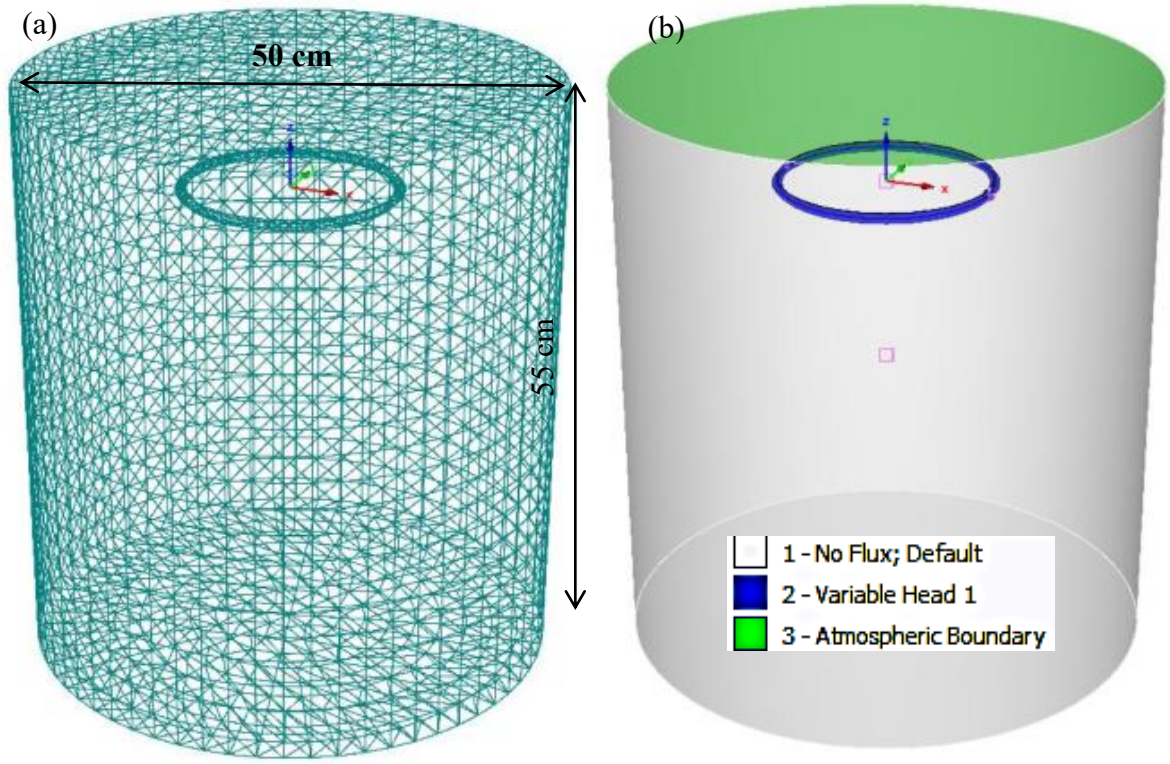

Figure 5.2 (a) A spatial discretization of a full three-dimensional simulation domain, (b) the boundary conditions were used in the numerical analysis of water flow from the buried ring-shaped emitter.

5.2.1. Model Simulation of Soil Water Flow using HYDRUS Full Three-Dimensional Flow Domain

The numerical simulations were carried out in a full three-dimensional domain (Figure 5.2a) so that the asymmetry in the hole configurations of the emitter could be modeled without any simplifications. Three-dimensional (3D) water movement simulation would be more adequate and realistic taking into account the uneven distribution of soil water dynamics in the root zone in many irrigation designs (Sansoulet et al., 2008; Kandelous et al., 2011; Simiunesei et al., 2016). The simulation domain was 55 cm in depth and 50 cm in diameter (Figure 5.2a). The ring-shaped emitter was placed at a depth of 15 cm, similarly as during the experiment (Chapter 4). The three-dimensional simulation domain was discretized into 41,016 triangular prismatic elements with finer elements around the emitter (with sizes of 1 cm) and gradually increasing element sizes farther from the emitter (up to 2.5 cm).

The comparison of wetted volumes around the buried ring-shaped emitters of different designs is not straightforward in the case of three-dimensional simulations. Calculated water contents at particular locations cannot provide sufficient information on the spatial extent of the wetted volumes. In this study, the effect of different emitter designs on the spatial extent of the wetted volume was assessed using the soil water stress a plant would have been exposed to. Assuming that the plant roots are distributed symmetrically around the buried ring-shaped emitter, a non-uniformity in the spatial extent of the wetted volume may cause stress to the plant roots. For example, when some parts of the soil are too dry, the plant roots in these regions cannot uptake water at an optimum rate. The uncompensated root water uptake model was first used to indirectly assess the non-uniformity of the spatial extent of the wetted volume around the buried emitter. The compensated root water uptake model with critical water stress index ($\omega_c = 0.25$) was then used to assess whether such non-uniformity would affect actual plant root water uptake. The simulations were carried out for two soil textures: silt and sand. The soil hydraulic parameters inversely estimated as described in Table 4.2 (Chapter 4) were used in water flow analysis.

5.2.2. Initial and Boundary Condition

The initial soil water content was estimated based on measurement of soil sensor value from the subsurface water flow experiment (Chapter 4). The initial water content value (θ_{in}) was set uniform across the flow domain. The observed average initial water content (θ_{in}) was assigned to the entire flow domain as the initial water content. The average initial water contents were 0.044 $cm^3\ cm^{-3}$ and 0.046 $cm^3\ cm^{-3}$ for silt and sand, respectively.

No flux boundary condition was set at vertical side and bottom of the flow domain (Figure 5.2b). The soil surface (upper domain) was subject to atmospheric boundary condition. The potential evapotranspiration was used to represent the atmospheric boundary condition. A typical potential evapotranspiration (T_p) rate of 6 mm d^{-1} (Shani *et al*., 2007), which corresponds to 720 cm^3 of water per day, was used in the analysis. The time-variable flux/head boundary condition was specified in the nodes representing the ring with the textile (blue dark parts in Fig. 5.2b). The inlet pressure head was kept constant at 1 cm during the water application in all the simulations following the experimental setup (Chapter 4). The graphical description of the boundary conditions adapted to three-dimensional flow in the model is shown in Figure 5.2b.

5.2.3. Root Distribution

Two model plants, tomato and strawberry, were considered in this study because of their contrasting spatial root distributions. It has to be mentioned that both crops are known for their high profitability as it is important to investigate the effectiveness of subsurface irrigation with the ring-shaped emitter for highly profitable crops. Fig.5.3 shows the spatial root distribution based on the Vrugt's model for both tomato and strawberry. The spatial root distribution was considered constant with time during the simulations (i.e., the root growth was neglected). While Table 5.1 summarizes the spatial root distribution parameters for tomato and strawberry, Table 4.2 lists the corresponding parameters of the stress response functions.

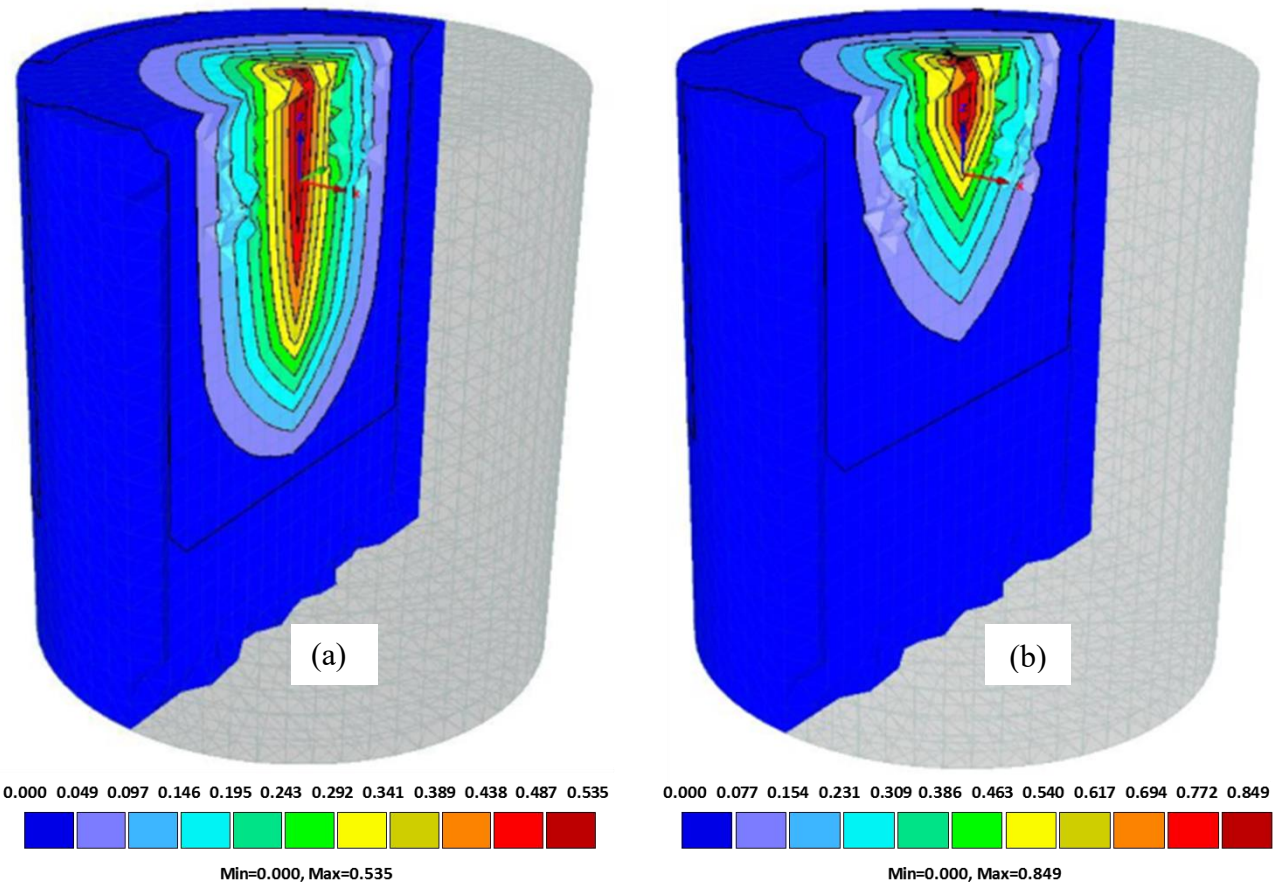

Figure 5.3 Spatial root distributions based on the Vrugt's model (Vrugt et al., 2001) for a) tomato and b) strawberry in a three-dimensional simulation domain. Different colors depict different root densities.

Table 5.1 Parameters describing the spatial root distribution of two model plants (tomato and strawberry) using the Vrugt model (Vrugt et al., 2001).

Parameters	Tomato	Strawberry
Maximum rooting depth, Z_m (cm)	40	30.5
Depth with maximum root density, z^* (cm)	25	5
Maximum rooting radius, X_m (cm)	20	20
Radius of Maximum intensity, x^* (cm)	0	0
Maximum rooting radius, Y_m (cm)	20	20
Radius of maximum intensity, y^* (cm)	0	0
Non-symmetry coefficient, P_z, P_x, and P_y	1, 1, 1	1, 1, 1
Surface area associated with transpiration (cm^2)	1200	1200

Table 5.2 The modified parameters for the stress response function of Feddes et al. (1978) for tomato and strawberry.

Threshold parameters	Value
Tomato	
h_1 (cm)	-10
h_2 (cm)	-20
h_3 (cm)	-100
h_4 (cm)	-150
Strawberry	
h_1 (cm)	-10
h_2 (cm)	-20
h_3 (cm)	-150
h_4 (cm)	-200

5.2.4. Simulation Scenarios

In this numerical analysis, the simulations were conducted firstly with short term simulation for 24 hours (i.e., 1 day) with two soil types, silt and sand, whereas in the second scenario, the simulations were run by considering 7 irrigation cycles. For the short-term simulation, water application was stopped when the predefined amount of water was injected. In this simulation, 720 cm^3 of water was applied daily to meet plant water requirement. The effect of the emitter design was assessed by simulating changes in the soil water content.

In practice, it is important to know the effect of preceding irrigations on the soil water dynamics during subsurface irrigation with the ring-shaped emitter. The simulations were thus also carried out for 504 hours (i.e., 21 days), during which water was applied 7 times (i.e., 7 irrigation cycles). In this numerical analysis, water was applied every three days (i.e., at 0, 72, 144, 216, 288, 350, 412, and 484 hours from the start of simulation). The amount of water applied during each irrigation cycle matched the cumulative potential transpiration of the model plants over 3 days. The inlet pressure head was again kept constant at 1 cm during the water application.

5.3. Results and Discussions

5.3.1. The Effect of Ring-Shaped Emitter Designs on Spatial Extent of Wetted Volume

Figure 5.4 shows simulated cumulative discharges as a function of the elapsed time for different emitter designs computed over 24 hours for initially dry silt and sand when 720 cm^3 of water was applied. For both soils, as expected, the duration needed to reach the same infiltration amount depended strongly on the number of holes. As the number of holes decreased, the duration increased. Although these simulation results show almost constant discharge rates regardless of the emitter design, it has to be mentioned that the emitter discharge rate during subsurface irrigation cannot be kept constant in practice unless a compensated emitter is used.

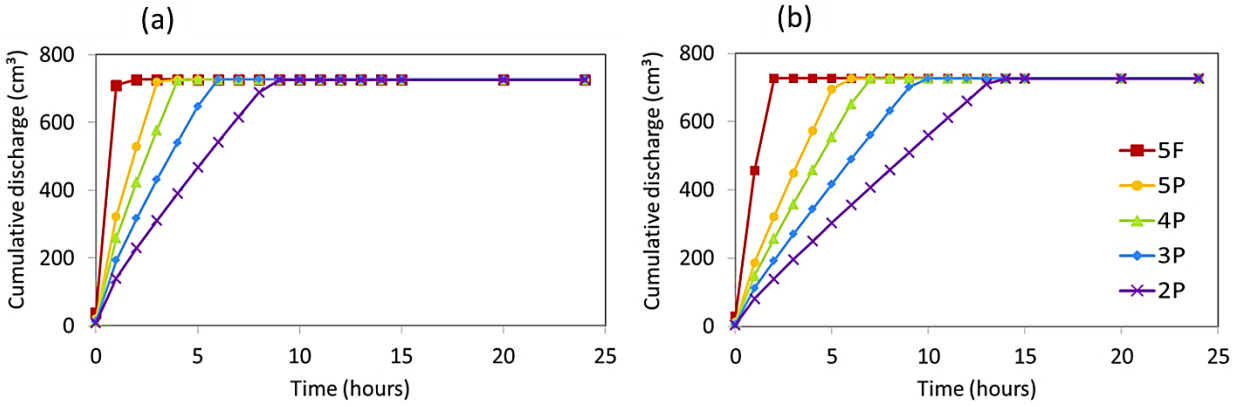

Figure 5.4 Cumulative irrigation discharge computed for different ring-shaped emitters using HYDRUS with the optimized soil hydraulic parameters for silt (a) and sand (b) under tomato cultivation.

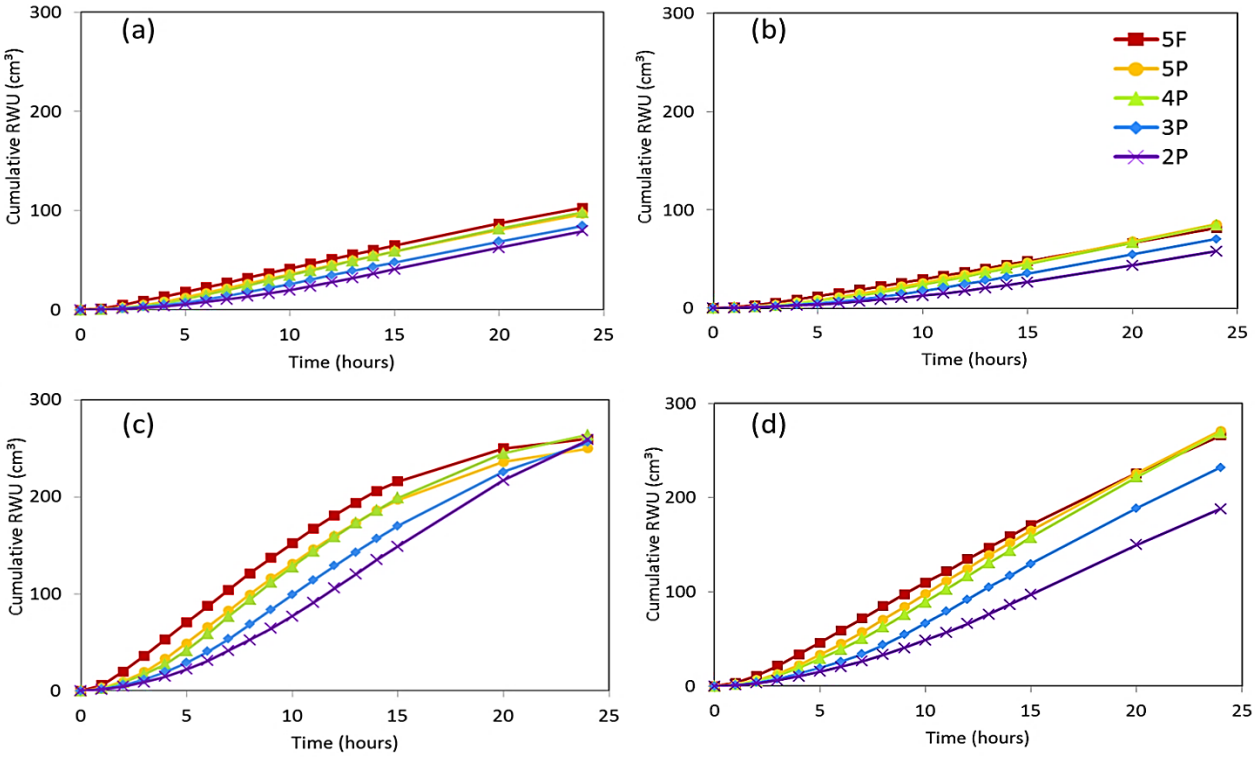

Figure 5.5 Uncompensated (a and b) and compensated (c and d) cumulative root water uptake computed for the buried ring-shaped emitters of different designs using HYDRUS with the optimized soil hydraulic parameters for both silt (a and c) and sand (b and d) in tomato.

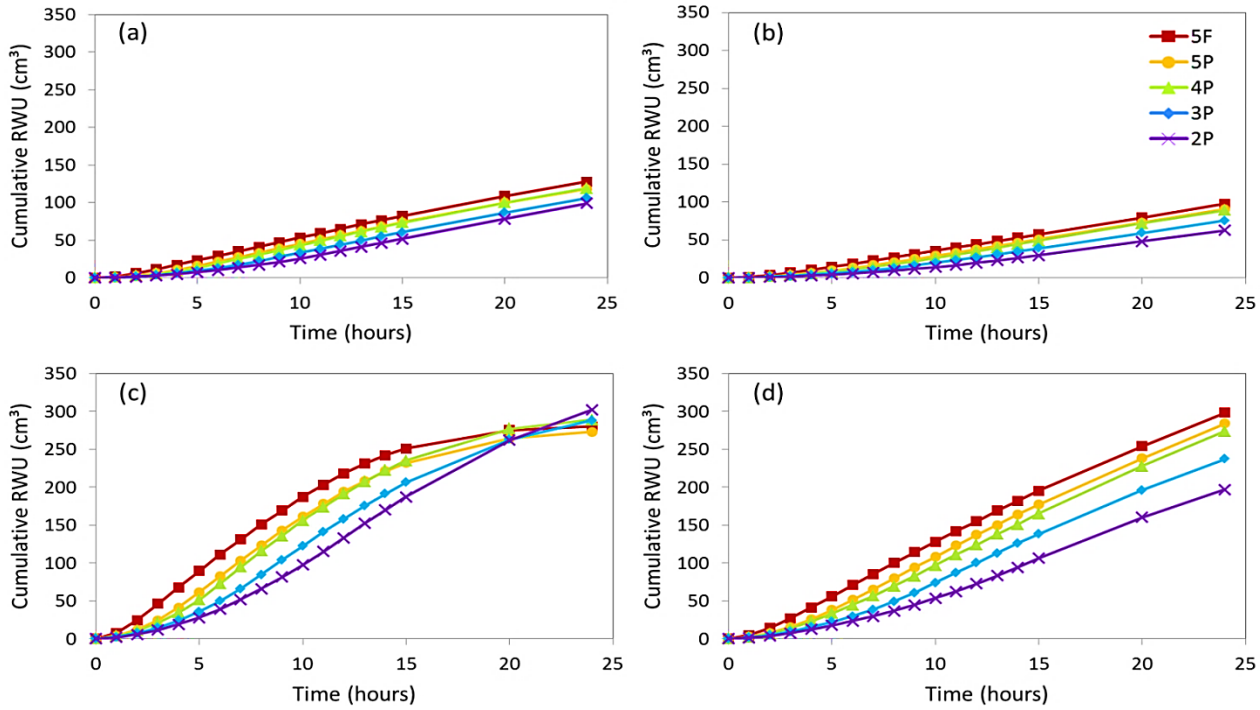

Figure 5.6 Uncompensated (a and b) and compensated (c and d) cumulative root water uptake computed for the buried ring-shaped emitters of different designs using HYDRUS with the optimized soil hydraulic parameters for both silt (a and c) and sand (b and d) in strawberry.

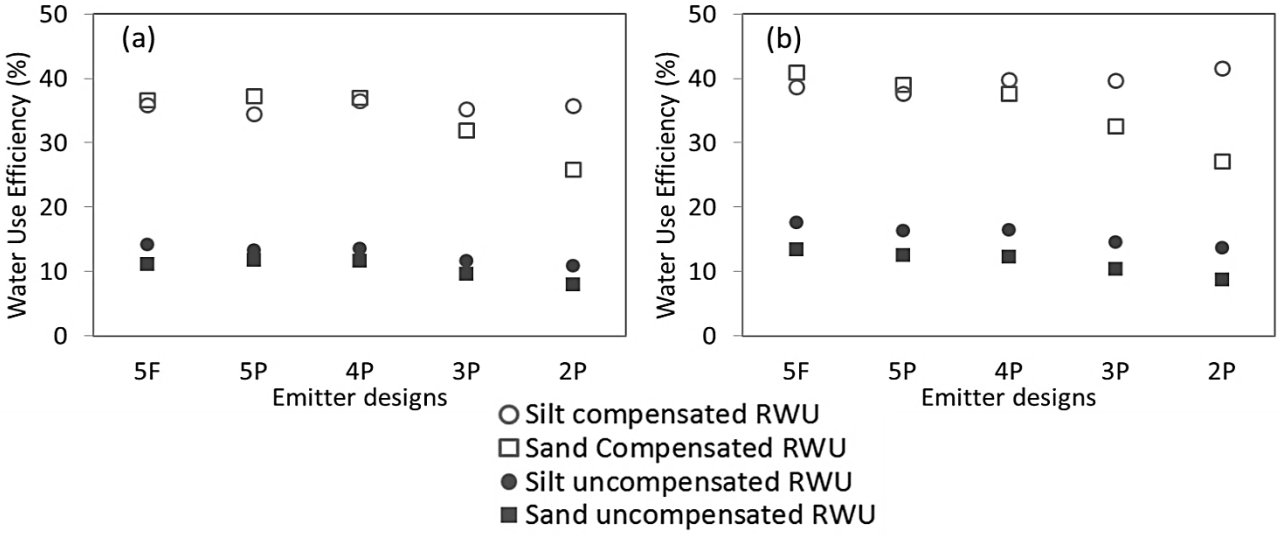

Figure 5.7 Water use efficiency (WUE) computed for emitters of different designs during 24-hour simulation under tomato (a) and strawberry (b) using compensated and uncompensated root water uptake models in HYDRUS.

Figure 5.5 and 5.6 show simulated uncompensated (top) and compensated (bottom) cumulative root water uptake (RWU) of tomato and strawberry over 24 hours in the silt (left) and sand (right) profiles for different ring-shaped emitters. Uncompensated RWU was used as an indirect, quantitative proxy measure of the non-uniformity in the wetted volume around the buried emitter. Compensated RWU was then computed to investigate whether such non-uniformity has any effect on actual plant RWU. The cumulative root water uptake was larger for shallow plant root system (strawberry) than of tomato. This was because the maximum root density located within the top 25 cm of the soil profile for strawberry.

Although uncompensated cumulative RWU in silt increased more slowly when the number of holes was reduced, cumulative uncompensated RWU was almost the same at the end of the simulation for all emitter designs (Fig. 5.5a and 5.6a). Even though the wet volume expanded more slowly with the smaller discharge rate in silt when the number of holes was smaller, uncompensated RWU eventually caught up with those for more holes as the wet volume evolved radially in all directions. As for sand, the initial trend is basically the same as for silt; the higher the number of holes, the higher uncompensated RWU. However, uncompensated RWU computed for the 3P or 2P emitters in sand, unlike in silt, could not catch up with those for 5F, 5P, or 4P after the water application was stopped. It was also observed that the 5F emitter had slightly smaller cumulative RWU after 24 hours compared to emitters that were partially covered (i.e., 5P and 4P). When the ring-shaped emitter with only a small number of holes is used in the sand profile, applied water

tends to move downward rather than radially around the emitter, as predicted numerically in the axisymmetrical three-dimensional domain for sand (Fig. 4.5bd).

Cumulative RWU increased significantly in both soils when the compensated RWU model was used (Fig. 5.5cd and 5.6cd). For silt, while compensated RWU with a smaller number of holes was much smaller than that for the emitter with more holes at earlier time, they were almost the same at the end of simulation for the model plant of tomato. While for strawberry, the cumulative compensated root water uptake kept increasing from the emitter which had fewer holes (i.e emitter 2P) for silt soil (Fig. 5.6c). This can be also seen in the computed WUE for compensated RWU for silt for both model plants (Fig. 5.7). As water was discharged slowly from the emitter with fewer holes, RWU slowly increased. This implies that reducing the number of holes does not affect the amount of water available for plant root uptake over 24 hours in silt. When the compensated RWU model was used for sand, the general trend was the same as for the uncompensated RWU model, except that cumulative compensated RWU was much larger.

The effect of emitter designs on water use efficiency for both types of soil, silt and sand under tomato and strawberry cultivation is summarized in Figure 5.7. In this study, the percentage of water transpired by plants to the total irrigation water was used for water use efficiency (WUE). In other words, WUE can be computed as the ratio of cumulative RWU to cumulative irrigation at 24 hours. WUE for both compensated and uncompensated RWU were computed. For silt, even though the number of holes decreased, WUE for the uncompensated RWU stayed almost constant for both plants. WUE increased for the compensated RWU as the number of holes decreased. On the other hand, for sand, WUE is at its peak when the ring covering method was changed from full cover to partially cover with 5 drilled holes (i.e., emitter 5P). The difference between silt and sand again can be attributed the difference in macroscopic capillary length of the soil as described in previous chapter (i.e., Section 4.4.1). As for silt soil, which has a higher capillary length allows plant roots to uptake water slowly in the zone of maximum root density where water moves radially from the emitter with fewer holes.

5.3.2. The Effect of Preceding Irrigation on Root Water Uptake

The effect of preceding irrigations was then assessed for different emitter designs by computing uncompensated and compensated cumulative RWU over 21 days (i.e., 504 hours), during which seven irrigation cycles were considered for cultivating tomato. Figure 5.8 depicts the cumulative irrigation discharge which meets the plant water requirement (i.e., potential

transpiration, Tp) for different emitter designs. Figure 5.9 shows the effect of emitter designs on cumulative uncompensated and compensated root water uptake.

For uncompensated RWU (Fig. 5.9ab), root water uptake was much lower in sand as compared to silt soil for all emitter designs. This difference was attributed to limited water-holding capacity in sand soil causing a faster downward movement of water when irrigation cycle was increased. As a result, plant roots could not extract water during the period between the two successive irrigation events, while the part of water that exceeded the soil water holding capacity percolated to the deeper soil layers by gravitation. Selim at al. (2012) reported the rate of root water uptake in sandy soil was less than that in other soil because of the rapid downward movement of water below the zone of maximum root density by gravitational force and the limited upward movement of water by capillarity. These simulation results clearly confirmed that sand soil had a low uniformity of soil water distribution compared to silt soil. When uncompensated RWU model was used, some parts of the root system were stressed due to the non-uniformity in the wet volume. The low uniformity of the wet volume led to the reduction of actual transpiration (i.e., actual cumulative root water uptake) in soil domain (Simionesei et al, 2016).

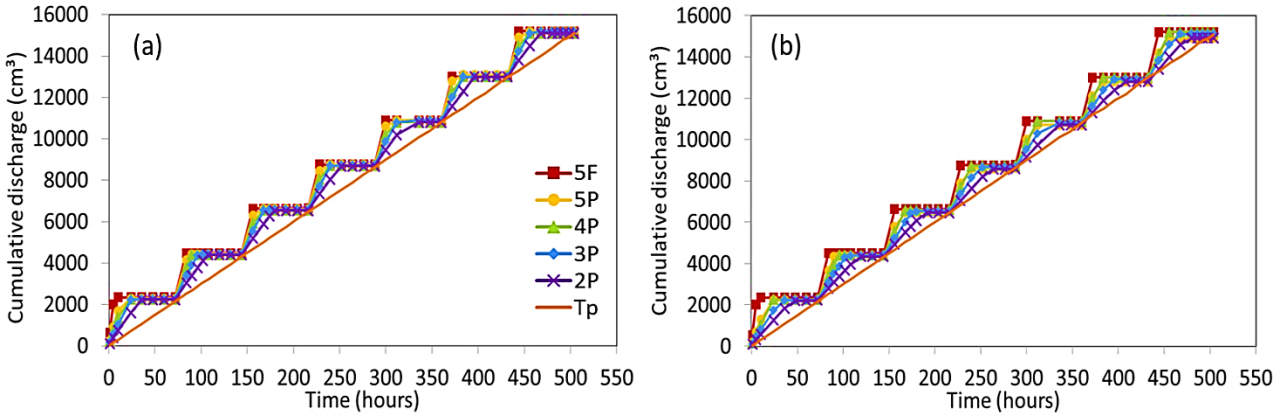

Figure 5.8 Cumulative infiltration computed for different ring-shaped emitters using HYDRUS with the optimized soil hydraulic parameters for silt (a) and sand (b) under tomato cultivation with seven irrigation cycles over 21 days.

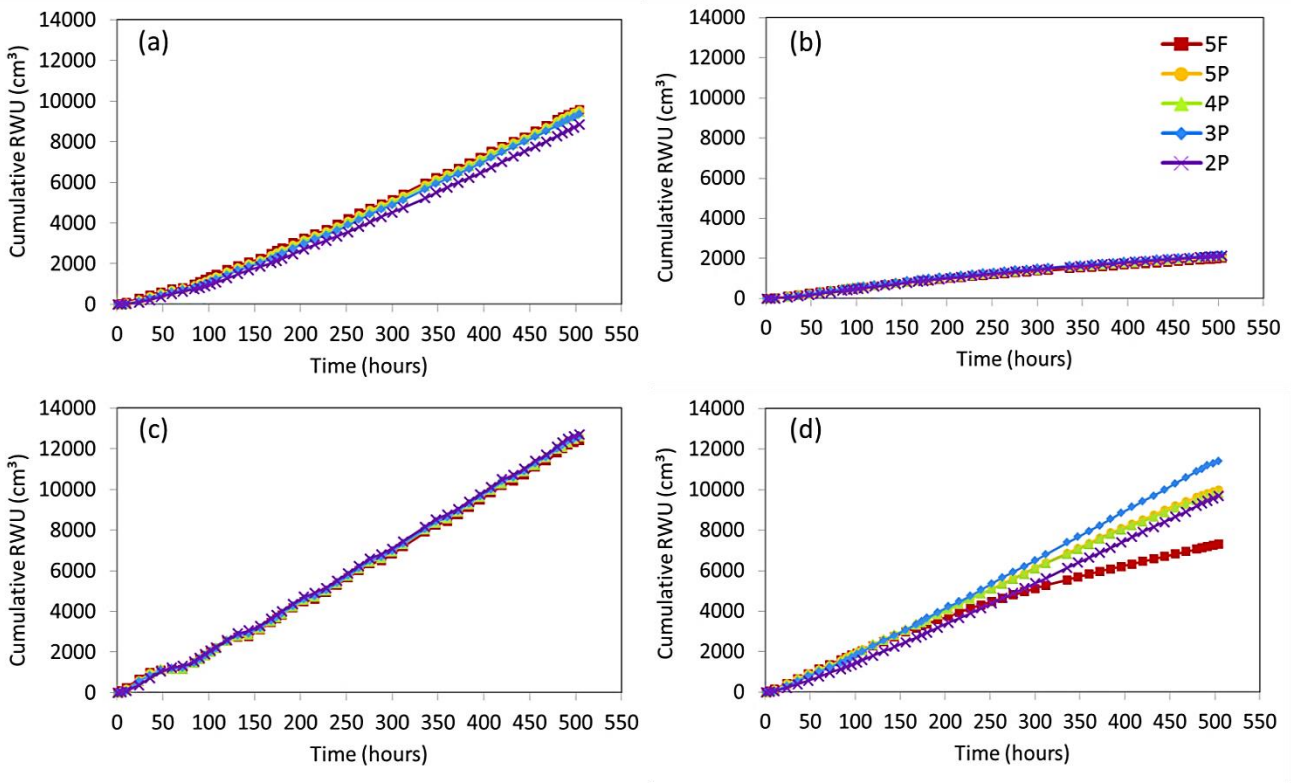

Figure 5.9 Cumulative infiltration computed for different ring-shaped emitters using HYDRUS with the optimized soil hydraulic parameters for silt (a) and sand (b) under tomato cultivation with seven irrigation cycles over 21 days.

Cumulative compensated RWUs after 21 days for different emitter designs were almost the same for silt. On the other hand, for sand, cumulative compensated RWU is strongly affected by the emitter design. For 5F, unlike the 24-hour simulation case shown in Fig. 5.6d, cumulative RWU starts being reduced after 8 days, while cumulative RWUs computed for the emitters with fewer holes continuously increase. At the end of the simulation, simulated cumulative RWU for 3P reaches the highest value, thus the highest WUE, among different evaluated designs. For 5F, the water application rate was too high for plant roots to uptake. As a result, there was a significant amount of water lost to deep percolation. For the emitters with fewer holes, the water application rate was smaller and consequently that there was much less water lost to deep percolations even for sand. In summary, these simulation results confirm that the number of holes can be reduced to 2 or 3 regardless of the soil types considered in this study.

5.4. Summary

With the optimized soil hydraulic parameters, HYDRUS was used to investigate the effects of alternative emitter designs on the spatial extent of the wet volume around the buried emitter during the subsurface water application. In this analysis, plant root water uptake was used as an indirect, quantitative proxy measure to assess the non-uniformity in the spatial extent of the wet volume around the emitter. Had the spatial distribution of the SWC been non-uniform, some parts of the plant root system would have been stressed, resulting in the reduction in root water uptake. Two model plants, tomato and strawberry, were considered because of their contrasting spatial root distributions. Both uncompensated and compensated RWU were computed. While the former was used to assess the non-uniformity in the spatial extent of the wetted volume, the latter was used to investigate whether such non-uniformity had any effect on the plant root water uptake.

In addition to the original 5-holes ring-shaped emitter that was fully covered by a permeable textile, four alternative emitter designs with a different number of holes were analyzed. The new emitter proposed in this study was only partially covered by the textile around the holes to simplify the maintenance of the emitter. Numerical simulations with these alternative emitter designs showed that the lower number of holes did not significantly affect uncompensated RWU in silt. However, in sand, cumulative uncompensated RWU decreased when the emitters with reduced number of holes were used in the initially dry soil, suggesting non-uniformity in the wet volume. The non-uniformity in the wet volume in silt for the emitter with fewer holes was not significantly different because water moved radially from the emitter, diminishing the effect of the spatial hole configuration. For sand, on the other hand, the non-uniformity in the wetted volume was larger, as indicated by uncompensated RWU.

Such non-uniformity in the wetted volume does not affect the long-term performance of the ring-shaped emitter with fewer holes even for silt soil because of the slow discharge rate. On the other hand, simulated compensated RWU showed that reducing the number of holes in sand significantly increased RWU when preceding irrigation was considered. As water slowly infiltrated from emitter which had few holes allowed plant roots to uptake water continuously.

These results show that, regardless of the soil type, reducing the number of holes and changing the covering method may result in a much better water use efficiency and easier maintenance. Overall, this study demonstrates that HYDRUS is a useful tool for analyzing soil water dynamics around the buried ring-shaped emitter during the subsurface water application.

Chapter 6. Performance of Ring-Shaped Emitter on Yield and Water Productivity of Bell Pepper (*Capsicum annum* L.)

6.1. Introduction

Efficient irrigation water use is important in arid and semi-arid regions where water supply is limited in supporting agriculture production. Soil water dynamics in the root zone under various environmental and crop systems are very complex and its understanding is critical for optimizing irrigation management. Thus, it is necessary to investigate soil water dynamics around buried ring-shaped emitters under such condition by considering several factors including crop management system as well as root distribution and crop water requirement in agro-climate conditions to enhance promoting ring-shaped emitters for subsurface irrigation to obtain higher water use efficiency.

A proper emitter design and effective water management are crucial in developing water-saving agriculture. In the previous chapter, an alternative ring-shaped emitter design (Saefuddin *et al*., 2018) was proposed by reducing the number of holes and changing the covering method. For modified ring-shaped emitter designs, the number of holes was reduced from 5 holes, which was originally used, to 2 holes to improve water use efficiency and was partially covered only around the holes for easier maintenance and repairing. The performance of the original and alternative ring-shaped emitter designs was evaluated numerically using HYDRUS 2D/3D software package (Šimůnek *et al*., 2016) under various soil types. In the numerical analysis, the effect of different emitter configurations on the evaluation of wet volumes around the emitter was assessed using soil water stress to the plant roots. Therefore, root water uptake was computed as an indirect indicator of how well the ring-shaped emitter distributed water around the emitter uniformly to the root zone. As a result, regardless of the soil type, the number of holes can be reduced from original 5 holes to 3 or 2 holes. The emitter with new hole configuration resulted in higher water use efficiency and provided a proper condition for plant roots to uptake water in the root zone. The emitter was partially covered with a permeable textile to simplify the repairing and maintenance.

Yield production is dependent on the amount of irrigation water and irrigation frequency. Bell pepper (*Capsicum annum* L.) is one of the most susceptible crops to water stress in horticulture (Ferarra *et al*., 2011). Costa and Gianquinto (2002) reported that continuous water stress significantly reduced the total fresh weight of fruit, while Antony and Singandhupe (2004)

concluded that the total pepper yield was poor at lower amounts of irrigation. Inappropriate irrigation schedule and management could result in water stress for the plant. Therefore, the precision irrigation is crucial to meet crop water requirement. In addition, soil water storage and soil water distribution in the root zone are one of the main factors to optimize irrigation. A better understanding of root density and distribution pattern and root water uptake under subsurface irrigation will allow for a more accurate simulation of soil water distribution for plants.

Numerical simulation of water flow and plant root water uptake can help in understanding dynamic process of soil water during irrigation. Because of the reliability and flexibility of HYDRUS 2D/3D to accommodate different types of boundary conditions and root water and nutrient uptakes, and because of its ease to use due to a graphical user friendly interface, the model has been widely and successfully used to investigate and evaluate the designing subsurface irrigation management practices involving a wide range of crops (Ityel *et al*., 2011; Bufon *et al*., 2012; Kandelous *et al*., 2012; Lila *et al. 2013;* El-Nesr *et al*., 2014; and Ghazouani *et al.* 2015). In previous chapters, HYDRUS has been used with a full three-dimensional flow domain to evaluate the effect of modifying the ring-shaped emitter design for subsurface irrigation without considering plant cultivation, e.g., crop growth, (Saefuddin *et al*., 2018). Therefore, experimental validation of the HYDRUS model by considering crop cultivation is needed to explore if subsurface irrigation with the ring-shaped emitter is suited for the real field conditions.

With these backgrounds in considerations, comprehensive experimental and simulation investigations were carried out under glass-house bell pepper cultivation. The main objectives of this chapter were 1) to investigate experimentally and numerically water dynamic around the buried ring-shaped emitter during bell pepper cultivation, and 2) to evaluate the performance of the ring-shaped emitter in terms of water productivity and irrigation water productivity. Initially, the simulated soil water contents and the measured soil water content in the cultivation experiments were compared to validate the performance of the HYDRUS three-dimensional model in simulating soil water movement around buried ring shaped-emitter. Then, parameters of the root water uptake model were computed to evaluate how well the ring-shaped emitter provided appropriate soil water in the root zone. Since a new version of the HYDRUS software package (Šimůnek *et al*., 2018) has been released recently that allows simulating plant root growth to characterize the actual of root water uptake, the observed plant growth data can be modeled for more comprehensive analysis. The results of the simulations were finally compared in terms of the ratio between actual transpiration

and the total amount of irrigation water, during the entire growing season, in other words in terms of water use efficiency.

6.2. Crop Water Consumption

Crops need water for transpiration. The plant roots uptake or extract water from the soil to live and grow. The main part of this water does not remain on the plant but escapes to the atmosphere as vapor through leaves and stems. This process is called transpiration**.** Transpiration happens mainly during the daytime. Water from an open water surface escapes as vapor to the atmosphere during the day. The same happens to water on the soil surface and to water on the leaves and stem of a plant. This process is called evaporation. The water need of a crop, thus consists of transpiration plus evaporation. Therefore, the crop water need is referred to as **"evapotranspiration".**

The potential evapotranspiration is defined as the value of evapotranspiration when soil is sufficiently wet, which is affected by atmospheric conditions such as net radiation, wind speed, air temperature and relative humidity. The value of the evapotranspiration usually ranges from 3 to 6 mm per day for summer crops in temperate-monsoon areas (Miyazaki et al., 1993).

Crop evapotranspiration (ET_c) is influenced by crop growth stages, environmental conditions and crop management. The crop water requirement (CWR) is the sum of ET_c for the entire crop growth period. When management or environmental conditions deviate from the optimal condition, the rate of evapotranspiration has to be adjusted to the prevailing conditions and is called *adjusted or actual crop evapotranspiration* (ET_c). Both *CWR* and ET_c concepts apply to either irrigated or rainfed crops.

For irrigated crops, the concept of *CWR* has to be complemented by that of an *irrigation water requirement* (*IWR*), which is the net depth of water [mm] required by a crop to fully satisfy its specific crop water requirement. The *IWR* is the fraction of *CWR* not satisfied by rainfall, soil water storage and groundwater contribution. When it is necessary to add a leaching fraction to assure appropriate leaching of salts in the soil profile, this depth of water is also included in *IWR*. In practice, *IWR* has to be converted into gross irrigation requirements to take into consideration the efficiency of the irrigation systems utilized.

In crop management practices, crop water requirement can be used as a guide to determine the balance between the amount of extractable soil water available for the crop and the amount of water needed to be supplied at a particular growth stage. In a wet soil, as water has a high potential

energy, it is relatively free to move and is easily taken up by plant roots. In a dry soil, however, as water is bound by capillary and absorptive forces to the soil matrix, it is less easily extracted by crop plants. When the potential energy of the soil water decreases to a threshold value (usually, the lower limit of plant extractable soil water), the crop is unable to extract the water from the soil and becomes water stressed.

Doorenbos et al. (1992) defined crop water requirements are the depth of water needed to meet the water loss through evapotranspiration (ET_c) of a disease-free crop. To calculate ETcrop a three-stage procedure is recommended by Doorenboos et al. (1992):

1. The effect of climate on crop water requirements is given by the reference crop evapotranspiration (ET_o). ET_o is expressed in mm per day and represents the mean value over the period based on the type of climatic data available. The most common method to calculate the reference evapotranspiration is based on the Penman-Monteith equation (Allen et al., 1998).
2. The effect of the crop characteristics on crop water requirements is given by the crop coefficient (*Kc*) which presents the relationship between reference (ET_o) and crop evapotranspiration (*ET*) or ETcrop = $Kc \; . \; ET_o$. Values of Kc vary with the crop, its stage of growth, growing season and the prevailing weather conditions. The unit of *ETc* is in mm day^{-1}.
3. The effect of local conditions and agricultural practices on crop water requirements includes the local effect of variations in climate over time, altitude, size of fields, advection, soil water availability, salinity, and method of irrigation and cultivation methods and practices.

6.3. Distribution of Plant Roots

Different irrigation systems influence root development by changing the availability of water at different depths in the soil profile. A healthy root system is essential for all crops because it facilitates the uptake of water and nutrients. Considering of the root zone at various stages of crop growth is important to determine the amount of irrigation depth and frequency. Shallow rooted crops can only extract water from a limited depth and may require short and frequent irrigations. Deep rooted plants, on the other hand, are able to extract water from deep down, but can be prone to root disease if the subsoil becomes saturated (Hillel, 1980).

One possible reason for the difference observed between the responses of pot-grown and of field-grown plants to the soil-water regime is the difference in root distribution with depth. In a pot,

root density can be fairly uniform, while in the field, it generally varies with depth. Furthermore, the roots present in different layers maybe exhibit different water uptake and transmission properties. For instance, the roots in the deeper layers may offer greater resistance to water movement within the plant than the roots of the upper layer (Hillel. 1980).

Rooting depth can be determined by digging out the whole plant, shaking the soil off or digging a soil pit and then measuring the depth of the root system. Rooting depth and depletion fraction (p), which is the fraction of total available water that can be depleted from the root zone before moisture stress occurs, are vital factors in determining how much water should be applied. The distribution of RWU in the soil profile is greatly affected by the spatial-temporal root distribution. More specifically, RWU is generally assumed to be a direct function of root length densities (RLDs) (Feddes et al., 2001). In order to represent the interactions between root development and soil water status, the dynamics of root distributions need to be properly accounted for (Krounbi and Lazarovitch, 2011). Direct measurements of RLD distributions and their temporal dynamics are important additional information that can be used to constrain other parameters related to stress and water uptake compensation functions in RWU models (Cai et al. 2017).

Root length density is defined by either the length per unit volume of soil [cm cm^{-3}] or the length per unit surface of soil [cm cm^{-2}]. The former is used to determine the root length distribution with depth, and the latter is used to determine the amount of roots per unit ground surface or crack surface. Root development influenced by the water supply (Miyazaki et al., 1993). Soil water uptake under different soil moisture regimes is a function of root growth, where under unfavorable soil water conditions plants improve their ability to increase water uptake by extensive root growth and proliferation in the soil matrix. In this regard, spatial and temporal variations of soil water content, soil texture, and soil structure have major impacts on root growth and distribution in soil matrix (Dexter, 2004).

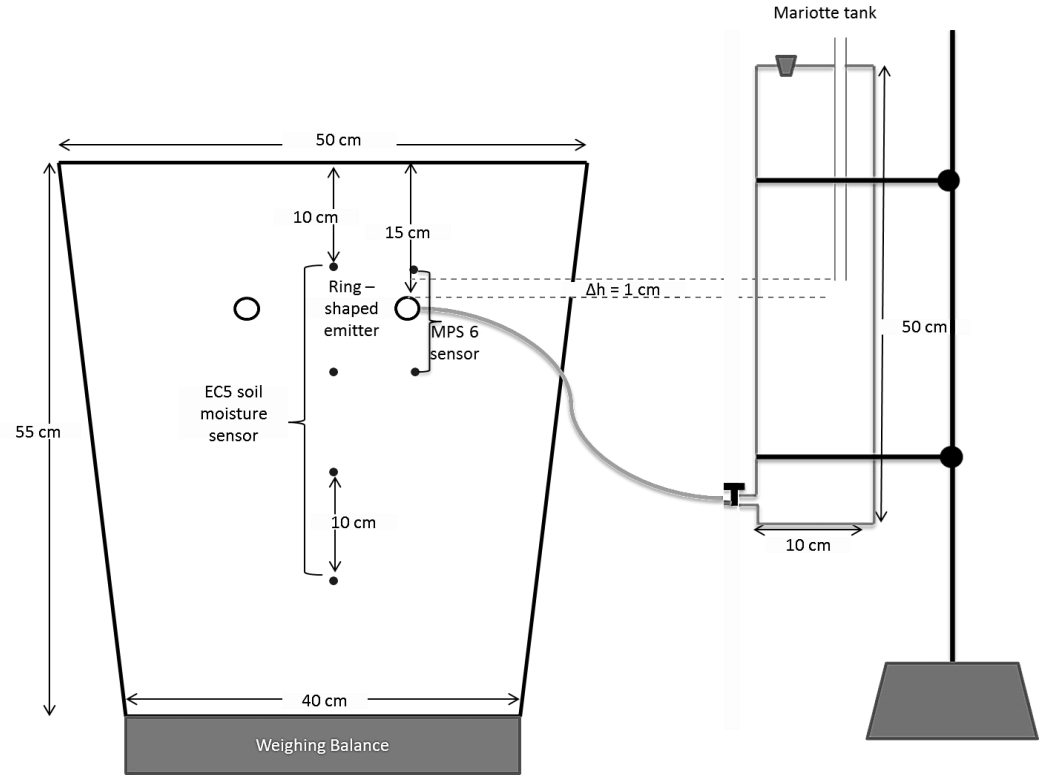

Figure 6.1 A cross-section view of the experimental set-up, showing the soil moisture sensors location.

Figure 6.2 Schematic presentation of bell pepper cultivation in a glass-house; a) Packing air dry andisol soil, b) Saturated ring-shaped emitter, c) transplanting bell pepper, d) monitoring bell pepper growth.

6.4. Materials and Methods

6.4.1. Cultivation Experiment

A glass-house experiment was carried out from June to November 2017 at the Agriculture experimental field of Tokyo University of Agriculture and Technology, Fuchu Campus. Bell peppers (*Capsicum annum* L.) were planted in the pots, which was filled with andisol soil as shown in Figure 6.1. Soil samples were taken from two depths (5-10, and 15-20) in the Saikaicho experimental field before the start of the experiment to obtain soil physical properties. The analysis revealed that the average bulk density was 0.74 g cm^{-3}. Bell peppers were transplanted 3 weeks after seeding. Figure 6.2 shows the preparation and experimental set-up of bell pepper cultivation in a glass-house. Before transplanting, Andisol collected from the field were sieved and cleaned from the roots, air dry soils were then placed in the pot with a 5-cm increment. Each addition was manually packed with a steel plate giving the predetermined bulk density of 0.74 g cm^{-3}.

Two designs of ring-shaped used in this study as comparison purpose, The first design was an original design that consisted of 5 small-holes and was covered entirely by a permeable textile (referred to emitter 5F), while a newly designed ring-shaped emitter had 2 holes and was covered partially only around the holes (referred to emitter 2P) are shown in Fig.6.3. For each pot, the ring-shaped emitter was placed at a depth of 15 cm and connected to the Mariotte tank to control the water pressure head applied at the inlet of the buried emitter (referred to as the inlet pressure). In this study, 1 cm constant pressure head was maintained for 2 hours to apply water through the ring-shaped emitter. During the experiments, the volume of water in the Mariotte tank was recorded every 10 minutes to obtain the emitter discharge rate.

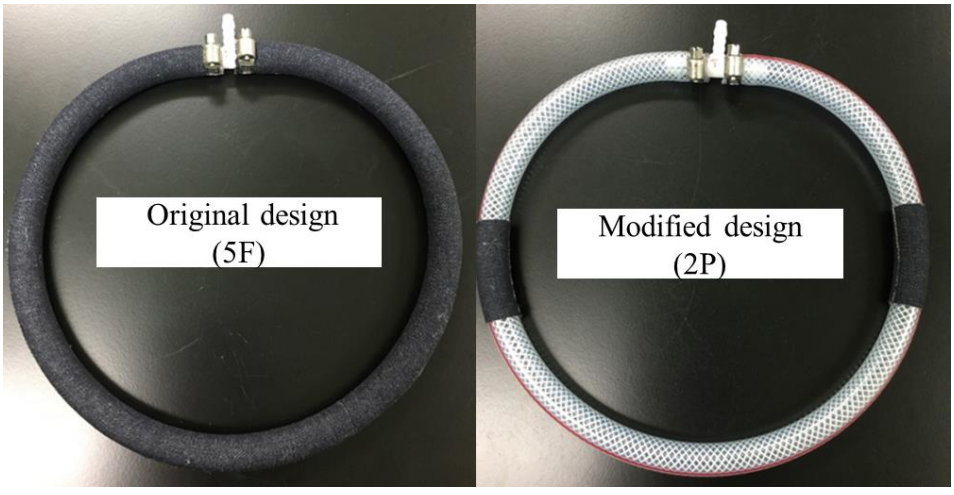

Figure 6.3 Ring-shaped emitter design used in the study.

6.4.2. Soil Water Content and Weather Monitoring

Meteorological data, including solar radiation, air temperature, and relative humidity and wind speed were monitored inside of the glass house using a set of meteorological sensors. Data were recorded at 1-h intervals, stored in data logger EM50, a product of METER environment, and regularly downloaded. Reference crop evapotranspiration (ET_o) was calculated using the Penman-Monteith equation (Allen et al., 1998). An electronic balance was used to measure the change in soil and plant mass in order to obtain the actual crop transpiration.

The soil water content (SWC) was measured using soil moisture sensors, 5TE and EC5 (product of Decagon). Two soil moisture sensor 5TE were installed at each a depth of 10 cm and 20 cm, while 2 EC5 sensors were installed at a depth of 30 and 40 cm. All soil moisture sensors were positioned at the center of the ring-shaped emitter (Figure 6.1). Sensor measurements were recorded in data logger EM50 and regularly downloaded. The observed SWC values at different depths were compared with the corresponding SWC values simulated by HYDRUS 2D/3D.

6.4.3. Laboratory Measurement of Soil Hydraulic Properties

At the beginning of the experiment, both disturb and undisturbed soil samples were collected from field experimental site of Saiwaikacho for the laboratory measurement of soil bulk density (BD), saturated hydraulic conductivity (Ks) and water content (θs). Undisturbed soil samples were taken using soil cores with a diameter of 5 cm and 5 cm in height from two representative layers (5-10 cm and 15-20 cm) to measure the dry bulk density (BD). The value of measured BD is listed in Table 6.1. Ks value of the disturbed soils was determined using a falling head method (Klute et al., 1986). The soil cores were first saturated from the bottom and then submerged in water for 24 h. After weighing, the saturated soil samples were dried at 105 °C to constant mass, and their mass-based saturated SWC was determined. θs values were determined by multiplying saturated mass-based soil water content with BD. Collected disturb soil samples from the field was used to determine soil water retention curve using pressure plate apparatus following the procedure by Richards (1942).

Table 6. 1 Bulk density

Depth (cm)	Core sample number	Bulk density (g cm^{-3})
5 – 10	C2	0.68
5 – 10	15	0.65
5 – 10	E6	0.55
15 – 20	53	0.88
15 – 20	A27	0.77
15 – 20	29	0.9
	Average	0.74

6.4.4. Root Sampling and Yield Measurements

Data about the horizontal and vertical distribution of plant root growth were obtained after breaking down of the pot at three different times as well as on August 25, October 11 and November 3. Resulting the maximum root depth and maximum radius at regular times in excavated transect was described in Table 6.2, while Figure 6.4 shows the root distribution of bell pepper.

Root sampling was conducted at the end of cultivation for each plant pot of where emitter 5F and 2P were installed in order to describe plant root distribution parameters for HYDRUS calculation. Following the sampling procedures of Mommer et al. (2017), a plant pot was divided into four quadrants. Soil cores with a diameter of 5.1 cm and height of 5 cm were inserted in every depth, from 0-5 cm down to 45 cm at 5-cm increments at each quadrat. The cores were taken to the laboratory and the roots were washed and separated from the soil. The clean roots were then digitized for root lengths and diameter using the root system scanner (perfection4870photo, Epson, Japan). The root lengths were analyzed with WinRHIZO software. The root length density at different depths was calculated by dividing the root length and the sampled soil volume (cm cm^{-3}) (Gao et al. 2010). The average of the root length density measurements was used an input in HYDRUS-2D/3D during the simulation period.

Table 6.2 Bell pepper root growth

Period of measurement	Maximum radius of root (cm)	Maximum root depth (cm)
25 August, 39 Days	18.	28
11 October, 47 Days	23	32
3 November, 23 Days	25	35

Figure 6.4 Root distribution of bell pepper after breaking down the pot.

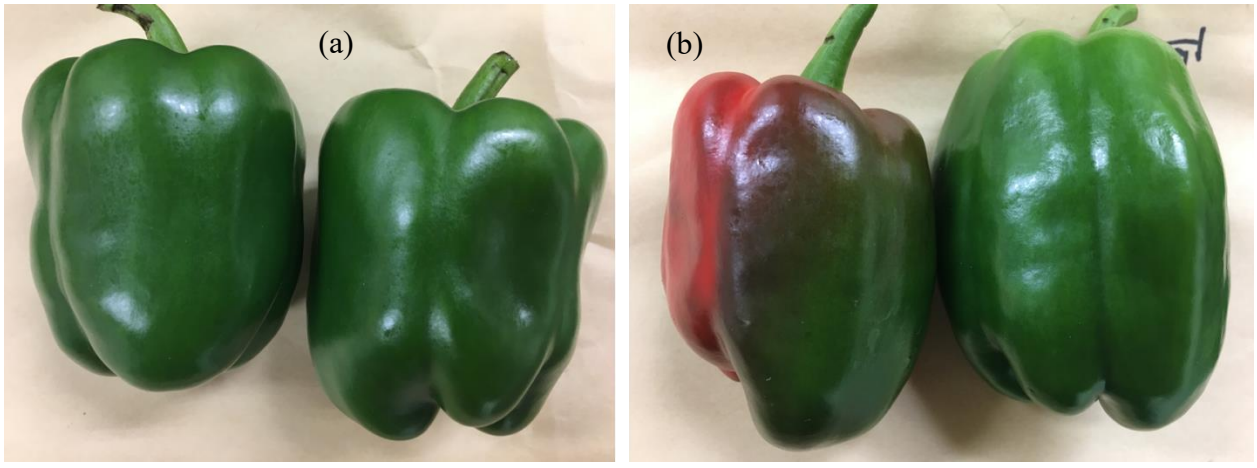

Figure 6.5 Harvested bell pepper fruits from emitter 5F (a) and emitter 2P (b).

Bell pepper fruits were hand harvested at 109 days after transplanting (DAT). Fruit diameters, lengths, and dry weights were measured for 2 fruits randomly selected per plant (Fig. 6.5). Fruit samples were then dried at 65^{o}C until the constant weight was obtained (3 days). After harvesting, the plants were cut off for measuring the dry aboveground biomass. Biomasses were dried at 80^{o}C to a constant weight. Water productivity (*WP*) and irrigation water productivity (*IWP*) were calculated by dividing the bell pepper fresh yield (kg/plant) with the crop evapotranspiration (ET_c) or with the total irrigation water applied as shown in Equations (2.3) and (2.5), respectively.

6.4.5. Irrigation and Fertigation

Irrigation of bell pepper started on the first day after transplantation where the soil profile remains relatively dry. This was evident from the initial soil water content data of soil profile based on soil moisture sensor measurement which varied from 0.098 – 0.132 $cm^3\ cm^{-3}$ in a pot which the emitter 5F was installed and 0.089 – 0.136 $cm^3\ cm^{-3}$ in a pot which the emitter 2P was installed. Irrigation was not uniformly scheduled during cultivation. Irrigation water was supplied every day in the first week after transplanting and approximately once in every 4 days during the crop full development stage. A total of 20 irrigation events was applied during cultivation.

Fertigation was initiated after bell pepper was in an establishing growth period (25 Days After Transplanting, DAT). Fertigation was performed for 2 hours every 2 weeks using liquid fertilizer with concentration of 22 cm^3 per 10-liter of water. Fertilizer consisted of 13 % nitrogen and 38% potassium, resulting in total of 6 fertigation events were applied during the crop growth season.

A glass-house experiment was conducted to collect two type data. First to gather the necessary input data to execute the HYDRUS-2D/3D model, and second to collect data used to test the model by comparing the measured and simulated values of soil water content.

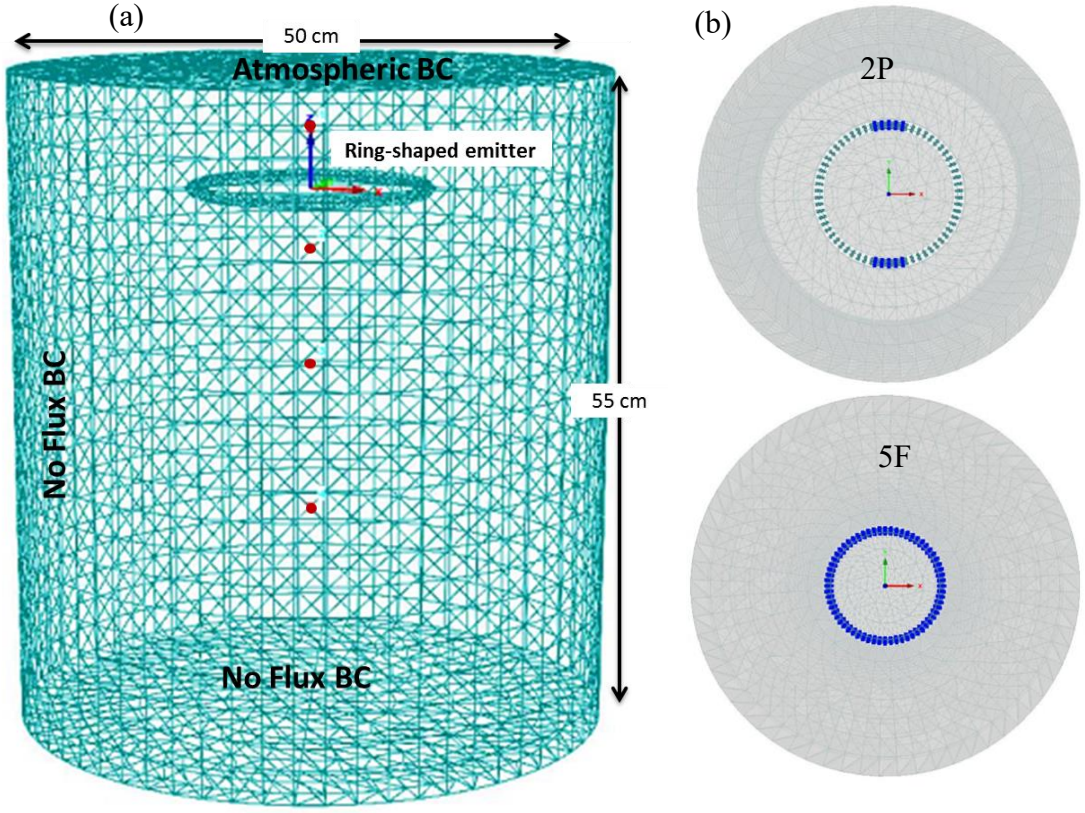

Figure 6.6 a) A schematic view of the simulated three-dimensional flow domain, displaying boundary conditions, spatial discretization, and the position of the ring-shaped emitter and observation nodes that correspond to soil moisture sensor locations; b) variable head boundary condition was imposed at the emitter where blue dark parts represent ring-shaped emitter with permeable textile cover, while light parts represent impermeable (without cover).

6.4.6. Numerical Simulation of Water Flow and Root Water Uptake during Cultivation

The main objective of this study is to evaluate the effects of the ring-shaped emitter design on soil water content distribution and root water uptake during subsurface water application during bell pepper cultivation. The HYDRUS software package version 3.0 (Šimůnek et al., 2018) was used to analyze collected experimental data since the software has been successfully used to simulate soil water dynamic around the buried emitter in various irrigation scenarios and crop management (Lazarovitch et al., 2005; Kandelous et al., 2012; Bufon et al., 2012; El-Nesr et al., 2014 and Ghazouani et al., 2015). The model additionally allows specification of root water uptake and root growth, which affect the spatial distribution of water between irrigation cycle.

In the cultivation experiment, a newly designed ring-shaped emitter with partially covered by permeable textile only around the hole was used. Therefore, asymmetry in hole configurations are required to be modeled in a fully three-dimensional flow domain to void over simplification.

The three-dimensional transport geometry used for the calculation is shown in Figure 6.6a. The depth of the transport domain was 55 cm and its diameter was 50 cm. The three-dimensional flow domain was discretized into 11,595 nodes, which corresponded to 41,016 three-dimensional triangular prismatic elements with very fine grid around the emitter (with sizes of 1 cm) and gradually increasing element sizes farther from the emitter (up to 2.5 cm). Four observation nodes, corresponding to the locations where volumetric soil water content sensors were installed, were placed in the center of emitter at a depth of 10, 20, 30, 40 cm from the soil surface. The initial soil water content was estimated based on the soil moisture sensor measured values from the plant pot after air-dried Andisol soil was packed into the pot. We assumed that initial soil water content was uniform in the entire flow domain at the average content of 0.121 $cm^3\ cm^{-3}$. The simulation was carried out for 109 days, corresponding to the experimental period.

In simulation, the "No-Flux" boundary condition was set at along vertical sides and bottom of the transport domain, while the "Atmospheric" boundary condition was specified in the top domain. The ring-shaped emitter was represented as a doughnut shape with a diameter of 20 cm, located in the center of the transport domain at a depth of 15 cm. The "Time-variable pressure head" was imposed in the nodal points representing the ring-shaped emitter covered with the textile (dark blue parts in Figure 6.6b). It should be noted that, water pressure head of 1 cm was kept constant at the inlet of the emitter during subsurface irrigation in the experiment. A constant pressure head boundary condition was switched to no flux boundary condition during periods without irrigation.

HYDRUS requires daily estimates of potential evaporation (*Es*) and transpiration (*Tp*) as input parameters so that it can simulate corresponding actual values of transpiration and evaporation. In this study, the potential transpiration is determined by the atmospheric demand as controlled by meteorological variables, such as net radiation, air temperature, wind speed and relative humidity. The potential evapotranspiration was obtained by combining the daily values of reference evapotranspiration (*ETo*), determined by the FAO Penman-Monteith method and the single crop coefficient approach (Allen et al., 1998), as follows;

$$ETp = Kc * ETo \qquad (6.1)$$

where *ETp* is the potential evapotranspiration [LT^{-1}], *Kc* is the crop coefficient, which represent the plant transpiration component, and *ETo* is reference evapotranspiration [LT^{-1}). A daily based of *ETo* was estimated with meteorological data using the FAO-56 Penman-Monteith combination equation (Allen et al., 1998) and *ETo* calculator, a software developed by the Land and Water Division of

FAO. The crop coefficient for bell pepper based on FAO 56 paper (Allen et al., 1998) is 0.6, 1.05 and 0.9 for the initial stage, middle and late growth stage, respectively. Since a plastic mulch was used to cover the soil surface in this study, the FAO 56 paper recommends reducing the value of crop coefficients by 10 – 30 %. A reduction of 15 % was therefore adopted in our study. The crop coefficients used for bell pepper were 0.51 at the initial stage (Kc_{in}), 0.89 and 0.77 at middle stage (Kc_{mid}) and late stage (Kc_{end}), respectively.

The potential transpiration and irrigation were used to represent the atmospheric boundary condition. Since in the cultivation experiment, soil surface was covered with plastic mulch, it was assumed evaporation from the soil surface was neglected and become zero in the simulation scenario, thus potential evapotranspiration represents transpiration only. The potential transpiration rate (Tp) was calculated with:

$$Tp = ETp - Ep, \text{ where } \quad Ep = 0$$

$$Tp = ETp \qquad (6.2)$$

Runnig the HYDRUS model requires reliable soil hydraulic parameters such as θr, θs, Ks, $alpha$, n and l as described in eq. 3.3 to 3.5. The soil hydraulic properties were modeled using the water retention and hydraulic conductivity functions described by van Genuchten-Mualem (van Genuchten, 1980). The soil hydraulic properties such as water retention curve, Ks and θs have been described in section 6.3.3. The van Genuchten- Mulaem hydraulic parameters were fitted against the soil water retention curve experimental data points using RETC program (Van Genuchten et al., 1991) to predict unsaturated hydraulic conductivity function. As for andisol soil used in this study, the soil hydraulic parameters fit are listed in Table 6.3.

Table 6.3 Soil hydraulic parameters of the van Genuchten-Mualem model used in the numerical simulation

Soil	θr (cm^3cm^{-3})	θs (cm^3cm^{-3})	α (1/cm)	n (-)	Ks (cm day^{-1})	l (-)
Andisol	0.09	0.543	0.025	1.422	14.33	0.5

θr is the residual water content, θs is the saturated water content, van Genuchten-Mualem shape parameters (α, n and l), and Ks is saturated hydraulic conductivity.

The root water extraction S (h, x, y, z, t) from the soil is computed according to the Feddes approach (Feddes et al., 1978), which is implemented in HYDRUS as explained more detail in Chapter 3, Section 3.2. The following parameters of the Feddes model were used in this work: h_1 = -10 cm, h_2 = - 20 cm, h_3 = -600 to -1500 cm, and h_4 = -3000 cm. The $h_1 - h_4$ represents different pressure head values which are affecting the root water uptake in the soil. The critical water stress index (ω_c) value was set equal to 1 in the simulation, since bell pepper is one of agricultural plants, which has a relatively high ω_c, therefore, their ability to compensate natural stress is limited (Šimůnek and Hopmans, 2009).

The standard approach of root distribution in HYDRUS 2D/3D version 2 only allows roots which are distributed constant with the time during the simulation. To extend the capabilities of the standard module of HYDRUS 2D/3D, a simple root growth model was implemented in Version 3. (Šimůnek et al., 2018). The rooting depth, L_R, now can be either constant (the standard approach) or variable during simulations. For annual vegetation, a growth model is required to simulate changes in rooting depth with time. Time-variable rooting depth values can be provided either using a table on input, or calculated by the program, assuming that the actual rooting depth is the product of the maximum rooting depth, L_m [L], and growth coefficient, f_r (t) [-], given by (Šimůnek et al., 2018);

$$L_R(t) = L_m \; f_{\mathrm{r}}(t) \tag{6.3}$$

For the growth coefficient, f_{r} (t) [-], the classical Verhulst-Pearl logistic growth function is implemented in the new version of HYDRUS 2D/3D;

$$f_{\mathrm{r}}(t) = \frac{L_0}{L_0 + (L_m - L_0)e^{-rt}} \tag{6.4}$$

where L_0 is the initial rooting depth at the beginning of the growing season [L], and r is the growth rate [T^{-1}]. The growth rate can be calculated either from assumption that 50% of the rooting depth will be reached after 50% of the growing season has elapsed or from given rooting depth data at the specified time. The same approach was also used for the horizontal extent of the rooting zone, except the maximum extent of the rooting zone in the horizontal direction is used instead of the maximum rooting depth (Šimůnek et al., 2018). In this study, both constant roots and the root growth approach were considered for comparison purpose. The observed bell pepper root growths, which are listed in Table 6.2, were used as input parameters of root growth in the simulation.

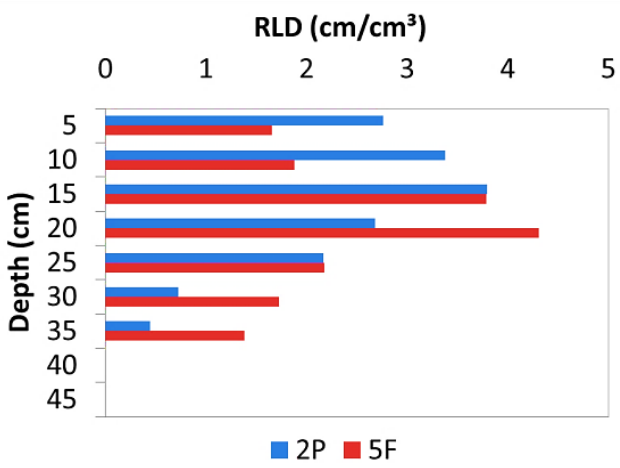

Figure 6.7 Root length density of bell pepper in different emitter designs.

The spatial distributions of roots which are described using the Vrugt (Vrugt et al., 2001) model function were selected in the numerical analysis (as described in Chapter 3). The location of the maximum root water uptake was observed to be concentrated mainly near the ring-shaped emitter where water and nutrient were applied. The root distribution was specified according to the measured distribution along the soil profile. Root sampling and plant roots distribution measurement were conducted after cultivation for each plant pot with different emitter design in order to obtain the plant roots distribution parameters used in the simulation. The observation of the bell pepper root distributions from different emitter designs, the emitters 2P and 5F, revealed that root length density (RLD) of the plant was highest at the depths of 20 cm and 15 cm for the original ring-shaped emitter (5F) and the modified ring-shaped emitter (2P), respectively as described in Figure 6.7. This finding contributed that the plant roots up-took water intensively near the buried water source (i.e., emitter). In addition, the maximum radius of roots (X_m and Y_m) was 25 cm in both emitter 2P and 5F, while the maximum depth of root (Z_m) was 35 cm. Table 6.4 shows the parameters of the spatial root distribution of the Vrugt model (Vrugt et al., 2001), which were used in the simulation. While Figure 6.8 visualizes the spatial root distributions computed by Vrugt's model for different emitters

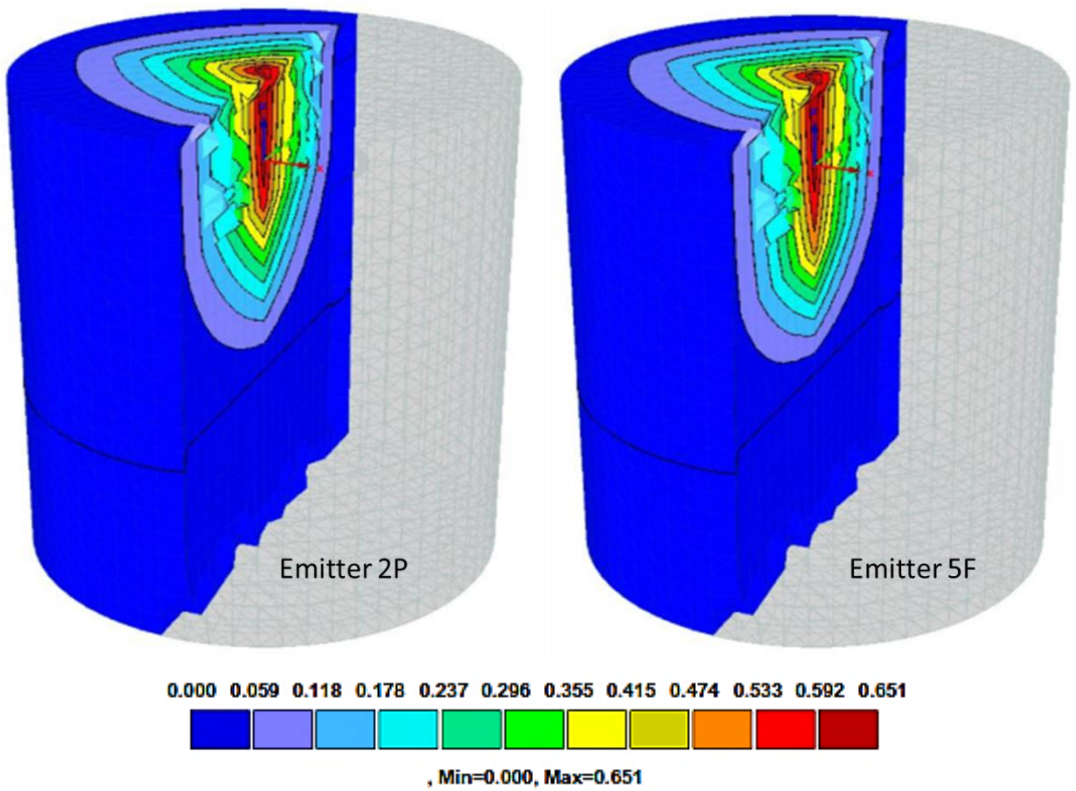

Figure 6.8 The three-dimensional spatial distribution of root water uptake based on Vrugt parameters for different emitter designs.

Table 6.4 The parameters of Vrugt root distribution function

Parameters	Emitter 2P	Emitter 5F
Maximum rooting depth, Z_m (cm)	35	35
Depth with maximum root density, z^* (cm)	15	20
Maximum rooting radius, X_m (cm)	25	25
Radius of maximum intensity, x^* (cm)	0	0
Maximum rooting radius, Y_m (cm)	25	25
Radius of maximum intensity, y^* (cm)	0	0
Non-symmetry coefficient, P_z, P_x, and P_y	1, 1, 1	1, 1, 1
Surface area associated with transpiration (cm^2)	1200	1200

6.5. Results and Discussions

6.5.1. Plant Growth and Water Consumption

The plants were transplanted into the pots on 17 July 2017. They were grown for 109 days during the experiment. The plant heights were measured every week during crop growth season, while crop biomasses and yield were determined after cultivation. The effect of ring-shaped emitter design on plant growth is described in Figure 6.9. The plant grew up during cultivation from 14 cm to 74 cm when water was applied with the modified ring-shaped emitter (2P). Since the original ring-shaped emitter applied more irrigation water compared to the modified ring-shaped emitter, the subsurface irrigation using the original ring-shaped emitter (5F) resulted in higher plants of about 84 cm, but they were not significantly different ($p>0.05$) from those with the modified emitter.

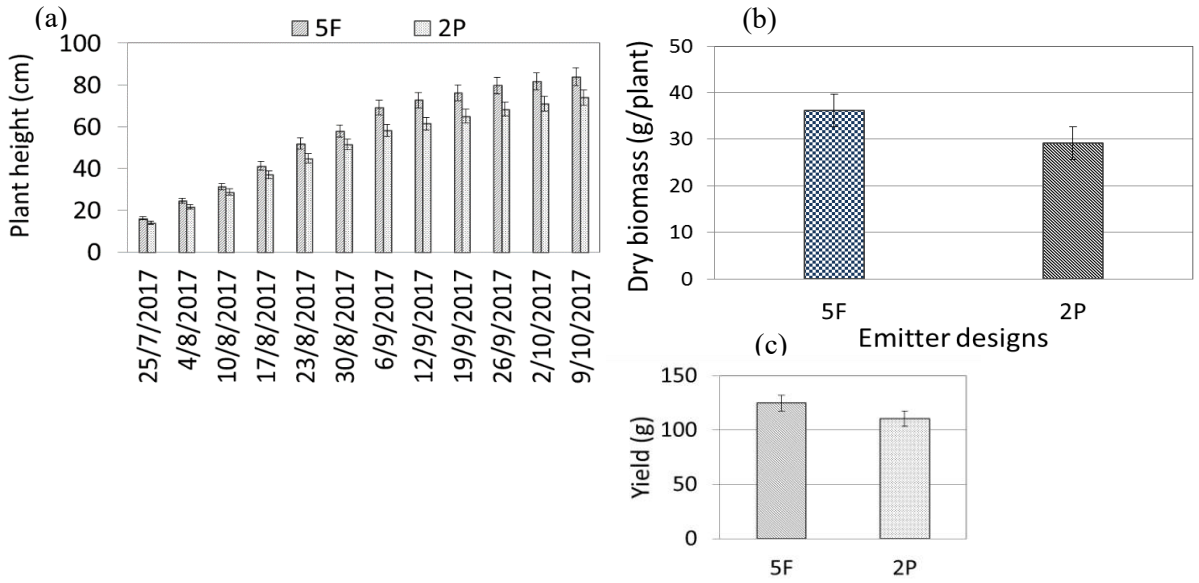

Figure 6.9 The effect of ring-shaped emitter designs on crop performance as well as (a) plant height and (b) dry biomass, (c) yield.

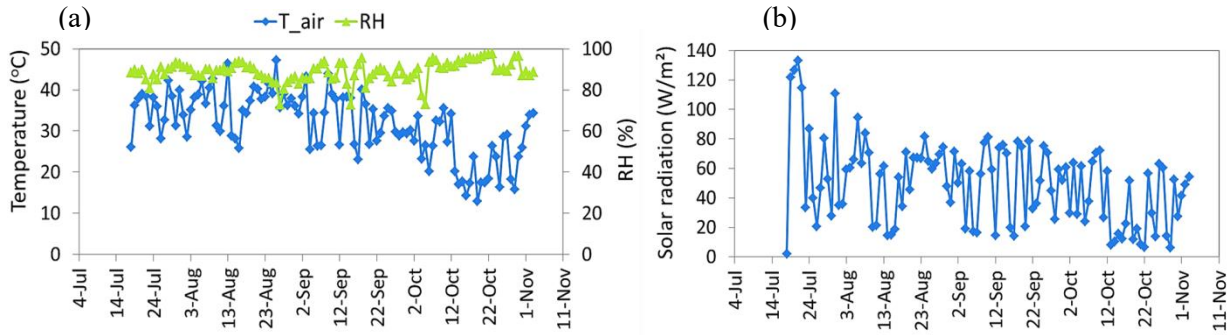

Figure 6.10 (a) Daily values of air temperature, Tair, and relative humidity, RH, (b) global solar radiation measured during the growing season.

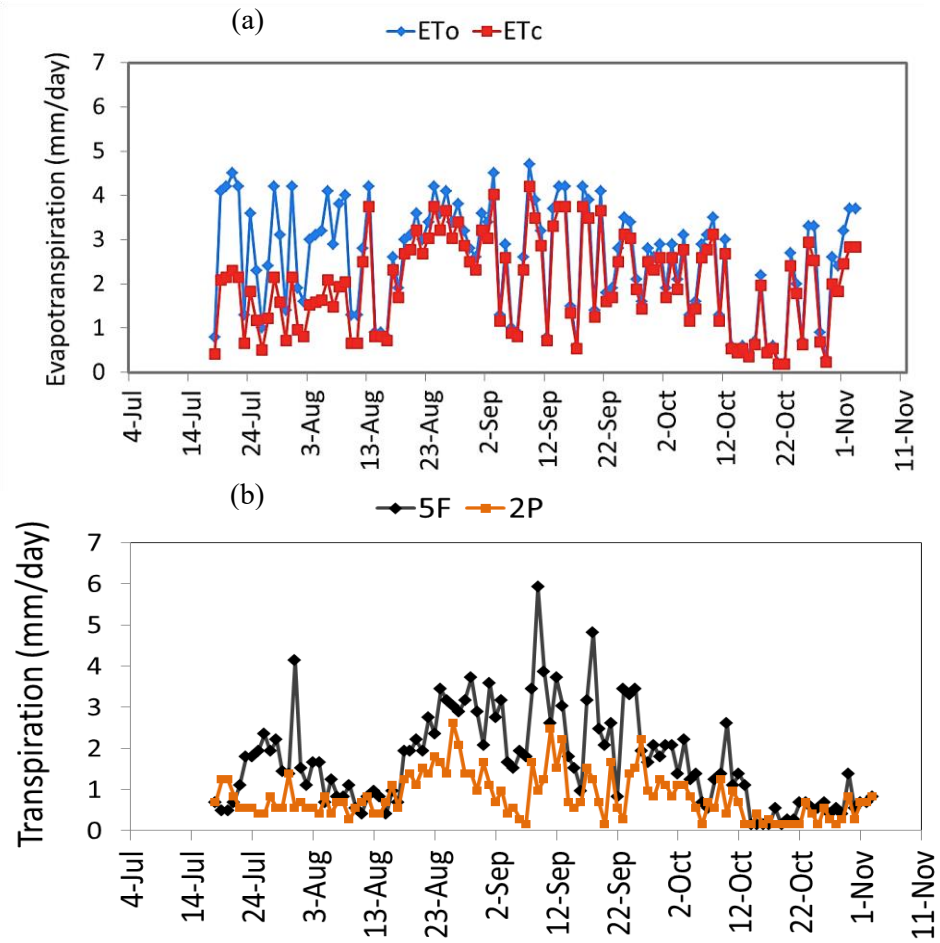

Figure 6.11 (a) Daily values of a reference evapotranspiration, ETo, and crop evapotranspiration, ETc based on Penman-Monteith calculation, (b) daily values of actual crop transpiration based on measurement of weighing balance for different emitter designs.

Dry biomass for different emitter designs is shown in Fig.6.9b. The total biomass was 36.9 and 29.14 g per plant for the emitter 5F and 2P, respectively. The dry biomass was low when subsurface irrigation with the emitter 2P was used, compared to the emitter 5F which had the largest biomass. The biomass increased as the amount of irrigation water increased. In addition, the yield was lower when the modified ring-shaped emitter, 2P, was used. The total yield of 111 g/plant achieved for the emitter 2P was lower compared to the emitter 5P which had the highest yield about 125 g/plant. The difference was not significant in both emitter designs (p>0.05) for three-replicates.

The growth progress was indicated by increasing daily water consumption. The daily water consumption was estimated based on the Penman-Monteith calculation, where the values of crop water requirement influenced by crop stages and environmental conditions as well as agro-meteorological variables. The dynamic of agro-meteorological variables (air temperature, humidity and global solar radiation) measured during the growing season are shown in Figure 6.10a and

6.10b. During cultivation, the air temperature decreased dramatically toward the end of October because the solar radiation was lower than usual due to continuous heavy rains occurred in October.

Figure 6.11a illustrates the computed daily potential evapotranspiration (*ETo*) and crop evapotranspiration of bell pepper (*ETc*). As can be observed, the crop evapotranspiration tends to increase during the growing season from mid of August to the end of September, rising 0.18 mm day^{-1} to about 4.19 mm day^{-1}. Shukla et al. (2013) reported that the crop evapotranspiration increased as the crop grew until it reached at maximum maturity. The cumulative crop evapotranspiration of bell pepper reached about 218 mm in the growing season.

Figure 6.11b describes the observed daily actual transpiration, which was determined by the depletion of the weighing balance of each soil pot before and after irrigation was applied from the subsurface ring-shaped emitter with the original design (5F) and modified one (2P). The bell pepper transpiration was higher during the development stage and reached its maximum value at the middle stage for both emitter designs 5F and 2P. The actual transpiration of bell pepper was highly dependent on variation of soil water storage during the growth season and the irrigation amount. As a result, the emitter which had 2 holes produced a small amount of water discharge into the soil profile causing reduction in the transpiration. The total amount of irrigation water applied from the modified ring-shaped emitter (2P) was about 93.9 mm lower than 244.7 mm applied from the original emitter (5F). The total cumulative transpiration of bell pepper was achieved 90.2 mm and 183.7 mm for the emitter with modified and original design, respectively. Sezen et al. (2015) reported that the seasonal bell pepper transpiration increased with increasing the amount of irrigation under both furrow and drip irrigation systems.

6.5.2. Comparison of Measured and Simulated Soil Water Contents

Water management of bell pepper is extremely important at all stages of plant development due to the influence on growth establishment, fruit set and quality. Profiles of soil water content variation at different depths during the growing season for each emitter design are shown in Figure 6.12. The soil water content distribution dynamics were monitored by soil moisture sensors installed at four different depths during bell pepper growth season. For each emitter design, a total of 4 soil moisture sensors was positioned at the center of the ring-shaped emitter. The figures show that the soil water content responded to the irrigation cycles. A total of 26 irrigation and fertigation events was applied during the cultivation experiment. As can be observed, at the depth of 20 cm, the soil water content jumped immediately after each irrigation event and gradually decreased due to

redistribution and root water uptake. Soil water content mainly changed in the upper root zone of 0-30 cm. As plant roots observation (Fig.6.7), the plant roots concentrated in the 5 – 35 cm layer during the development stage while soil water content varied in the corresponding depth.

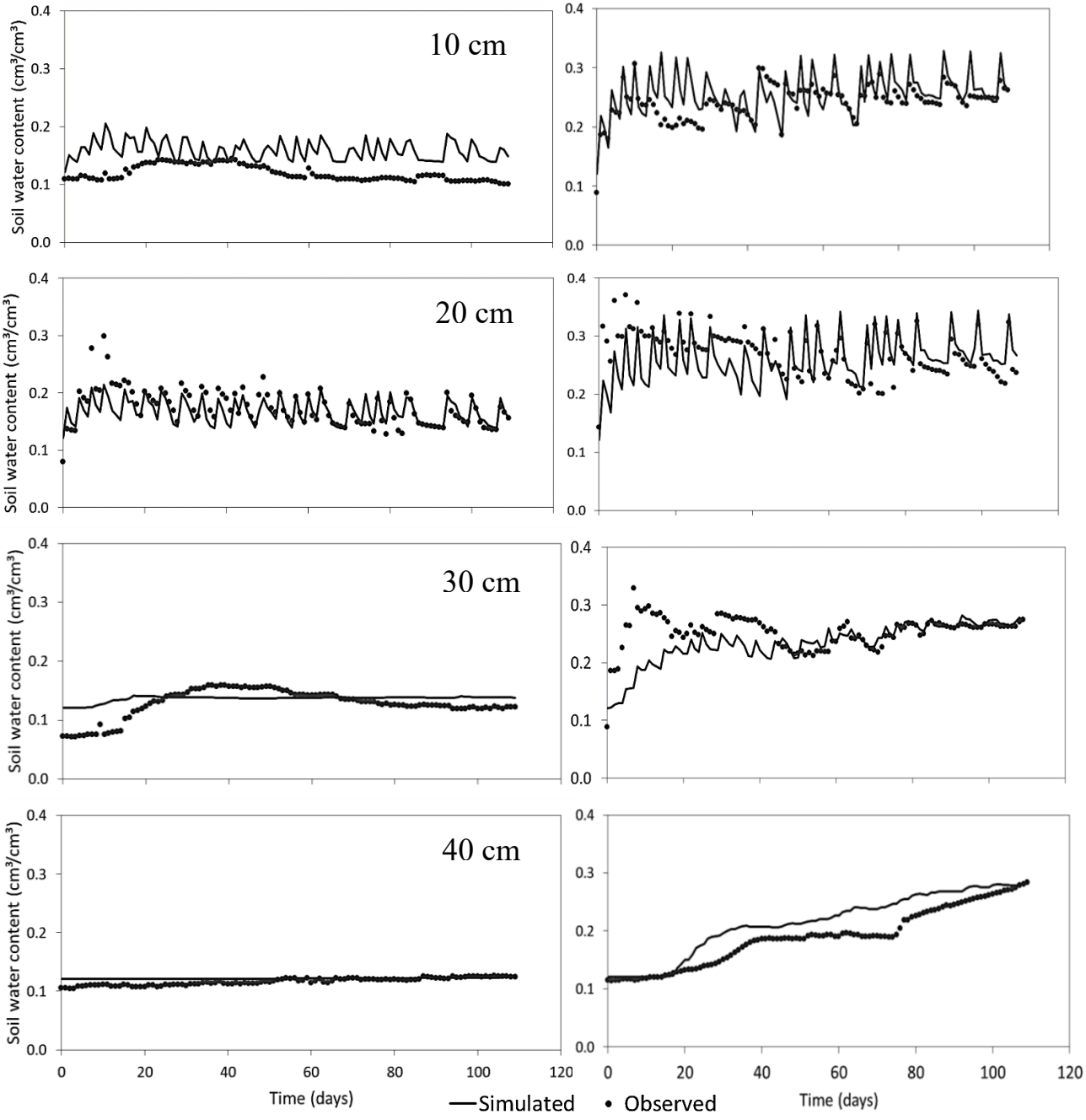

Figure 6.12 Comparison between measured and simulated soil water content at depth of 10 cm, 20 cm, 30 cm and 40 cm from the emitter 2P (left) and 5F (right). The simulation scenario based on HYDRUS standard approach which the plant root was considered as constant with time.

As is the depicted in Fig. 6.12 (left), the emitter with 2 holes (2P) can maintain the soil water content approximately from 0.205 to 0.301 $cm^3 cm^{-3}$. It never reached to the saturated condition. In addition, because the wet volume expanded slowly with smaller discharge rates from the emitter, it allows redistribution of water radially. The soil water content at the depth of 30 cm then increased initially and stayed almost constant. As the soil water content remained almost constant at lower values at the depths of 10 cm and 40 cm, there was a minimal water loss either due to deep percolation or evaporation from the soil surface. On the other hand, for subsurface water application using the original design ring-shaped emitter, the soil water content reached at near the saturated condition at the depth of 20 cm in the early stage of irrigation cycle (Fig.6.12 right). Generally, the soil water content remained high in all observation depths compared to subsurface irrigation with the modified ring-shaped emitter. This comparison revealed that the modified ring-shaped emitter allows maintaining the soil water content in the root zone and eliminating water stress for the plant roots. For this reason, the modified ring-shaped emitter can prevent evaporation and deep percolation water losses. Providing better soil water distribution near the active roots and the absence of evaporation losses could explain observed higher productivity with subsurface irrigation (Shukla e al., 2013).

The measured volumetric soil water content values were compared with the model simulated values at different soil depth for different emitter designs. The dots represent observed soil water content values, while line represents simulated soil water content values (Fig.6.12). Figure 6.12 documents that a relatively good agreement between experimental and simulated data was obtained. Overall, temporal changes in soil water contents in the upper soil layers (0-30 cm) were larger than in the deeper layers, as these layers were more directly affected by irrigation, and transpiration.

Table 6.5 Error analysis for different emitter designs at different depths

Depth	Error ($cm^3 cm^{-3}$)	Emitter 5F	Emitter 2P
10 cm	RMSE	0.061	0.109
	MAE	0.014	0.04
20 cm	RMSE	0.092	0.028
	MAE	0.011	0.007
30 cm	RMSE	0.099	0.029
	MAE	0.020	0.009
40 cm	RMSE	0.049	0.003
	MAE	0.025	0.005

Since the emitter was installed at 15-cm depth, soil water contents at a depth of 20 cm increased quickly corresponding to irrigation event. During the entire growing season, the root mean square errors (RMSE) and mean absolute errors are computed (Table 6.5). Generally, the simulated soil water content values computed with HYDRUS were in good agreement with the measured soil water contents, despite some discrepancies. The difference between simulated and observed soil water content values was higher at a depth of 10 cm when emitter 2P was used. It might be due to the wetted volume from emitter 2P was distributed based on the hole of emitter configuration, therefore the fluctuation of soil water content was less pronounced in the experiment. The discrepancies might be partially attributable to spatial heterogeneity and observation errors. Ramos et al. (2012) explained that relate to field measurement, the measurement of SWC by sensors is not free of errors due to numerous assumptions and inherent complexities in the soil which can be potential reasons for discrepancies.

Although some discrepancies between simulations and measurements occurred in some depths, the overall accuracy of the HYDRUS model for simulating the soil water content was satisfactory where the RMSE values and MAE were low in the deeper soil layer. This result agreed well with that of Yao et al. (2011), who used HYDRUS 2D/3D to simulate the soil water dynamics in a section of the jujube root zone and RMSE values decreased with the increasing of soil depth below a drip tube. One possible reason for these variations was that the root water uptake activity was most intense in the shallow soil zone (Xi et al., 2013). Therefore, it can be concluded that the accuracy of the simulations for different emitter designs was satisfactory and that HYDRUS 2D/3D is well suited for simulating water content in subsurface irrigation with ring-shaped emitter under environmental and crop conditions.

6.5.3. Comparison of Measured and Simulated Actual Transpiration of Bell Pepper

Crop transpiration (T) and soil evaporation are the main mechanisms by which water is cycled in cropland areas, and the ratio of transpiration and evapotranspiration are very important for understanding the ecological mechanisms of the crop water transport (Scanlon et al., 2005). However, few studies have modeled transpiration and compared the simulated results with observed data. To evaluate the HYDRUS model for predicting transpiration and provide support for field management, in this study, the constructed HYDRUS 2D/3D model version 3 was used to compute the daily actual transpiration (Fig.6.13) under different ring-shaped emitter designs.

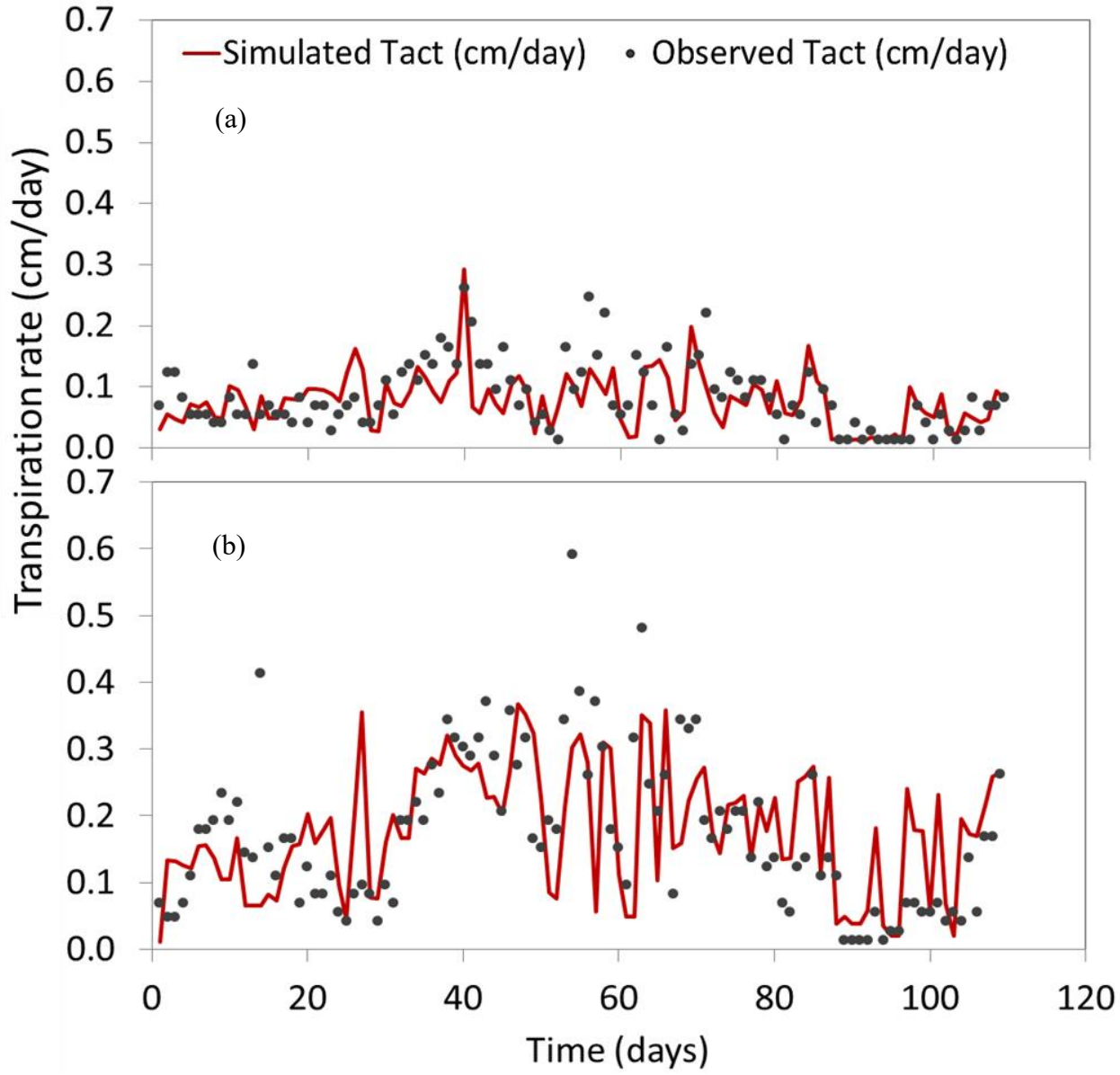

Figure 6.13 Comparison of the measured and simulated values of actual transpiration (Tact) during crop growing season for emitter 2P (a) and emitter 5F (b).

Table 6.6 Errors analysis of actual transpiration simulation results for different emitter designs

Paremeter	Errors	Emitter 5F	Emitter 2P
	RMSE (cm day^{-1})	0.543	0.137
Tact	MAE (cm day^{-1})	0.006	0.006

RMSE is the root mean square error, MAE is mean absolute error, Tact is the actual transpiration.

As for emitter 2P, the values of actual transpiration were lower than potential transpiration compared to emitter 5F, the potential transpiration values were close to the actual transpiration values. The reduction of the actual transpiration rate from the emitter 2P was mainly affected by the availability of water storage in the soil column. As can be seen in Fig. 6.12 the soil water content was maintained relatively lower compared to emitter 5F. Transpiration is affected by soil properties such as soil water potential and hydraulic conductivity of the soil. The low soil water potential (i.e., the low water content) and the low hydraulic conductivity, both of which impede the conduction of sufficient water to plant roots, keep stomata close, to avoid dehydration of the plant. As a result, the transpiration rate is reduced to a low value. Empirically, it is well known that the rate of the plant activities such as transpiration and growth is a function of available soil water depletion (Miyazaki, 1993). Denmead and Shaw (1962) investigated the transpiration rates of plants as a function of soil water content for various conditions of the atmosphere. They found under clear and dry conditions, the transpiration rate decreased from 6.5 mm day^{-1} to 2 mm day^{-1} when soil water content decreased from 0.34 cm^3 cm^{-3} to 0.28 cm^3 cm^{-3}. On the other hand, under heavily overcast and humid conditions, the transpiration rate was small (1.3 mm day^{-1}) and constant when the water content was more than 0.23 cm^3 cm^{-3} but decreased to 0.2 mm day^{-1} when water content less than the wilting point (0.22 cm^3 cm^{-3}). They concluded that available water for plants was not constant but depends on the atmospheric condition or evaporative demand.

The accuracy of the HYDRUS 2D/3D model to simulate actual transpiration was evaluated by comparing the simulation results and observed data. The mean absolute errors were varied from 0.006 to 0.011 and -0.006 to 0.020 for emitter 5F and 2P, respectively. This indicated that the simulated actual transpiration values agreed well with the measured values. Although, some discrepancies were found between simulated and observed values of actual transpiration during simulation, overall, HYDRUS 2D/3D can be used as a tool to accurately simulate the transpiration during the entire growth period. In addition, various environmental factors, particularly, can cause errors in the simulation, such as, temperature, soil water availability and soil strength, can influence the plant root development and root distribution in soil.

6.5.4. Yield and Irrigation Water Productivity

Water application and irrigation design extremely important to provide the appropriate amount of water for crop development. Table 6.7 presents the data on the total amount of irrigation and actual transpiration of bell pepper during the growing season for different emitter designs. The

bell pepper weight increased with an increase the amount of water applied. Since the actual transpiration was higher in emitter 5F, the yield was also higher about 137.94 g per plant. Bell pepper transpiration was highly dependent on the variation of soil water storage in growth season, and irrigation amount. As presented in Table 6.7, the total amount of water irrigation was 244.46 mm applied by emitter 5F. The simulated of total irrigation had slightly less discrepancies with measured data. Therefore, HYDRUS 2D/3D can be used as a tool to determine the irrigation water use efficiency in term of water productivity.

In the following, the term of water productivity is related to the amount of irrigation water provided to produce yield. The results obtained for the water productivity (Table 6.7) demonstrated that the lower the irrigation dose, the higher the water productivity. This can be clearly seen in the pot which was irrigated by emitter 2P had lower the amount of irrigation water can increase the water productivity of 1.28 g mm^{-1}.

Water productivity of bell pepper was estimated by dividing the measured yield by the seasonal actual transpiration. Water productivity and irrigation water productivity influenced the cumulative water irrigation discharge. When using the modified ring-shaped emitter, water productivity and irrigation water productivity were larger than those with the original design emitter (5F). Dukes et al. (2003) reported irrigation water productivity values for drip irrigated bell pepper ranging from 16 to 52.6 kg m^{-3} in Florida. In another study, Sezen et al. (2015) reported water productivity of bell pepper under full irrigated by drip irrigation in Mediterranean areas varied from 5.5 to 7.1 kg m^{-3}.

Table 6.7 Yield, Transpiration, Irrigation, Water productivity and Water use efficiency of bell pepper in different emitter designs.

Parameters	Emitter 5F		Emitter 2P	
	Simulated	Observed	Simulated	Observed
Fresh weight (gr per plant)		137.94		120.14
Transpiration (mm)	209.17	183.74	88.64	90.18
Irrigation (mm)	243.18	244.46	94.32	93.90
Water productivity (g mm^{-1})	0.66	0.75	1.36	1.33
Irrigation water productivity (g mm^{-1})	0.57	0.56	1.27	1.28
Water use efficiency (%)	86.0	75.2	94.0	96.04

6.6. Summary

In this chapter, the effect of different emitter designs on plant growth performance and irrigation water productivity was assessed during bell pepper cultivation. In order to achieve the objectives, the cultivation was conducted in glass-house during summer season of 2017. Two emitter designs were used for comparison; emitter 5F and 2P. Emitter 5F was the original ring-shaped emitter design which was fully covered by a permeable textile and consisted of 5 holes. Whereas emitter 2P was a modified ring-shaped emitter design with reduced number of holes into 2 holes and partially covered only around the holes. Bell pepper was transplanted into a pot which filled with andisol soil. For each emitter design had 3 plant pots and 3 additional pots for destructive sampling of plant roots. Thus, a total of plant pots was 9. During the experiment, the changes in soil water content in different depths were monitored and crop water requirement was estimated following the procedure from FAO-56 paper. Measured data as well as soil water content and actual transpiration were used to calibrate the capacity of the HYDRUS 2D/3D model. The input parameters for HYDRUS model were based on experimental data and field conditions.

Both experimental and numerical results indicated that water productivity and irrigation water productivity values can be increased when using the modified ring-shaped emitter, 2P even though, emitter 2P produced lower yield than emitter 5. The increases in water productivity and irrigation water productivity corresponded to the total amount of irrigation that was applied by different ring-shaped emitter configurations. The results found in this work seem to indicate that the use of the modified design of the ring-shaped emitter could be a recommendable option to save water in areas where water resources are particularly scarce without compromising the crop yield. In addition, the modified ring-shaped emitter design allows easy to repair and maintain.

Chapter 7. Long-term Effect of Subsurface Irrigation on Subsurface Environment in Arid Region

7.1. Introduction

Subsurface ring-shaped emitter irrigation has been introduced and developed in the East Lombok Regency of West Nusa Tenggara, Indonesia since 2014. East Lombok is considered one of the water scarce regions in Indonesia. Generally, the climate condition of the region is classified as dry with average annual rainfall from 500 – 1000 mm (Sumarsono et al., 2018). According to climate classification of the Oldeman, the area is categorized in the zone of E4 agroclimatic where the wet season is characterized for 4 months (the dry season is therefore 8 months). Currently, farmers intensively use subsurface irrigation with ring-shaped emitters for cultivating vegetable crops such as hot pepper. Pumped groundwater is stored in a small reservoir with the capacity of 300 cm3. Water is delivered from the reservoir to irrigate land through a pipeline network.

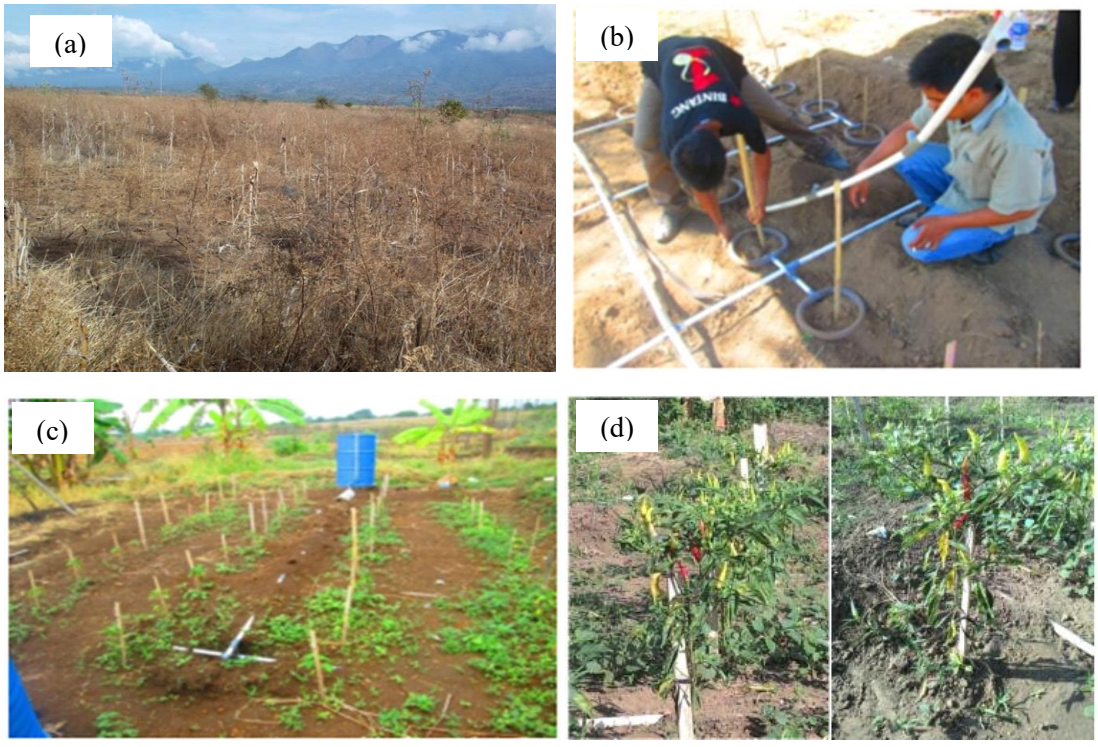

Figure 7.1 Bare land in East Lombok without any cultivation during dry season, b) Farmer installed ring-shaped emitter at a depth of 10 cm for subsurface irrigation, c) Cultivation hot pepper under subsurface irrigation with ring-shaped emitter, which water is supplied from a water tank, d) maturity of hot pepper in farmer's land under subsurface irrigation with ring-shaped emitter (Source: Saptomo et al., 2014; Sumarsono et al., 2018).

Increasing irrigated areas for intensive horticulture cultivation in arid lands can contribute increases in the nitrate concentration in shallow aquifers because of nitrate leaching (Siemens et al., 2008; Ramos et al., 2012). Excessive application of N fertilizer and poor management of water lead to nitrate pollution of groundwater. Thus, the monitoring of the nitrate concentration in aquifers needs to be complemented with the control of nitrate beyond the root zone.

Although subsurface irrigation has many advantages such as an increase in irrigation water saving, one of the potential problems associated with this irrigation technique is nutrient leaching due to deep percolation beyond the root zone (Ajdary et al., 2007; Doltra and Munoz, 2010). Therefore, a proper management of water and nutrient during subsurface irrigation for cultivating crops is very important to obtain sustainable yield, to save precious water, and to prevent nitrate pollution in groundwater due to deep percolation. Understanding the relationship between the amount of water and nutrient application, crop root water uptake, and leaching risk can be helpful in providing better irrigation practices and management. In addition, to provide sustainable irrigation with the ring-shaped emitters, it is crucial to evaluate the long-term effects of subsurface irrigation with the ring-shaped emitters on the root zone and the aquifer.

Direct measurements of simultaneous water movement and solute distribution around a buried ring-shaped emitter in the field scale are labor intensive, time consuming and expensive. Simulation models have been proved to be valuable tools for assessing and predicting the long- and short-term effect of subsurface irrigation on soil properties, crop yield, nitrate leaching, and groundwater environment (Hanson et al., 2006; Ajdary et al., 2007, Doltra and Munoz, 2010; Wang et al., 2014). The interaction between soil water and solute with the plant root water uptake is implemented in the HYDRUS software package (Šimůnek et al., 2006; 2012; 2018). This model is therefore selected for the present study to simulate the water movement and solute transport during subsurface irrigation with the ring-shaped emitter under field condition for a long period.

In this chapter, the effect of a long-term application of the alternative ring-shaped emitter for subsurface irrigation in the cultivated arid land East Lombok, Indonesia, was assessed numerically. HYDRUS 2D/3D was used to investigate soil water movement, solute distribution and deep percolation.

7.2. Materials and Methods

7.2.1. Study Area

The study area was located in Pringgabaya village, in the East Lombok of West Nusa Tenggara, Indonesia (8°31'58.32"S, 116°37'44.85"E). Hot pepper (Capsicum frutences L.) was cultivated during the dry season from June to November (Sumarsono et al., 2018). The original design ring-shaped emitter was used in the field experiment. The climate is a continental arid temperate zone with an annual average precipitation of 1042 mm from 2008 to 2017. Most precipitation occurred during November to February. The annual reference average evapotranspiration was 1675.19 mm from 2008 to 2017. The fluctuation of precipitation and potential evapotranspiration during 10 years is described in Figure 7.2. The lowest and the highest temperatures are about 22.5°C in January and 36.3°C in August, respectively. Soil texture in the study area was characterized as sandy clay loam. The main soil properties are presented in Table 7.1

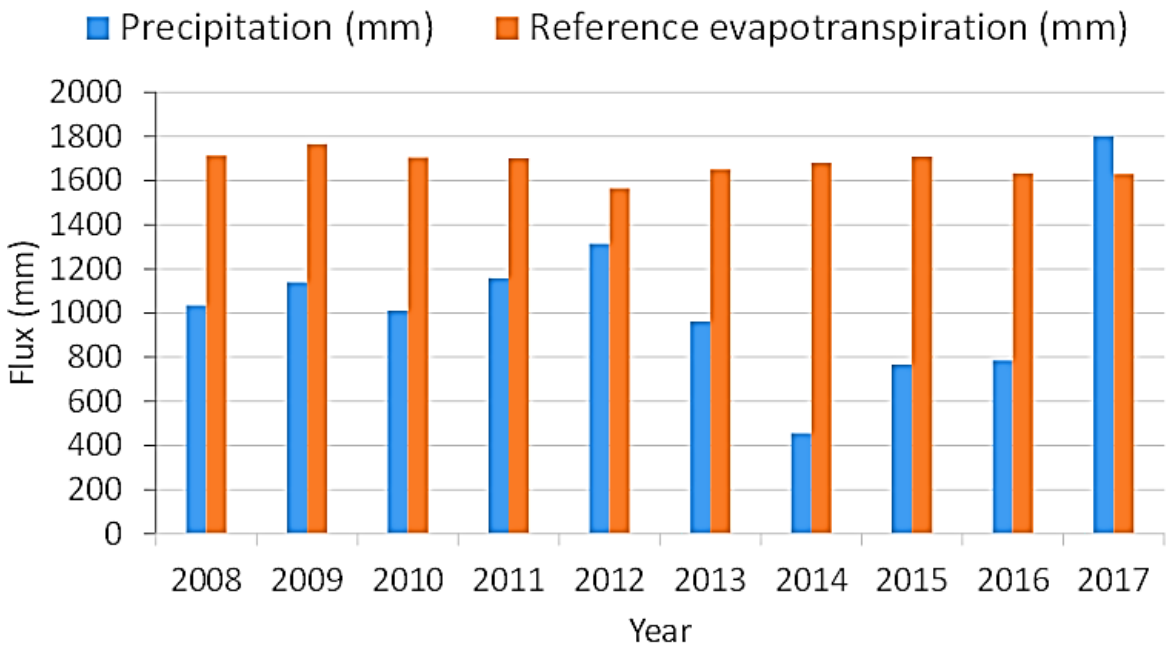

Figure 7.2 Annual of precipitation and evapotranspiration in East Lombok Regency, West Nusatenggara, Indonesia for 10 years.

Table 7.1 Measured soil properties of the study area

Parameters	Unit	Plot 1		Plot 2	
		0-15 cm	15-30 cm	0-15 cm	15-30 cm
Available water content	$cm^3\ cm^{-3}$	0.12	0.09	0.11	0.09
Field water content	$cm^3\ cm^{-3}$	0.35	0.32	0.38	0.41
Porosity	$cm^3\ cm^{-3}$	0.61	0.6	0.66	0.52
Bulk density	$g\ cm^{-3}$	0.96	0.98	0.88	1.18
Particle density	$g\ cm^{-3}$	2.44	2.48	2.56	2.47
Ks	$cm\ h^{-1}$	5.34	3.76	7.86	4.87
Ks	$cm\ day^{-1}$	128.16	90.24	188.64	116.88

(Source data; Saptomo et al., 2014)

7.2.2. Long-term HYDRUS Simulations of Water Flow and Solute Distribution

In order to simulate the long-term effects of subsurface irrigation with the ring-shaped emitter on spatial extent and temporal dynamics of water and solute in the root zone, the three-dimensional model of HYDRUS (Šimůnek et al., 2008; 2018) was used. The three-dimensional transport domain was used for simulating water flow and solute transport in soil as shown in Fig.7.3. The dimension of the transport domain was 100 cm in depth, 80 cm in width, and 100 cm in length. The transport domain was discretized into 12,586 nodes and 50,753 three-dimensional finite element mesh. The ring-shaped emitter was located at a depth of 20 cm below the soil surface. Mesh refinement of 1 cm was done around the buried ring-shaped emitter where rapid change in flux occurs. In order to describe solute distributions in soil profiles, 4 observation points were located in the center of ring-shaped emitter for different depths (i.e., 10 cm, 30 cm, 50 cm and 70 cm).

An atmospheric boundary condition was set at the top of the transport domain. Precipitation, evaporation, and evapotranspiration were accounted as the atmospheric boundary condition during the simulation. It was assumed that during cultivating hot peppers, the soil surface was covered by rice straw mulch, therefore the potential evapotranspiration was taken equal to the potential crop transpiration while the potential evaporation was ignored. Since cultivation was conducted only once a year and there was no crop rotation, thus the evaporation rates which occurred from the bare soil surface were considered in the model at the atmospheric BC during non-cultivation periods.

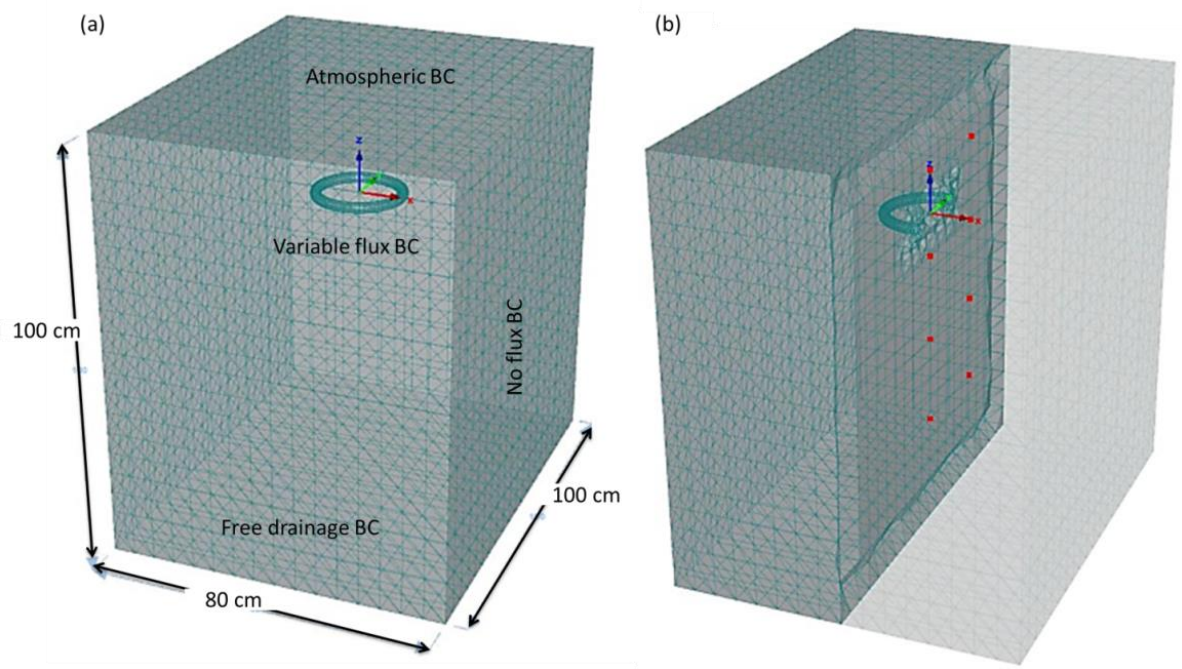

Figure 7.3 Conceptual geometry of simulated area showing ring-shaped emitter location and boundary conditions used in HYDRUS 2D/3D simulations, b) red dots represents the location of observation points in the soil profile.

No flux boundary conditions were assumed along the vertical sides of the transport domain. A free drainage boundary condition was applied at the bottom of the soil profile. A variable flux boundary condition along the buried ring-shaped emitter surface was considered during the irrigation time and no flux during the fallow time. The constant flux in the aforementioned boundary condition was defined based on the amount of water applied of 1500 cm^3 in each irrigation event, which corresponded to the irrigation flux rate of 9.14 cm day^{-1}. The irrigation period was 8 h per day. Since it is common to irrigate vegetables every 2-3 days (e.g., Allen et al., 1998), the irrigation water was applied every 3 days with the duration of 8 h. A third type Caucy boundary condition along the emitter surface was used to evaluate the effect of nitrogen application from fertigation on nutrient uptake and solute distribution in the soil during a given fertigation event. In the simulation, fertigation was applied every 2 weeks with NO_3-N concentration of 1.07 mmol L^{-3} (Phogat et al., 2014). The total of 10 fertigation events was considered in one cultivation period. The fertigation involved applying fresh water for the first 4 h and fertilizer with irrigation water for the next 4 h. The initial conditions of soil water content and solute concentration were assumed uniform throughout the soil profile with the value of 0.103 cm^3 cm^{-3} for soil water content and zero for initial solute concentration.

7.2.3. Root Water and Nutrient Uptake Parameters

The parameters of the spatial root distribution based on Vrugt et al (2001) model were considered in the simulation. The roots of the hot pepper were assumed concentrated mainly below the buried ring-shaped emitter where the water and nutrient were applied and expanded horizontally into all available space between crop lines. The parameters of root distribution are summarized in Table 7.2 while the spatial root distribution is shown in Figure 7.4. The reduction of root water uptake due to the water stress, α_1 (h), was modeled based on the Feddes approach (Feddes et al., 1978), which is implemented in HYDRUS. The reduction in root water uptake due to salinity stress, α_2 (h) was described by adopting the Maas and Hoffmann (1977) salinity threshold and slope function. The parameters of water stress reduction function of Feddes et al. (1978) and osmotic reduction parameters of Maas and Hoffman (1977) are listed in Table 7.3.

Table 7.2 Root distribution parameters from Vrugt et al. (2001) for hot pepper

Zm (cm)	*Z** (cm)	*Xr* (cm)	*Yr* (cm)	*Pz*	*Px*	*Py*
60	35	25	25	1	1	1

Table 7.3 Root water uptake parameters and osmotic reduction parameters (From Feddes et al., 1978) and Maas and Hoffman, 1977, respectively)

Po (cm)	-10	Osmotic Reduction	
Popt (cm)	-20	Treshold (dS/m)	2.5
P_2H (cm	-800	Slope (%)	9.9
P_2L (cm)	-1500	Osmotic coefficient	1
P_3 (cm)	-3000	cRoot	0.2
r_2H (cm/day)	0.5		
r_2L (cm/day)	0.1		

Table 7.4 Soil hydraulic parameters used in HYDRUS-2D/3D water flow simulations.

Soil texture	θr (cm³ cm^{-3})	θs (cm³ cm^{-3})	α (1/cm)	n	Ks (cm day^{-1})	l
Sandy clay loam	0.09	0.524	0.045	1.623	90.27	0.5

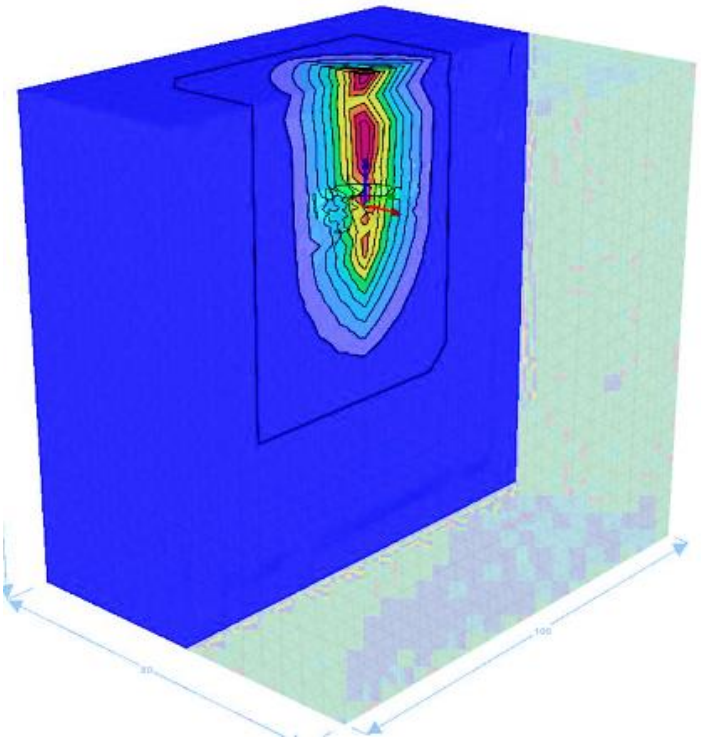

Figure 7.4 A spatial root distribution used in the simulation based on Vrugt et al. (2001) parameters.

7.2.4. Properties of Soil and Solutes Considered in HYDRUS Simulations

Simulations were carried out for sandy clay loam as represent the soil texture used in the study area. The soil hydraulic parameters of van Genuchten-Mualem are given in Table 7.4. The Crank-Nicholson and Galerkin finite element schemes were used to solve the advection-dispersion equations of solute transport with the recommended value of the stability criterion in the simulation. A non-reactive tracer was considered in solute transport simulations. The longitudinal dispersivity equal to one-tenth of the profile depth and transversal dispersivity equal to one-tenth of longitudinal dispersivity, which are recommended in many studies (Ajdary et al., 2007; Ramos et al., 2012 and Doltra and Muňoz, 2010), were used. Thus, the longitudinal and transversal dispersivities were set to 10 cm and 1 cm, respectively. Since the effect of long-term subsurface irrigation with ring-shaped emitter on water and physical solute distribution in soil was the main concern in this study, the chemical interaction and biological process of solute degradation were ignored. The value used for maximum solute concentration of the water removed from the flow region by root uptake (cRoot) was set to 0.2 (Doltra and Muňoz, 2010). No Nitrogen reaction or transforming process was considered, assuming chemicals were either both that taken up by the crops and or transported by water flow in the soil (part of them will be that lost through leaching).

To evaluate the long-term effect of subsurface irrigation with the ring shaped emitter, a long-term simulation was conducted for 10 years using the series meteorological data from 2008 to 2017. The series of meteorological data used in the study area such as precipitation, air temperature, relative humidity, wind speed and solar radiation downloaded from the website of National Oceanic and Atmospheric Administration (http://www.1.ncdc.noaa.gov.) Two emitter designs were compared, the emitter 5F as the original design and the emitter 2P which is an alternative design (e.g., emitter design has been explained in previous chapter). The simulations were done by adjusting the same amount of water applied for both emitter 5F and 2P.

7.3. Results and Discussions

7.3.1. Long-term HYDRUS Simulations

Fig. 7.5 shows the simulated nitrogen concentrations over 10 years for the emitters 2P and 5F at 4 observation points in the center of the emitter. The nitrogen concentration tended to increase during the fertigation event and decrease as the root uptake nutrient for their development. Since the active root zone concentrated at the depth of 0 - 35cm, solute concentration was the highest at a depth of 30 cm, which is classified as an active root zone. The general trend of nitrogen concentration mainly changed in the depth of 10 cm and 30 cm during growth season. As for emitter 2P, the average nitrogen concentration was 0.25 mmol cm^{-3} higher than 0.19 mmol cm^{-3} of emitter 5F. Therefore, because of high concentration of nitrogen in the root zone, more nitrogen can be extracted by the roots when emitter 2P was used. As water infiltrates slowly into the soil profile, it allows plant root to uptake water and nutrient at the optimum rate.

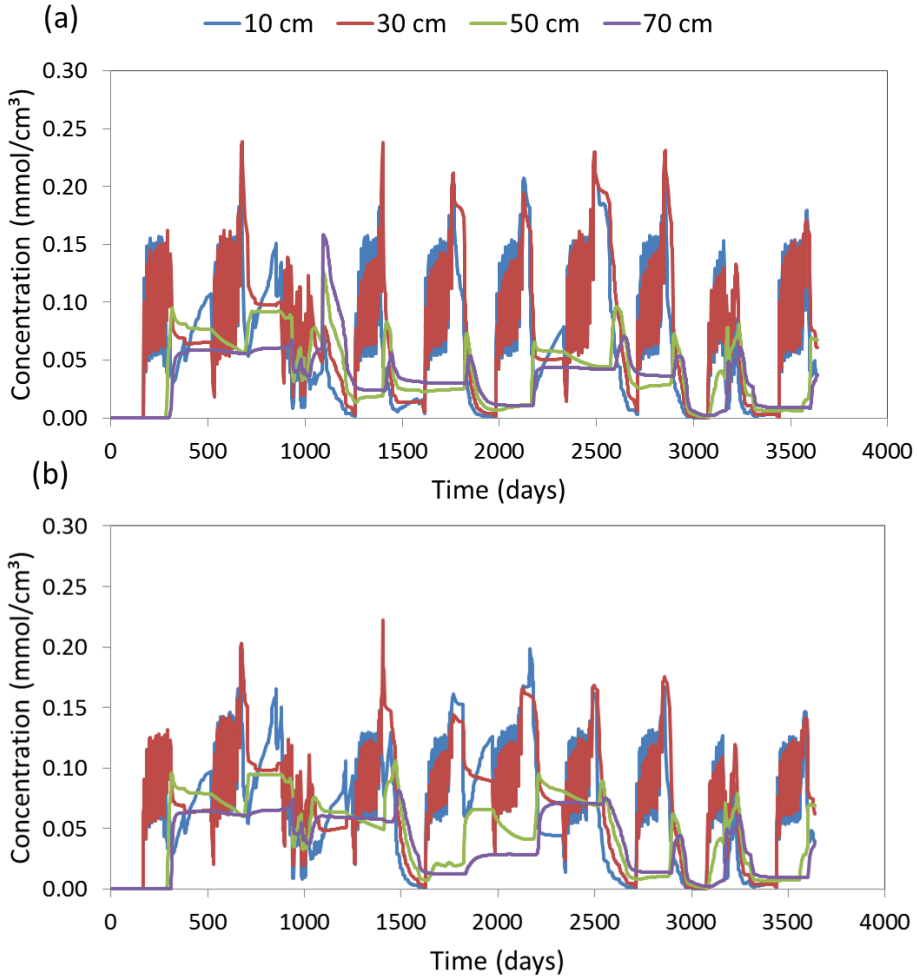

Figure 7.5 Simulated solute distribution at different soil layers when nitrogen fertilizer was applied by (a) emitter 2P and (b) emitter 5F for 10 years.

The fertigation increased the nitrogen content in the soil profile every year, as is evident from an increasing concentration below the buried emitter (i.e emitter depth is 20 cm) as the season progressed. As depicted in Fig.7.5, the concentration of nitrogen was high at a depth of 30 cm, which was about 0.25 mmol cm-3 and 0.20 mmol cm^{-3} for emitter 2P and emitter 5F, respectively. This indicates that the plant was not able to take up all nitrogen added through fertigation. Thus, nitrogen remained in the soil at the end of the crop season. Ultimately, nitrogen started moving downwards after cultivation season, when there was high rainfall. This nitrogen is expected to continue leaching downwards over time and become a potential source of hazard pollution to the shallow ground water and subsurface environment. Alva et al. (2006) found greater variations in nitrogen concentrations in the 0-15 cm depth of soil layer in a field experiment under citrus cultivation, which the seasonal concentration of nitrogen in the soil profile varied from 0.01 – 7.03

mmol cm^{-3}. Phogat et al. (2014) reported the concentration of nitrogen remained high at a depth of 25 cm and seasonal root zone nitrogen concentrations ranging from 0 to 8 mmol cm^{-3} in the end of cultivation season.

Additionally, the concentration of nitrogen was lower during the growing season in 2010 due to higher precipitation occurred in the middle of August. During the crop season the intensity of rainfall was higher than other years, thus, the about 50% of total infiltrated water was lost through deep percolation. This indicates that the amount of 28. 4 % nitrogen leached out from the root zone due to deep percolation from excess water through irrigation and precipitation at the same time.

Simulated spatial nitrogen distributions in the soil profiles under different emitter designs from 2008 to 2017 are depicted in Figure 7.6. The figure reveals that the difference in nitrogen concentration was more at the depth of 10 – 30 cm, which is near from the emitter location. The nitrogen concentration increased with depth up to 30 cm thereafter decreased as the plant roots actively up took nutrient during the growing season. The fluctuation of the solute concentration in the deeper layer was less than the upper layer. While the plant uptake reduced at the end of the crop cultivation season, excess water further mobilized nitrogen out from the root zone, as is evident from 300 DOY and beyond. At the end of cultivation, the amount of solute concentration remained in the soil profile. The accumulated nitrogen might be leaching out to the deeper layer when precipitation occurred and become a potential pollutant to groundwater environment. On the other hand, when the evaporation rate increased at the soil surface, the accumulation of nitrogen increased at the soil surface.

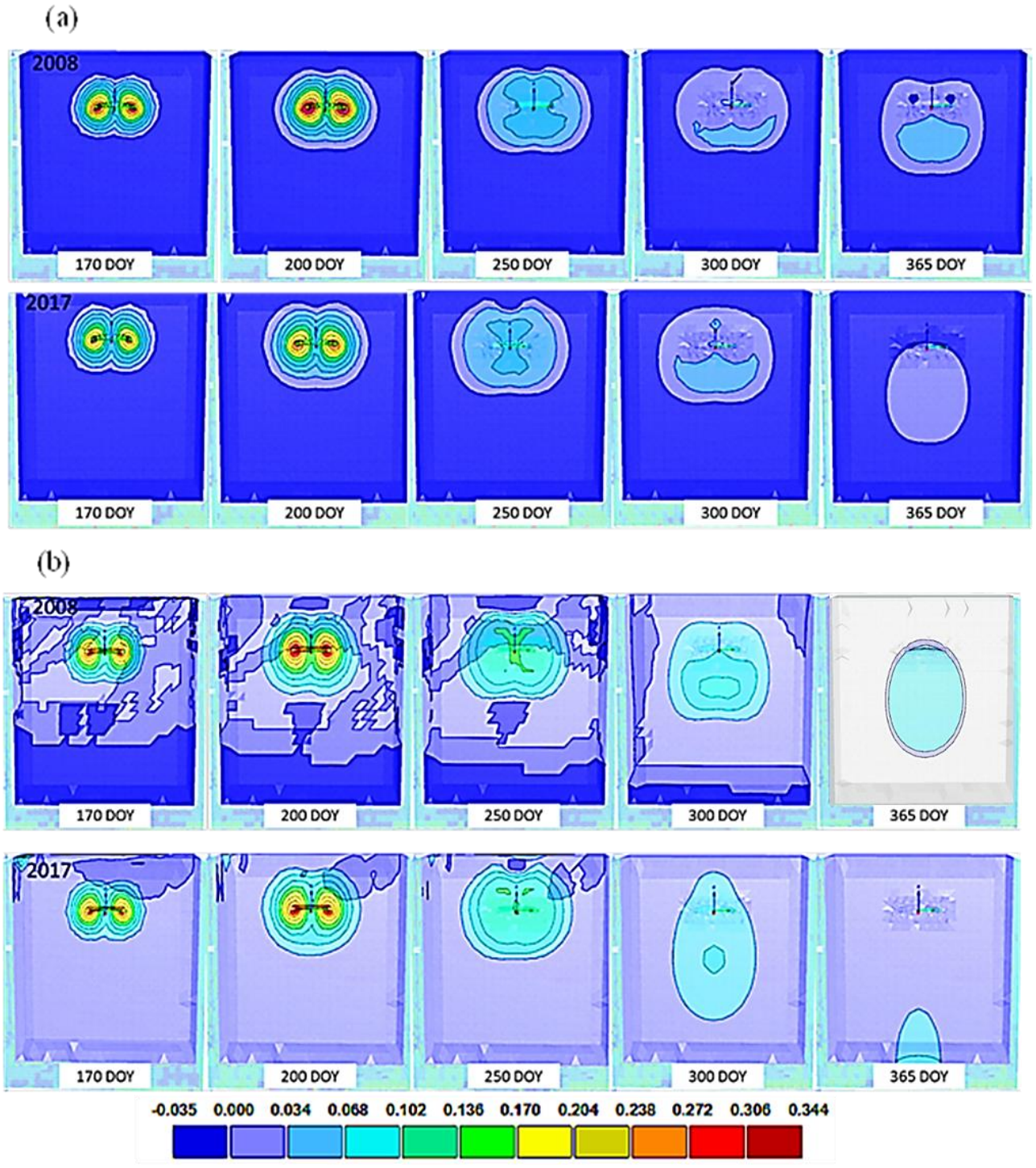

Figure 7.6 Spatial distribution of simulated solute transport over 10 year simulation for emitter 2P (a) and emitter 5F (b).

The effect of emitter design on the nitrogen distribution is shown in Fig.7.6. Although the same amount of fertilizer was injected during each fertigation event, the emitter design affected evidently the nitrogen distribution. As for the emitter 2P, the nitrogen moved less downward as water was applied slowly from the emitter 2P. It indicated that more nitrogen was taken by plant roots when nitrogen remained in the active root zone. At the end of the crop cultivation, as the nitrogen remained in the soil profile, nitrogen did not leach to the deepest layer. On the other hand, the nitrogen in the root zone for the emitter 5F was higher in the early fertigation event and moved downward to a deeper soil layer immediately due to the high discharge rate of emitter 5F. The amount of solute leached below the root zone was about 7,755 mmol higher than of that emitter 2P (2,565 mmol) over 10 years. It indicated that more solute leaching occurred to shallow groundwater when the emitter 5F was used. Thus, potential groundwater pollution more pronounce in emitter 5F.

7.3.2. Crop Nutrient Uptake

The cumulative nutrient uptake was computed by adjusting the amount of nutrient applied same for all the emitter designs. Figure 7.7 shows the cumulative nutrient root uptake during the cultivation season for different emitter designs. The figure shows that the root nutrient uptake was high and solute leaching was virtually eliminated when the emitter 2P was used. The ratio of the cumulative nutrient uptake to the cumulative nutrient applied for the emitter 2P was about 93.6 %, which is higher than that of emitter 5F (82.1%). Despite the lower irrigation discharge rate for the emitter 2P, allowing the plant roots to uptake more nutrient in the active root zone. At the same time, it reduced the nutrient leaching from the root zone due to excess water from irrigation events. However, the cumulative nutrient uptake was lower than the nutrient applied every year, indicating that the plant was not able to uptake all nutrients applied through fertigation event.

On the other hand, when the nutrient applied through emitter 5F, the nutrient uptake by plant roots was lower than emitter 2P. Although the same amount of water and nutrient applied in all emitter designs, the cumulative nutrient uptake was low in emitter 5F. This may be due to the fact that the higher emitter discharge rate facilitated more water and nutrient movement in downward directions. Therefore, more nutrients leached below the root zone. Furthermore, because of the high intensity of precipitation during the growing season of 2010 and 2016, more nutrients leached below to the root zone.

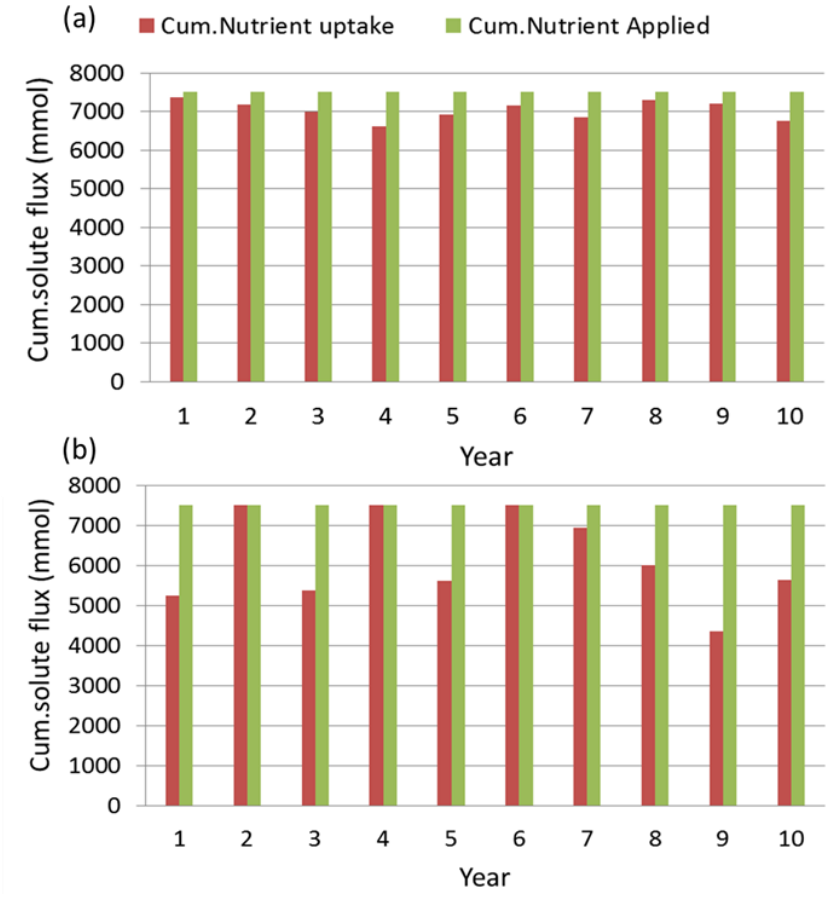

Figure 7.7 Cumulative nutrient uptake when the cumulative nutrient was applied same in (a) emitter 2P and (b) emitter 5F.

7.3.3. Solute Leaching

The amount of solute leached below the root zone was determined by computing the amount of solute flux drainage freely in the bottom boundary (i.e., 100 cm depth). The cumulative leached solute under different emitter designs is plotted in Figure 7.8. The leached solute was considerably higher when the emitter 5F was used. Nutrient leaching most likely occurred following a fertigation event for emitter 5F. This might be due to the fact that larger emitter discharge rate pushed the nutrient below the root zone. Wang et al. (2014) reported a great emitter discharge resulted in a large amount of deep percolation and nutrient leaching rate. An increase nutrient leaching was also greatly dependent on precipitation. A great precipitation during growing season produced more drainage. This fact was confirmed by simulating deep drainage in 2010 and 2016 where the precipitation was higher during the irrigation season. Arbat et al. (2013) indicated that nutrient leaching during the irrigation season was considerably higher when heavy precipitation events occurred and water consumption of crop roots was relatively small.

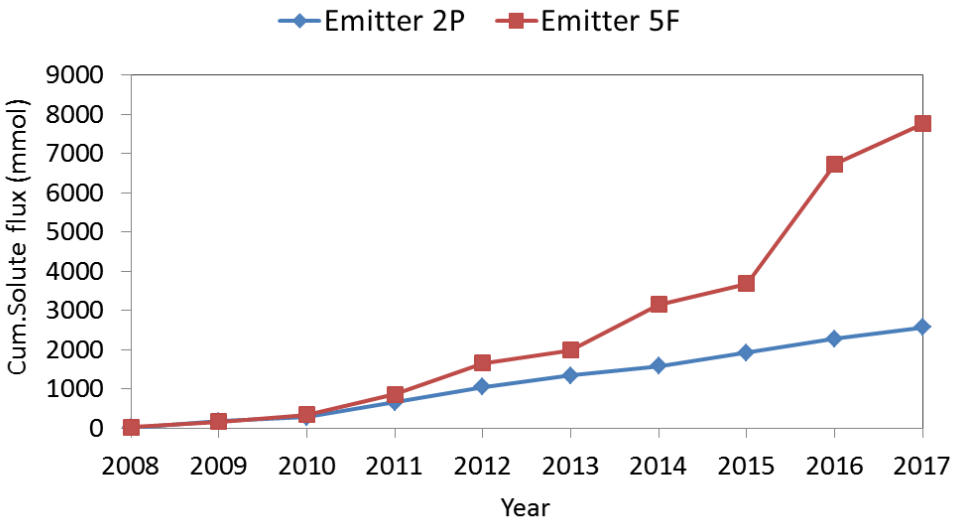

Figure 7.8 Cumulative solute leaching over 10 years when the same amount of fertigation was injected in emitter 2P and emitter 5F.

On the other hand, there was only limited leaching below the root zone and fertilizers remained accessible to the plant roots when the emitter 2P was used. As for the emitter 2P, water infiltrated slowly because of the low emitter discharge rate, resulted less nutrient moved downward during the growing season. The lower irrigation discharge rate facilitated root nutrient uptake and minimized the nutrient losses due to deep percolation. For the emitter 2P, the remained nutrient at the end of crop season leached out during rainy season. Therefore, the nutrient leaching was mainly due to the high precipitation instead of excessing water from irrigation events.

7.4. Summary

The long-term effect of subsurface irrigation with the ring-shaped emitter on water movement and solute distribution was evaluated numerically using HYDRUS. Two emitter designs were compared as well as: the emitters 2P and emitter 5F. The simulation results were extended by to 10 years in order to understand the effect of irrigation and nutrient applied on the shallow groundwater environment. The simulation results showed that potential solute leaching was higher when emitter 5F was used over 10 years. It can give negative impact to the ground water environmental as it increased the hazard pollutant from chemical fertilizer application. On the other hand, by applying fertigation through emitter 2P, which had the low discharge rate, the amount of nutrient leaching can be minimized. The simulation results confirmed that 93.6% of nutrient applied was taken by plant roots. Therefore, in order to minimize the leaching losses in fertigation cycle, the

application of emitter with low flow discharge rate can be considered. In this chapter, the assessment of irrigation and fertigation for long period is important to evaluate the design and management of subsurface irrigation with ring-shaped emitter in arid regions by considering climate conditions, crop, and soil types besides controlling environmental contaminations.

Chapter 8. Conclusions and Recommendations

8.1. Conclusions

This study has presented the performance of ring-shaped emitter for sustainable subsurface irrigation practices in arid regions. The experimental and numerical analysis was combined to evaluate irrigation design and practices by considering soil hydraulic characteristics, amount of water and nutrient application and crop system. This study was divided into several sub studies to address the specific objectives as follows:

1. Investigation subsurface water movement around buried ring-shaped emitter

In order to understand subsurface water flow around buried ring-shaped emitter, the laboratory experiments and numerical analysis were conducted. Knowledge of water movement in different soil characteristics and amount of water application is essential for the design and evaluating of subsurface irrigation with ring-shaped emitter. Subsurface water application experiments were carried out using the original ring-shaped emitter, 5F. Numerical model HYDRUS was used to simulate water movement around buried emitter. This study presented several conclusions;

a. Soil hydraulic properties greatly influence the wetted volume in infiltration processes during subsurface water was applied through buried ring-shaped emitter. Water moved radially around the emitter in silt, while downward water movement was dominant in sand. The difference in the flow pattern can be attributed to the difference in the macroscopic capillary length of the soil, which can be interpreted as a measure of the contribution of capillarity as opposed to gravity's effect on unsaturated water movement.
b. Water pressure head applications were significantly affected the wetted area. As water pressure head irrigation increase, the wetted area (e.g., wet volume) increase. Simulation results revealed that when the inlet pressure head was increased to 5 cm, wet volume reached near to soil surface for silt soil over 10 hour irrigation. It indicated that potential water loss from soil surface in silt soil due to the evaporation when the high water pressure head applied. On the other hand, as for sand soil, when the applied inlet pressure head was 5 cm, the preferential-type flow may have occurred underneath the drilled holes of the emitter that enhanced downward water movement. This type of flow

clearly creates a non-uniform asymmetrical wetted volume around the buried emitter, which may not be an ideal situation for plant roots to uptake water. It may, therefore, is not a good idea to apply a high inlet pressure when a ring-shaped emitter is installed in a sandy soil profile.

c. The simulated soil water contents (SWCs) using HYDRUS were fitted well with the observed soil water contents for silt. Whereas, for sand, SWCs above the buried emitter were overestimated, and those directly below the emitter were underestimated. Generally numerical model HYDRUS can capture reasonably how ring-shaped emitter with the original design for subsurface irrigation works.

2. Numerical evaluation of ring-shaped emitter designs for subsurface irrigation

This study addresses the improvement ring-shaped emitter design which is not only easy to maintained and operated but also to increase water productivity. Thus, modified ring-shaped emitter by reducing the number of holes in the emitter and changing the covering method into partially covered only around the hole was proposed. The effect of alternative emitter designs on the spatial extent of the wetted volume around the buried emitter during the subsurface water application was investigated numerically using HYDRUS. Had the spatial distribution of the SWC been non-uniform, some parts of the plant root system would have been stressed, resulting in the reduction in root water uptake. In this analysis, plant root water uptake (RWU) was therefore used as an indirect, quantitative proxy measure to assess the non-uniformity in the spatial extent of the wetted volume around the emitter. Two model plants, tomato and strawberry, were considered because of their contrasting root distributions. Both uncompensated and compensated RWU were then computed. While the former was used to assess the non-uniformity in the spatial extent of the wetted volume, the latter was used to investigate whether such non-uniformity had any effect on the plant root water uptake. In addition, the effect of preceding irrigation by considering several irrigation cycles was simulated to get more reliable for field practices. The presented study obtained several findings:

a. The non-uniformity in the wetted volume in silt for the emitter with fewer holes was not significantly different because water moved radially from the emitter, diminishing the effect of the spatial hole configuration. For sand, on the other hand, the non-uniformity in the wetted volume was larger, as indicated by uncompensated RWU. When the number of holes was reduced, the effect of the spatial hole configuration

could not be attenuated in sand as the downward movement was dominant due to gravity force was higher in sand soil.

b. Based on the compensated RWU model, the emitters with fewer holes tended to increase cumulative root water uptake for silt soil which corresponded to increase water use efficiency. As water was slowly discharged from the emitter with few holes, RWU slowly increased. Simulation results showed that water use efficiency was highest when the number of holes reduced to 2 holes (e.g., emitter 2P). This implies that reducing the number of holes does not affect the amount of water available for plant root uptake over 24 hours in silt.
c. Simulated compensated RWU revealed that cumulative root water uptake is strongly affected by emitter designs when preceding irrigation was considered in the simulation. As the number of holes was reduced to 3 holes (e.g., Emitter 3P), resulted the highest cumulative root water uptake.
d. In summary, these simulation results clearly confirmed that the number of holes can be reduced to 2 or 3 regardless of the soil types considered in this study.

3. The performance of ring-shaped emitter designs for subsurface irrigation during crop cultivation.

A combination between experimental and numerical analysis was conducted in order to evaluate the performance of ring-shaped emitter designs. Bell pepper (*Capsicum annum* L.) cultivation experiments were carried out in a glass-house. In the experiment, a bell pepper nursery was planted in a plant pot in which the ring-shaped emitter was buried at a depth of 15 cm. In addition to the modified design emitter with 2 holes, which was partially covered by the permeable textile, the original fully covered emitter with 5 holes was used in this experiment for a comparison purpose. Initially, the changes in soil water content at given positions and meteorological data were monitored during growing season as input parameters to assess the effects of ring –shaped emitter designs on soil water distribution and plant root water uptake. A numerical model, HYDRUS was used to validate the observed soil water content and actual plant root water uptake. The performance of ring-shaped emitter designs in terms of water productivity and irrigation water productivity was then evaluated. The results showed that:

a. Soil water content fluctuated at a depth of 10 cm and 20 cm that corresponded to irrigation events and crop transpiration.

b. The emitter which had few holes can minimize water loss due to evaporation in soil surface and deep percolation from the deep layer. As can be observed the amount of water applied was maintained in the root zone (e.g., 15 – 30 cm).
c. Soil water content remained high in all observation layers when subsurface water was applied through emitter which had more holes, emitter 5F.
d. Plant root distribution was strongly affected by emitter designs. Since soil water content remained high in all observation depths, root distributed uniformly from a depth of 5 to 35 cm. The maximum root length density was found at a depth of 15 cm and 20 cm for emitter 2P and 5F, respectively. It indicated that root uptake water intensively near from emitter location.
e. Simulation results documented that predicted water contents were a good agreement with observed data which the value of RMSE and MAE was low. In addition, although some discrepancies were found, but generally simulated actual root water uptake (i.e., actual transpiration) during cultivation was fitted well with observed values.
f. However emitter 2P had lower yield and growth performance, both experimental and numerical analysis confirmed that water productivity and irrigation water productivity can be increased when emitter 2P was used. The increases in water productivity and irrigation water productivity corresponded to the total amount of irrigation that was applied by different ring-shaped emitter designs.

4. Numerical evaluation of long-term effect of subsurface irrigation with ring-shaped emitter in arid region.

In order to provide food security besides environmental protection and suitable development, it is necessary to evaluate the long-term utilization of subsurface irrigation with ring-shaped emitter by considering water and nutrient movement during irrigation practices. For this purpose, prediction and simulation for long-term period can be used for developing sustainable irrigation and fertigation operation. In this study, HYDRUS model was used to simulate water and nitrogen distribution in the soil through buried ring-shaped emitter. In the simulation results showed that solute has a very high leaching potential during the plant growth season when the original design of ring-shaped emitter was used. Solute transfer to shallow groundwater due to the high irrigation discharge rate was injected in emitter 5F and precipitation occurred at the same time. Therefore, optimization irrigation and fertigation scheduling are necessary by considering solute

leaching and its accumulation in the soil profile when emitter 5F was used for long-term period. On the other hand, by applying fertigation through emitter 2P, the amount of nutrient leaching can be minimized. The simulation results confirmed that 93.6% of nutrient applied was taken by plant roots. Therefore, in order to minimize the leaching losses in fertigation cycle, the application of emitter with low flow discharge rate can be considered.

Overall, this study clearly demonstrated that in designing subsurface irrigation with ring-shaped emitter involves with many factors, including the selections of an appropriate water pressure head application (i.e. emitter discharge rate), soil hydraulic characteristics, crop and climate conditions as well as plant root distribution, root and nutrient uptake, transpiration and evaporation. Understanding water and nutrient movement in the vadose zone are important for an efficient irrigation water use and prevention of solute transport to groundwater environment. Thus, Numerical model HYDRUS can be a useful tool to predict those parameters and evaluate subsurface irrigation with ring-shaped emitter when the number of experiments were limited. A proper design of ring-shaped emitter for subsurface irrigation with the reduced number of holes is likely to be recommended to increase irrigation water productivity in arid regions. In addition the modified design with partial cover can be easily maintained and operated by the farmers.

8.2. Recommendation for Future Works

In the light of the obtained results and during the investigation presented in the current study, it was thought that the following research lines could be carried out in the further investigations:

1. Study of the effect of capillary barrier on coarser soil textures under subsurface irrigation with ring-shaped emitter.

   Since the investigation of soil water movement in sand resulted preferential flow and non-uniformity flow, installation capillary barrier at given depth can be proposed to prevent water loss due to deep percolation.
2. Study of the effect emitter depths and emitter spacing in the crop line on soil water distribution and nutrient transport during annual crop cultivation to improve irrigation water productivity.

   This study will improve the optimization of ring-shaped emitter installation in a depth and space between crops. In order to reach this objective, it will be better to apply different depth installations by considering root distribution, water and nutrient uptake

by plant roots. The cultivation experiment will be conducted in the field instead of pot cultivation in order to understand the real factors which can influence the crop growth.

3. Evaluation of fertigation scheduling in order to get optimum irrigation and fertigation practices.

   This study will address the improvement fertilizer use efficiency under subsurface irrigation with ring-shaped emitter. Understanding the reactive transport of urea, ammonium, and nitrate during fertilizer application with irrigation water in the root zone will be helpful to develop fertigation and irrigation management. Numerical model can be used to quantify the movement and transformations of various nitrogen forms.

References

Ajdary K., 2005. Modeling of water and nitrogen movement under drip fertigation. PhD thesis. Division of agricultural engineering, Indian Agricultural Research Institute, New Delhi, India.

Ajdary K., Singh D.K., Singh A.K., Khanna M., 2007. Modelling of nitrogen leaching from experimental onion field under drip fertigation. *Agric. Water Manag.* 89; 15-28. https://doi.org/10.1016/j.agwat.2006.12.014

Al-Omran, A.M., Sheta, A.S., Falatah, A.M., and Al-Harbi, A.R. 2005. Effect of drip irrigation on Squash (*Cucurbitapepo*) yield and water use efficiency in sandy calcareous soils amended with clay deposits. *Agric. Water Manag.* 73; 43-55. DOI: 10.1016/j.agwat.2004.09.019.

Allen R.G., Pereira L.S., Raes D., Smith M., 1998. Crop evapotranspiration, guidelines for computing crop water requirements. FAO irrigation and drainage paper 56, Food and Agriculture Organization of the United Nations (FAO), Rome.

Alva A.K., Paramasivam. S., Obreza T.A., Schumann A.W., 2006. Nitrogen best management practice for citrus tree: I. Fruit yield, quality and leaf nutritional status. *Sci. Hortic*. 107; 233-244.

Antony E., Singandhupe R.B., 2004. Impact of drip and surface irrigation on growth, yield and WUE of capsicum (*Capsicum annum* L.) *Agric. Water Manag.* 65; 121-132. DOI: 10.1016/j.agwat.2003.07.003.

Arampatzis G., Tzimopoulos C., Sakellariou-Makrantonaki M., Yannopoulos S., 2001. Estimation of unsaturated flow in layered soils with the finite control volume method. *Irrig Drain* 50; 349–358.

Arbat G., Rosello A., Olive D., Barques J., Linas G., Ros D.E., Pujol J.M., Cartagena D.R., 2013. Soil water and nitrate distribution under drip irrigated corn receiving pig slurry. *Agric. Water Manag*. 120; 11-22.

ASAE, 2001. ASAE Standard S256.2 JAN 01. Soil and Water Terminalogy. American Society Agricultural Engineers. St. Joseph, Michigan. 21 pp.

AQUASTAT, 2011. Irrigation in Southern and Eastern Asia, AQUASTAT Survey, 2011. FAO Water Report 37. Food and Agriculture Organization of the United Nations, Rome.

BPS (Central Bureau of statistics of Indonesia; Biro Pusat Statistic), 2018. The population projection of Indonesia by province 2010-2035. Available on: https://www.bps.go.id/statictable/2014/02/18/1274/proyeksi-penduduk-menurut-provinsi-2010-2035.html (Accessed on 17 January 2019)

Batchelor, C., Lovel, C., and Murata, M., 1996. Simple micro irrigation techniques for improving irrigation efficiency on vegetable gardens. *Agric. Water Manag.* 32(1); 37-48. DOI: 10.1016/S0378-3774(96)01257-7.

Batra B.R., Inder M., Arora S.K., and Mohan I., 2000. Effect of irrigation and nitrogen levels on dry matter production by okra (*Abelmochus esculentus* L.Moench). *Haryana J.Hortic. Sci.* 29 (3-4); 239-241.

Bear J., 1972. Dynamics of fluids in porous media. Elsevier, New York.

Ben Gal, A., Lazarovitch, N., and Shani, U. 2004. Subsurface drip irrigation in gravel filled cavities. *Vadose Zo. J.* 3, 1407–1413.

Bhattari S.P., Huber S., and Midmore D.J., 2004. Aerated subsurface irrigation gives growth ad yield benefits to zucchini, vegetavle soybean and cotton in heavy clay soils. *Ann. Appl. Biol.* 144; 285-298.

Bryla D.R., Banuelos G.S., and Mitchell, J.P., 2003. Water requirements of subsurface drip-irrigated faba bean in California. *Irrig. Sci*. 22; 31-37.

Bufon, V.B., Lascano, R.J., Bednarz, C., Booker, J.D., Gitz, D.C., 2012. Soil water content on drip irrigated cotton: Comparison of measured and simulated values obtained with the Hydrus 2-D model. *Irrig. Sci*. 30; 259–273. https://doi.org/10.1007/s00271-011-0279-z.

Cai G., Vanderborght J., Vereecken H., Couvreur V., Mboh C.M., 2017. Parameterization of root water uptake models considering dynamic root distributions and water uptake compensation. *Vadose Zo. J*. DOI:10.2136/v zj2016.12.0125

Camp CR., 1998. Subsurface drip irrigation: a review. *Trans ASAE.* 41(5); 1353–1367.

Cancela J.J., Fandino M., Rey B.., Martinez E.M., 2015. Automatic irrigation system based on dual crop coefficient, soil and plant water status for Viris vinifera (*cv Godelloand cv Mencia*). *Agric. Water Manag.* 151; 52-63.

Celia M.A., Bouloutas E.T., Zarba R.L., 1990. A general massconservative numerical solution for the unsaturated flow equation. *Water Resou Res.* 26(7):1483–1496.

Clausnitzer V., Hopmans .W., 1994. Simulteneous modeling of transient three-dimensional root growth and soil water flow. *Plant Soil.* 165; 299-314.

Cirelli A.F., Arumi J.L., Rivera D., and Booch P.W., Environmental effect of irrigation of arid and semiarid regions. *J. Agric. Res.* 69 (1); 27-40

Coelho E.F., and Or D., 1999. Root distribution and root water uptake patterns of corn under surface and subsurface drip irrigation. *Plant and Soil*. 206; 123-136.

Costa DL., Gianquinto G., 2002. Water stress and water table depth influence yield, water use efficiency and nitrogen recovery in bell pepper, lysimeter studied. *Australian J. Agric. Res.* 53; 201-210.

Cote, C.M., Bristow, K.L., Charlesworth, P.B., Cook, F.J., Thorburn, P.J., 2003. Analysis of soil wetting and solute transport in subsurface trickle irrigation. *Irrig. Sci*. 22; 143–156. https://doi.org/10.1007/s00271-003-0080-8

Dekker, L.W., Ritsema, C.J., 1994. How water moves in a water repellent sandy soil: 1. Potential and actual water repellency. *Water Resour. Res*. 30; 2507–2517. https://doi.org/10.1029/94WR00749

DeMalach, Y., Pasternak, D., 1993. Agriculture in a desert saline environment, a case study. In MaraniBettolo, G.B. (Ed.). Agriculture and the Quality of Life, New Global Trends. Proceeding of an international conference held at The Pontificia Academia Scientiarum, Ex Aedibvs Academicis in Civitate Vaticana, Rome, Italy, pp. 97-26.

Denmead O.T., and Shaw R.H., 1962. Availability of the soil water to plants as affected by moisture content and meterological conditions. *Agro. J.* 4; 385-390.

Dexter A.R., 2004. Soil physical quality: Part I. Theory, effects of soil texture, density, and organic matter, and effects on root growth. *Geoderma.* 120(3-4);201-214.

Doorenbos J., Pruitt W.O., Aboukhaled A., Damagnez J., 1992. Crop water requirements; FAO Irrigation and Drainage paper 24. Food and Agriculture Organization of The United Nations, Rome.

Doltra J., Munoz P., 2010. Simulation of nitrogen leaching from a fertigated crop rotation in a Mediterranian climate using the EU-Rotate_N and HYDRUS-2D models. *Agric. Water Manag*. 97; 277-285.

Dukes M.D., Simmone M.H., Davis W.E., Studstill D.W., Hochmuth R., 2003. Effect of sensor-based on high frequency irrigation on bell pepper yield and water use. Water for sustainable world-limited supplies and expanding demand. in *Proceeding of the second international conference on irrigation and drainage,* Phoenix, Arizona 12-15 May; 665-675.

El-Nesr, M.N., Alazba, A.A., Šimůnek, J., 2014. HYDRUS simulations of the effects of dual-drip subsurface irrigation and a physical barrier on water movement and solute transport in soils. *Irrig. Sci*. 32, 111–125. https://doi.org/10.1007/s00271-013-0417-x

Fandino M., Cancela J.J., Rey B.J., Martibez E.M., Rosa R.G., Pereire L.S., 2012. Using the dual Kc approach to model evapotranspiration of Albarino vineyards (*Viris vinifera* L.cv. Albarino) with consideration of active ground cover. *Agric. Water Manag.* 112; 75-87.

FAO, 2015. Towards a water and food secure future; Critical perspective for policy makers. FAO White paper. Food and Agriculture Organization of The United Nations, Rome and World Water Council, Marseille.

FAO. 2011b. The state of the world's land and water resources for food and agriculture (SOLAW)-Managing system at risk. FAO and Earthscan, Rome and London.

Fares A., Parsons L.R., Wheaton T.A., Morgan K.T., Šimůnek J., van Genchuten M.Th., 2001. Simulated drip irrigation with different types of soils. *Proc Fla State Hort Sci*. 114:22–24.

Feddes R.A., Kowalik, P.J., Zaradny, H., 1978. Simulation of Field Water Use and Crop Yield. John Wiley & Sons, New York.

Feddes R.A., Hoff H., Bruen M., Dawson T., de Rosnay P., Dirmeyer P., Jackson R.B., Kabat P., Kleidon A., Lilly A., Pitman A.J., 2001. Modeling root water uptake in hydrological and climate model. *Am. Meteorological Soc.*. 82 (12); 2797-2810. http://doi.org/10.1175/1520-0477(2001)082<2797:MRWUIH>2.3.CO;2.

Feddes R.A., Raats P.A.C., 2004. Parameterizing the soil-water-plant root system. In Feddes R.A., de Roij G.H., van Dam J.C. (Eds.), Proceeding of the Unsaturated Zone Modeling: Progress, Challenges and Appliaction.

Ferrara A., Lovelli S., Di Tommaso T., Perniola M., 2011. Flowering, growth and fruit setting in greenhouse bell pepper under water stress. *J. Agro.* 10; 12-19.

Gärdenäs, A.I., Hopmans, J.W., Hanson, B.R., Šimůnek, J., 2005. Two-dimensional modeling of nitrate leaching for various fertigation scenarios under micro-irrigation. *Agric. Water Manag*. 74; 219–242. https://doi.org/10.1016/j.agwat.2004.11.011

Ghazouani, H., M'Hamdi, B.D., Autovino, D., Mguidiche Bel Haj, A.M., Rallo, G., Provenzano, G., Boujelben, A., 2015. Optimizing subsurface dripline installation depth with Hydrus 2D/3D to improve irrigation water use efficiency in the central Tunisia. *Int. J. Metrol. Qual. Eng*. 6; 1–9. https://doi.org/10.1051/ijmqe/2015024

Gao Y., Duan A., Qiu X., Liu Z., Sun J., Wang H., 2010. Distribution of roots and root length density in a maize soy bean strip inter cropping system. *Agric. Water Manag.* 98; 199-212.

Hanson, B.R., 1995. Drip irrigation of row crops: An overview. In: Proceedings Fifth International Microirrigation Congress, Orlando, FL, April 2-6, pp. 651-655.

Hanson B.R., Šimůnek J., Hopmans J.W., 2006. Evaluation of urea-ammonium-nitrate fertigation with drip irrigation using numerical modeling. *Agric. Water Manag.* 86; 102-113.

Hanson B., Hopmans J.W., Šimůnek J., 2008. Leaching with subsurface drip irrigation under saline, shallow ground water conditions. *Vadose Zo. J.* 7(2); 810-818.

Hillel D., 1980. Applications of soil physics. Academic Press Inc. New York.

Hopmans J.W., Bristow K.L., 2002. Current capabilities and future needs of root water and nutrient uptake modeling. *Adv Agron*. 77:104–175.

Hoffman, G.J., Mead, R.M., Ziska, L.H., Francois, L.E., Gatlin, P.B., 1986. Salt tolerance of mature plum trees yield. Water Management Research Laboratory Annual Report, USDA, Fersno, CA, pp. 62-63.

Imanudin M.S and Prayitno, 2015. Pengembangan irigasi bawah pemukaan untuk irigasi mikro melalui metoda kapilaritas tanah. Proceeding Seminar of Swasembada Pangan. 29 April 2015, pp 376-381 (In Indonesian).

Ityel E., Lazarovitch N., Silberbush ., Ben-Gal A., 2011. An artificial capillary barrier to improve root zone condition for horticultural crops: physical effects on water content. *Irrig.Sci.* 29; 171-180.

Jarvis N.J., 1989. A simple empirical model of root water uptake. *Hydrol. J.* 107; 57-72.

Ju S.H., Kung K.J.S., 1997. Mass types, element orders and solution schemes for Richards equation. *Comp Geosci.* 23(2); 175–187.

Kandelous, M.M., Šimůnek, J., 2010a. Comparison of numerical, analytical, and empirical models to estimate wetting patterns for surface and subsurface drip irrigation. *Irrig. Sci*. 28, 435–444. https://doi.org/10.1007/s00271-009-0205-9

Kandelous M.M., Simunek J., 2010. Numerical simulations of water movement in a subsurface drip irrigation system under field and laboratory conditions using HYDRUS. *Agric. Water Manag.* 97; 1070-1076.

Kandelous M. M., Šimůnek J., van Genuchten M.Th., Malek K., 2011. Soil water content distributions between two emitters of subsurface drip irrigation system. *Soil Sci. Soc. Am. J.* 75; 488-497.

Kandelous, M.M., Kamai, T., Vrugt, J.A., Šimůnek, J., Hanson, B., Hopmans, J.W., 2012. Evaluation of subsurface drip irrigation design and management parameters for alfalfa. *Agric. Water Manag*. 109; 81–93. https://doi.org/10.1016/j.agwat.2012.02.009

Kavetski D., Binning P., Sloan S.W., 2002. Non-iterative time stepping schemes with adaptive truncation error control for the solution of Richards equation. *Water Resour Res* 38(10):1211–1220.

Keller, Jack, 2002, Evolution of Drip/ Micro Irrigation: Traditional and Nontraditional Uses, Keynote address at the International Meeting on Advances in Drip/ Micro Irrigation, December 2002, Spain

Klute A., Dirksen C., 1986. Hydraulic conductivity and diffusivity: Laboratory methods of soil analysis, part 1, 2nd edn. Agronomica monograph 9, ASA amd SSSA, Madison. Pp 687-734.

Kreij D.C., van der Burg, and Runia W.T., 2003. Drip irrigation emitter clogging in Dutch greenhouses as affected by methane and organic acids. *Agric. Water Manag.* 60 (2); 73-85

Keller, Jack and Andrew Keller, 2005, Mini–irrigation Technologies for Smallholders, Proceeding of the World Water and Environmental Resources Congress, 15–19 May 2005, Alaska, USA.

Krounbi, L., and N. Lazarovitch. 2011. Soil hydraulic properties affecting root water uptake. In: J. Gliński et al., editors, Encyclopedia of gro-physics. Springer, Dordrecht, the Netherlands. p. 748–754.

Kulkarni, S.A., 2005, Looking Beyond Eight Sprinklers, Proceedings of the National conference on Micro Irrigation, June 2005, G.B. Pant University of Agriculture and Technology, Pantnagar, Uttaranchal, India

Lamm, F.R., Ayars, J.E., and Nakayama, F.S., 2007. Micro irrigation for crop production; Design, Operation and Management. First Edition, Elsevier. B.V. The Netherland

Lazarovitch. N., Shani, U., Thompson. T.L., Warrick. A.W., 2006. "Soil Hydraulic Properties Affecting Discharge Uniformity of Gravity-Fed Subsurface Drip Irrigation Systems. *J. Irrig. Drain. Eng.* 132 (6); 531-536. DOI:10.1061/ASCE0733-9437(2006)132:6 (531).

Lazarovitch, N., Warrick, A.W., Furman, A., Šimůnek, J., 2007. Subsurface Water Distribution from Drip Irrigation Described by Moment Analyses. *Vadose Zo. J.* 6; 116. https://doi.org/10.2136/vzj2006.0052 .

Lila A.T.S., Berndtsson R., Persson M., Somaida M., El-Kiki M., Hamed Y., Mirdan A., 2013. Numerical evaluation of subsurface trickle irrigation with brackish water. *Irrig. Sci.* 31; 1125-1137.

Lowder, S.K., Skoet J., Singh, S., 2014. "What do we really know about the number and distribution of farms and family farms worldwide?", Background of paper for *The State of Food and Agricultur*e 2014, ESA Working Paper No. 14-02, Food and Agriculture Organization of the United Nation, Rome

Maas E.V., Hoffman G.J., 1977. Crop salt tolerance-current assessment. *J. Irrig.Drain.* 103; 115-134.

Maas E.V., 1986. Salt tolerance of plants. *Appl. Agric.Res.* 1(1); 12-25

Maas E.V., 1990. Crop salt tolerance. In Tanji K.K. (ed), Agricultural Salinity Assessment and Management. ASCE Manual and Report on Engineering Practice 71. *Am. Soc. Civ. Eng.* New York, pp. 262-304.

Maas E.V., and Grattan S.R., 1999. Crop yields as affected by salinity. *J.Agric. Drain.* 38; 55-108.

Machado R.M.A., Oliviera M.D.G., 2005. Tomato root distribution, yield and fruit quality under different subsurface drip irrigation regimes and depths. *Irrig Sci.* 24; 15-24.

Martines J., and Reca J., 2014. Water use efficiency of surface drip irrigation versus an alternative subsurface drip irrigation method. *J.Irrig. and Drain. Eng*. 140. DOI:10.1061/(ASCE)IR.1943-4774.0000745.

Marquardt, D.W., 1963. An algorithm for least-squares estimation of nonlinear parameters. SIAM J. Appl. Math. 11,431–441.Naglič, B., Kechavarzi, C., Coulon, F., Pintar, M., 2014. Numerical investigation of the influence of texture, surface drip emitter discharge rate and initial soil moisture condition on wetting pattern size. *Irrig. Sci*. 32; 421–436. https://doi.org/10.1007/s00271-014-0439-z

Miguel A., and Fransisco M., 2007. Response of tomato plants to deficit irrigation under surface and subsurface drip irrigation. *J. App. Hortic.*, 9(2); 97-100

Miyazaki T., Hasegawa S., Kasubuchi T., 1993. Water flow in soils. Marcel Dekker Inc. New York.

Mommer L., and Visser E., "Protocol;Root distribution in soils I. Root core sampling and destructive pot harvests", was accessed 11/12/2017 at http://prometheuswiki.org/tiki-index.php?page=Root+distribution+in+soils+I.+Root+core+sampling+destructive+pot+harvest

Mualem Y., 1976. A new model for predicting the hydraulic conductivity of unsaturated porous media. *Water Resour Res.* 12:513–522.

Mulyani A. and Sarwani M., 2013. The characteristic and potential of suboptimal land for agriculture development in Indonesia. Jurnal Sumber Daya Lahan. 7(1): 47-55. (In Indonesian with English abstract).

Nagazawa K., Zhang J., Nishimura T., Saito H., Kato M., 2008. Impact of pressure heads applied to porous bottles on water supply characteristics for subsurface irrigation. *J. Arid Land Studies*. 18(1); 11-20.

Naglicˇ B, Kechavarzi C., Coulon F., Pintar M., 2014. Numerical investigation of the influence of texture, surface drip emitter discharge rate and initial soil moisture condition on wetting pattern size. *Irrig Sci*. 32 :421–436. DOI 10.1007/s00271-0140439-z.

National Oceanic and Atmospheric Administration. The U.S Department of Commerce. 2018. Weather data resources in West Nusa Tenggara, Indonesia. Available on: http://www1.ncdc.noaa.gov . (Accessed on 23 October 2018).

Oron, G., DeMalach, Y., Hoffman, Z., Keren, Y., Hartmann, H., Plazner, N., 1990. Wastewater disposal by subsurface trickle irrigation. In: Proceedings, Fifteenth Biennial Conference, IAWPRC, Kyoto, Japan, July 29-Aug. 3, pp. 2149-2158

Oron, G., DeMalach, Y., Gillerman, L., David, I., 1995. Pear response to saline water application under subsurface drip irrigation. In: Proceedings Fifth International Microirrigation Congress, Orlando, FL, April 2-6, pp. 97-103.

Palada M., Mercado A.C., Roberts M., Ella V.B., Reyes M.R., Susila A.D., Ha D.T., Wu D.L., and Bhattarai M., 2011. Farmers experiences with low-pressure drip irrigation for vegetable production in Southeast Asia and the Pasific. *Acta Hortic*. 921; 49-56. https://doi.org/10.17660/ActaHortic.2011.921.5

Patel N and Rajput T.B.S., 2008. Dynamic and modeling of soil water under subsurface drip irrigated onion. *Agric. Water Manag*. 95; 1335-1349. https://doi.org/10.1016/j.agwat.2008.06.002

Perry C., 2011. Accounting for water use terminology and implications for saving water and increasing production. *Agric. Water Manag.* 98; 1840-1846.

Phene, C.J., Davis, K.R., Hutmacher, R.B., McCormic, R.L., 1987. Advantages of subsurface irrigation for processing tomatoes. In: Proceedings, International Symposium on Integrated Management Practices for Tomato and Pepper Production in the Tropics, Shanhua, Taiwan, ROC, pp. 325-338.

Phene, C.J., Davis, K.R., Hutmacher, R.B., Bar-Yosef, B., Meek, D.W., 1990. Effect of high frequency surface and subsurface drip irrigation on root distribution of sweet corn. *Irrig. Sci. J.,* 12; 135-140.

Phene C.J., Davis KR, Hutmacher RB, Bar-Yosef B, Meek DW, Misaki J., 1991. Effect of high-frequency surface and subsurface drip irrigation on root distribution of sweet corn. *Irrig Sci*. 12; 135–140.

Philip J.R., 1968. Setady infiltration from buried point source and spherical cavities. *Water Resour Res.* 20; 1039-1047.

Philip J.R., 1991b. Effects of root and sub irrigation on evaporation and percolation losses. *Soil Sci Soc Am J.* 55; 1520–1523.

Philip J.R., 1992. What happens near a quasi-linear point source?. *Water Resour Res.* 28:47–52.

Phogat V., Skewes M.A., Cox J.W., Sanderson G., Alam J., Šimůnek J., 2014. Seasonal simulation of water, salinity and nitrate dynamics under drip irrigated mandarin (*Citrus reticulata*) and assessing management options for drainage and nitrate leaching. *J.Hydrol.* 513; 504-516. http://dx.doi.org/10.1016/j.jhydrol.2014.04.008.

Postel, S. 2000. Redesigning irrigated agriculture. State of The World, Vol. 272; 39-58.

Provenzano G., 2007. Using HYDRUS-2D simulation model to evaluate wetted soil volume in subsurface drip irrigation systems. *J. Irrig Drain Eng*. ASCE 133(4):342–349.

PSDA (Direktorat Pengelolaan Sumber Daya Air; Directorate General of Water Resources), 2008. Pedoman teknis pengembangan irigasi bertekanan (Manual book of low-pressure irrigation; drip and sprinkler irrigation). pp 42 (In Indonesian).

PU (Kementrian Pekerjaan Umum: Minstry of Public Work), 2016. Irigasi mikro. Available in http://litbang.pu.go.id/berita/view/814/air-mahal-terapkan-irigasi-mikro. (accessed in 17 January 2018)

Purwartini T.B and Suhaeti R.N., 2017. Small scale irrigation: performance, problems and solutions. Forum Penelitian Agro Ekonomi 35(2): 91-105. (in Indonesian with English Abstract). DOI: 10.21082/fae.v35n2.2017.91-105.

Radcliffe D., Šimůnek J., 2010. Soil physics with HYDRUS: modeling and applications, CRC Press. Taylor and Francis Group, Boca Raton, FL.

Radin, J. W., Mauney, J. R., and Kerridge, P. C., 1989. Water uptake by cotton roots during fruit filling in relation to irrigation frequency. *Crop Sci.*, 29; 1000–1005.

Ramos T.B., Simunek J., Gonsalves M.C., Martins J.C., Prazeres A., Pereira L.S., 2012. Two-dimensional modeling of water and nitrogen fate from sweet sorghum irrigated with fresh and blended saline waters. *Agric Water Manag*. 111; 87-104.

Rawlins, S. L., and Raats, P. A. C., 1975. Prospects for high-frequency irrigation. *Science*, 188; 604–610.

Richards L.A., 1942. A pressure-membrane extraction apparatus for soil solutions. *Soil Sci.* 53: 241-248

Rodrigues G.C., Pereire L.S., 2009. Assessing economic impacts of deficit irrigation as related to water productivity and water costs. *Biosystems Eng.*, 103; 536-551.

Scanlon B.R. Levit D.G., 2005. Ecological controls on water-cycle response to climate variability in deserts. *Proc. Natl. Acad. Sci.* 102(17); 6033-6038.

Saefuddin R., Setiawan B.I., Saptomo S.K., Mustaningsih P.R.D., 2014. Performance Analysis of Emitter Ring Irrigation System. *Jurnal Irigasi. 9*; 63-74 (in Indonesian with English Abstract). https://doi.org/10.13140/RG.2.1.1102.6647

Saefuddin R., Saito H., Šimůnek J., 2018. Experimental and numerical evaluation of ring-shaped emitter for subsurface irrigation. *Agric. Water Manag. 211; 111-122.* https://doi.org/10.1016/j.agwat.2018.09.039

Sagi., 2006. Dripper resistance to clogging with use of effluent water; a case study. *Int. Water Irrig.* 26 (2); 42-43

Sansoulet J, Cabidoche Y-M, Cattan P, Ruy S., Šimůnek J., 2008. Spatially distributed water fluxes in an Andisol under banana plants; experiments an three-dimensional modeling. *Vadose Zo.J.* 7: 819-829.

Saptomo S.K., Setiawan B.I., Mustaningsih P.R.D., Chadirin C., Sumarsono J., 2014. Development of solar power irrigation in arid region using micro irrigation system. Research Project Report. (In Indonesian with English Summary).

Selim A. L., Berndtsson R., Persson M., Somaida M., El-Kiki M., Hamed Y., Mirdan A., 2012. Numerical evaluation of subsurface irrigation with brackish water. *Irrig.Sci*. 31; 1125-1137.

Sezen SM., Yazar A., HayarS., Baytorun N., Yildiz D., Asiye A., Servet T., Derya O., Erdal A., Yelderem A., Ozkan G., 2015. Comparison of drip-and furrow-irrigated red pepper yield, yield component, quality and net profit generation. *J. Irrig. Drain.* 64(6). DOI: 10.1002/ird.1915.

Shani U., Xue, S., Gordin-Katz, R., and Warrick, A. W., 1996. Soil limiting flow from subsurface emitters. I: Pressure measurements. *J.Irrig. Drain. Eng*., 122(5); 291–295.

Shani U., Ben-Gal, A., Tripler, E., Dudley, L.M., 2007. Plant response to the soil environment: An analytical model integrating yield, water, soil type, and salinity. *Water Resour. Res*. 43; 1–12. https://doi.org/10.1029/2006WR005313

Shukla S., Jaber FH., Goswami D., Srivastava S., 2013. Evapotranspiration losses for pepper under plastic mulch and shallow water table conditions, *Irrig. Sci. J.* 31; 523-536.

Siedel S.J., Schutze N., Fahle M., Mailhol J.C., and Ruelle P., 2015. Optimal irrigation scheduling, irrigation control and drip line layout to increase water productivity and proit in subsurface drip-irrigated agriculture. *J. Irrig. Drain.*, 64; 501-518. DOI: 10.1002/ird.1926.

Siemens, J., G. Huscheka, C. Siebe, and M. Kaupenjohanna. 2008. Concentrations and mobility of human pharmaceuticals in the world's largest wastewater irrigation system, Mexico City-Mezquital Valley. *Water Res*. 42; 2124-2134.

Simionesei L., Ramos T.B., David B., Jauch E., Pedro C.L., 2016. Numerical Simulation of soil water dynamics under stationary sprinkler irrigation with MOHID-LAND. *J.Irrig.and Drain.* DOI: 10.1002/ird.1944.

Skaggs T.H., Trout T.J., Šimůnek J., Shouse P.J., 2004. Comparison of HYDRUS-2D simulations of drip irrigation with experimental observations. *J Irrig Drain Eng.* ASCE. 130(4):304–310.

Šimůnek J., Sejna M., van Genuchten M.Th., 1999. The HYDRUS-2D software package for simulating two-dimensional movement of water, heat and multiple solutes in variably saturated media, Version 2.0. Rep. IGCWMC-TPS-53, p 251, International Ground Water Model. Cent., Colo. Sch. of Mines, Golden, CO.

Šimůnek J., 2005. Models of water flow and solute transport in the unsaturated zone. In: MG Handerson (ed) *Encyclopedia of Hydrol Sci*; 1171–1180.

Šimůnek J., van Genuchten M.Th., Šejna M., 2006. The HYDRUS software package for simulating two-, and three-dimensional movement of water, heat and multiple solutes in variably saturated media, Technical manual, Version 1.0, PC Progress, Prague, Czech Republic. P.241.

Šimůnek J., van Genuchten M.Th., 2008. Modeling non equilibrium flow and transport with HYDRUS. *Vadose Zo. J.* 7(2); 581-586.

Šimůnek J., and Hopmans J.W., 2009. Modeling compensated root water uptake and nutrient uptake. *Ecol. Modelling.* 220; 505-521. DOI:10.1016/j.ecolmodel.2008.11.004

Šimůnek J., van Genuchten M.Th., Šejna M., 2012. Hydrus: model use, calibration and validation. Tansac Asabe, 55(4): 1261-1274.

Šimůnek, J., van Genuchten, M.Th., Šejna, M., 2016. Recent developments and applications of HYDRUS computer software packages. *Vadose Zo. J.* 6; 1–25. https://doi.org/0.2136/vzj2016.04.0033

Šimůnek, J., Šejna, M., van Genuchten, M.Th., 2018. New features of version 3 of the HYDRUS (2D/3D) computer software package. *J. Hydrol. Hydromech.*66(2); 133-142. DOI: 10.1515/johh-2017-0050.

Siyal A.A., van Genuchten M.T., Skaggs T.H., 2009. Performance of pitcher irrigation system. *Soil Sci.* 174; 312-320.

Steudle E., and C.A. Peterson. 1998. How does water get through roots? *J. Exp. Bot*. 49:775–788. 10.1093/jexbot/49.322.775

Subbaiah R., 2013. A review of models for predicting soil water dynamics during trickle irrigation. *Irrig Sci* . 31:225–258. DOI 10.1007/s00271-011-0309-x.

Su D., Tian, Y., and Gao, Q. Z., 2000. Application of gravity and low head drip irrigation techniques in solar greenhouses." *Trans. Chinese Soc. Agric. Eng.* 16, 73–76 in Chinese with English abstract.

Sumarsono J., Setiawan B.I., Subrata, I.D.M., Waspodo, R.S.B., Saptomo S.K., 2018. Ring-typed emitter subsurface irrigation performances in dryland farmings. *Int. J. Civ. Eng. Technol*. 9; 798-806.

Sun S.M., An, Q.X., Yang P.L., Lu X.B., and Gu K.K., 2016. Effect of irrigation depth on root distribution and water use efficiency of jujube under indirect subsurface drip irrigation. *J. Trans. Chinese Soc. Agric. Machinery.* 47 (8); 81-90.

Syuaib M.F., 2016. Sustainable agriculture in Indonesia: Facts and challenges to keep growing in harmony with environment. *Agric.Eng.Intl-The CIGR.* 18(2): 170-184.

Taylor S.A., Ashcroft G.M., 1972. Physical edaphology. Freeman and Co., San Fransisco, CA, pp.434-435.

Van Genuchten M.Th., 1980. A closed form equation for predicting the hydraulic conductivity of unsaturated soils. *Soil Sci. Soc. Am. J.*, 44; 892–898.

Van Genuchten M.Th., and Hoffman G.J., 1984. Analysis of crop salt tolerance data. *In:* Shainberg I., and Shalhevet J. eds. *Soil salinity under irrigation: processes and management. Ecological Studies.* 51; 258-271.

Van Genuchten M.T., Leij, F.J., Yates, S.R., 1991. The RETC Code for Quantifying the Hydraulic Functions of Unsaturated Soils. United States Environ. Research. Lab. 93. https://doi.org/10.1002/9781118616871

Vazifedousta M., van Dam J.C., Feddes R.A., Feizi M., 2008. Increasing water productivity of irrigated crops under limited water supply at field scale. *Agric. Water Manag*. 95 (2); 89-102.

Vrugt J.A., Van Wijk, M.T., Hopmans, J.W., Šimunek, J., 2001. One-, two-, and three-dimensional root water uptake functions for transient modeling. *Water Resour. Res*. 37; 2457–2470. https://doi.org/10.1029/2000WR000027

Wang Z., Jin M., Šimůnek, J., van Genuchten M.T., 2013. Evaluation of mulched drip irrigation for cotton in arid Northwest China. *Irrig. Sci.* DOI: 10.1007/s00271-013-0409-x

Wang Z., Li J.S., Li Y.., 2014. Simulation of nitrate leaching under varying drip system uniformities and precipitation patterns during growing season of maize in the North China Plain. *Agric. Water Manag.* 142; 19-28.

Warrick A. W., and Shani, U., 1996. Soil-limiting flow from subsurface emitters. II: Effect on uniformity." *J. Irrig. Drain. Eng*. 122(5), 296–300.

Wesseling J.G., Elbers, J.A., Kabat P., van den Broek B.J., 1991. SWARTE: Instructions for input. International Note. Winand Staring Centre. Wageningen, The Netherland.

Xi B., Wang Y., Bloomberg M., Li G., Di N., 2013. Characteristic of fine root system and water uptake in a triploid Populus tomentosa plantation in the North Cina plain: Implications for irrigation water management. *Agric. Water Manag.* 117; 83-92.

Xu F., Li W., Li J.S., Fan Y.S., Feng J.J., 2003. Hydraulic characteristics of emitter in soil of subsurface drip irrigation system. *J. Transactions of The CSAE.* 19 (1); 85-88

Xu F., an Y.S., Li H., Guo Z.X., Li J.S., Li W.C., 2004. Clogging of emitter in subsurface drip irrigation system. *J. Transactions of The CSAE.* 20 (1); 80-83

Yao P., Dong X., Hu A., 2011. Using HYDRUS-2D simulate soil water dynamic in jujube root zne under drip irrigation. Internaional Symposium on Water Resource and Environmental Protection (ISWREP), 1;684-688.

Zhou Q.Y., Kang S.Z., Zhang L., 2007. Comparison of APRI and Hydrus-2D models to simulate soil water dynamics in a vineyard under alternate partial root zone drip irrigation. *Plant Soil* 291:211–223.

Zwart S.J.Z., Bastiaanssen W.G.M., 2004. Review of measured crop water productivity values for irrigated wheat, rice, cotton and maize. *Agric. Water Manag. 69 (*2);115-133